# MOLECULAR LEVEL CHARACTERIZATION AND MOBILITY OF RADIONUCLIDE-CARRYING NATURAL ORGANIC MATTER IN AQUATIC ENVIRONMENTS

A Dissertation

by

CHEN XU

Submitted to the Office of Graduate Studies of
Texas A&M University
in partial fulfillment of the requirements for the degree of

DOCTOR OF PHILOSOPHY

August 2011

Major Subject: Oceanography

Molecular Level Characterization and Mobility of Radionuclide-Carrying Natural

Organic Matter in Aquatic Environments

# MOLECULAR LEVEL CHARACTERIZATION AND MOBILITY OF

# RADIONUCLIDE-CARRYING NATURAL ORGANIC MATTER IN AQUATIC

# ENVIRONMENTS

A Dissertation

by

CHEN XU

Submitted to the Office of Graduate Studies of
Texas A&M University
in partial fulfillment of the requirements for the degree of

DOCTOR OF PHILOSOPHY

Approved by:

| | |
|---|---|
| Co-Chairs of Committee, | Peter H. Santschi |
| | Robin L. Brinkmeyer |
| Committee Members, | Luis A. Cifuentes |
| | Robin L. Autenrieth |
| | Kathleen A. Schwehr |
| Head of Department, | Piers Chapman |

August 2011

Major Subject: Oceanography

# ABSTRACT

Molecular Level Characterization and Mobility of Radionuclide-Carrying Natural

Organic Matter in Aquatic Environments.

(August 2011)

Chen Xu, B.S. Xiamen University, China;

M.S., Texas A&M University

Co-Chairs of Advisory Committee:  Dr. Peter H. Santschi
Dr. Robin L. Brinkmeyer

Radionuclides, $^{129}I$ and $^{239,240}Pu$, are major products or by-products of nuclear fission and among the top risk drivers for waste disposal at the Savannah River Sites (SRS) and Rocky Flats Environmental Technology Sites (RFETS), respectively, due to their perceived mobility in the environment, excessive inventory, toxicity, and long half-life. The objective of this study is to investigate the role of natural organic matter in retarding or facilitating the migration of $^{129}I$ and $^{239,240}Pu$ in the Department of Energy (DOE) sites.

Measurements of $^{127}I$ and $^{129}I$ in humic acids (HAs) and fulvic acids (FAs) obtained by five successive alkaline, two glycerol and one citric acid-alkaline extractions, demonstrated that these extractable humic substances (HS) together account for 54-56% and 46% of the total $^{127}I$ and $^{129}I$ in the soil, respectively. The variations among $^{127}I$ and $^{129}I$ concentrations, isotopic ratios ($^{129}I/^{127}I$), chemical properties of all these humic substances indicated iodine was bound to a small-size aromatic subunit (~10

kDa), while the large-size subunit (~90 kDa), which likely linked the small-size unit through some weak chemical forces, determined the relative mobility of iodine bound to organic matter.

Soil resuspension experiments simulating surface runoff or stormflow and erosion events were conducted with soils collected from SRS. Results showed that 72-77% of the newly-introduced $I^-$ or $IO_3^-$ were irreversibly sequestered into the organic-rich soil, while the rest was transformed into colloidal and dissolved organo-iodine by the soil. The resulting iodine remobilization contradicts the conventional view that considers only $I^-$ or $IO_3^-$ as the mobile forms.

Quantitative structure analysis by $^{13}$C DPMAS NMR and solution state $^1$H NMR on these humic substances indicate that iodine is closely related to the aromatic regions containing esterified products of phenolic and fomic acid or other aliphatic carboxylic acids, amide functionalities, quinone-like structure activated by electron-donating groups (e.g., $NH_2$) or hemicelluloses-lignin-like complex with phenyl-glycosidic linkage. The micro-molecular environment, such as the hydrophobic aliphatic periphery hindering the active aromatic cores and the hydrophilic polysaccharides favoring its accessibility towards hydrophilic iodine species, play another key role in the interactions between iodine and SOM.

NMR spectra of the colloidal organic Pu carrier which can potentially be released from the soil during the surface runoff or stormflow showed Pu was transported, at sub-pM concentrations, by a cutin-derived soil degradation products containing siderophore-like moieties and virtually all mobile Pu.

# DEDICATION

To my husband Liang Ma, my daughter Joanna and my parents Bi Lin and Zhuhua Xu

# ACKNOWLEDGEMENTS

I would like to express my deepest appreciation to my committee chair, Dr. Peter H. Santschi, who is like a loving father to me and who was a constant source of instruction and encouragement. I give many thanks to my co-chair Dr. Robin Brinkmeyer, and committee members, Dr. Luis A. Cifuentes, Dr. Robin Autenrieth and Dr. Kathleen Schwehr, for their guidance and support throughout the course of this research.

I am grateful for my excellent colleague, Dr. Saijin Zhang, who is always ready to help, and show me the greatest "troubleshooting" skill. I highly appreciate the constant help and instruction from my other colleagues, Eric J. Miller, Chia-Ying Chuang, Hsiu-Ping Li, Yi-Fang Ho and Read Ebersole, whose contributions to formation of some of the ideas in my dissertation are greatly appreciated.

Special thanks are given to Dr. Junyan Zhong and Dr. Patrick G. Hatcher, who kindly introduced me into the state-of-art techniques (NMR) which were applied in my dissertation and gave me incredible help in the data interpretation. Thanks is also given to Dr. Yuelu Jiang, for her assistance with the training of the spectrofluorometer.

I express my gratitude to Drs. Daniel Kaplan, Chris Yeager, and Kimberly Roberts, from the Savannah River National Laboratory (SRNL), who were kind enough to show me a lot of wonderful aspects of geochemistry and microbiology and send me the precious samples from the heavily-contaminated DOE remediation sites, which I don't have access to.

**TABLE OF CONTENTS**

# LIST OF FIGURES

# LIST OF TABLES

CHAPTER I

INTRODUCTION TO THE PROBLEM


**1.1 Introduction**

**1.1.1 Biogeochemical cycling of iodine in the soil and groundwater: speciation and mobility**

**1.1.1.1  Sources of $^{129}$I and its environmental significance**

Iodine is a biophilic element (Wong et al., 1985) that has several short-lived isotopes (e.g., $^{131}$I with $t_{1/2}$ of eight days; $^{125}$I with $t_{1/2}$ of 60.1 days), with only one naturally-occurring and long-lived radioactive isotope, $^{129}$I ($t_{1/2}$=15.6 million years) and one stable isotope, $^{127}$I. Its biophilic nature is demonstrated by a high concentration factor of ~1200 in mixed plankton and up to $10^4$ in brown algae (Mauchline and Templeton, 1964; Bruland, 1983). The element is required in trace amounts by all animals and some plants, being by far the heaviest element known to be essential to living organisms. Iodine deficiency in some areas of the world has caused thyroid disease in humans, especially in children, resulting in stunted growth, mental retardation, problems in movement, speech and hearing, etc.

The total inventory of natural $^{129}$I from cosmic ray-induced spallation of Xe in the atmosphere and spontaneous fission of $^{238}$U in the earth's crust is ~100-260 kg. This testing (1953-1962, ~50-150 kg); Chernobyl reactor accident (1986, ~1.3 kg);

---

This dissertation follows the style of *Geochimica et Cosmochimica Acta*.

has been overwhelmed by anthropogenic release, which included atmospheric bomb

atmospheric release by the Hanford nuclear facility in Washington (1944-1972, ~260

kg); fuel reprocessing releases from facilities in La Hague in France and Sellafield in

England (~2600 kg) to the ocean and about a decade ago, ~ 6 kg/yr to the atmosphere

(Santschi and Schwehr, 2004). From 1944 through 1972, the plutonium-production

operation at the Hanford Site in Washington released about 266 kg of $^{129}$I into the air

while the operation of production reactors in the Savannah River Site (SRS) in South

Carolina released about 32 kg of $^{129}$I into the air from 1953 to 1990. By comparison, the

geological repository for storing high-level nuclear waste at Yucca Mountain of Nevada

will reach as much as 13,300 kg $^{129}$I based on the proposed storage of 70,000 tons of

nuclear waste (Table 1).

Due to its long half-life and high perceived mobility, the large inventory in some

DOE sites (e.g., 26 Ci at the SRS), and its property as an essential nutrient for humans

that highly accumulates in certain organs (e.g., thyroid), $^{129}$I has recently been

recognized by the U.S. Department of Energy's Office of Environmental Management

(DOE-EM) as a high risk radionuclide in groundwater at these DOE sites such as the

SRS (Denham et al., 2009). These factors then determined the maximum contaminant

level, MCL, of $^{129}$I in groundwater of 1 pCi/L issued by EPA to be the lowest among all

radionuclides. Even though $^{129}$I makes up only a very small portion (~0.00002%) of the

total radiological release from the site, it contributes 13% to the offsite population dose.

This is a six orders magnitude higher risk than that of any other radionuclide (Kaplan et

al., 2011). Thus, it needs to be considered not only as a major risk driver for DOE, but

also as a potential threat to the environment and human health.

Table 1.1  Major source terms of $^{129}$I in the environment (Hu et al., 2007).

| Source | $^{129}$I | |
|---|---|---|
| | (kg) | (Tbq) |
| Natural hydrosphere | 100 | 0.65 |
| Natural atmosphere | 0.0005 | 0.000003 |
| Atmospheric testing | 50 | 0.32 |
| Chernobyl | 1-2 | 0.01 |
| Savannah River Site | 32 | 0.21 |
| Hanford Reservation | 266 | 1.7 |
| NTS underground nuclear testing | 10 | 0.065 |
| Yucca Mountain repository | 13,300 | 87 |
| Spent fuel reprocessing (Europe) | 2,360 | 15 |

**1.1.1.2 Iodine content and speciation in the soil, sediment and groundwater**

The median concentrations of $^{127}$I in the different environmental compartments are:

0.46 ppm in the earth's crust (Earnshaw and Greenwood, 2005), 30-400 pmol/m$^3$ in the

atmosphere (Yoshida and Muramatsu, 1995), ~600 nM in seawater (Schwehr and

Santschi, 2003, and references therein), 10-2,000 nM in freshwater (Oktay et al., 2001;

Moran et al., 2002; Schwehr and Santschi, 2003). Iodine concentrations in groundwater

largely lie in the range of $7.87 \times 10^{-2} - 567$ nM (BGS, 2000), depending on geographical

location, local geology and geochemical properties of soils. Iodine is found at low

concentrations in most rocks because it is incompatible with most rock-forming silicate

minerals. The average iodine content in surface soils (usually sampled to 15 cm depth) on a worldwide basis is about 5 mg/kg (Whitehead, 1984). The total iodine contents in 15 U.S. surface soils ranged from 0.46 to 5.42 mg/kg (Hu et al., 2007). In contrast, generally higher total iodine contents were found in 132 surface soils of various types in the United Kingdom (UK) and in more than 50 soils in Japan, varying from 0.5 to 98.2 mg/kg with a mean value of 9.2 mg/kg and from 0.2 to 150 mg/kg, respectively. This higher range in Japan can be ascribed to the proximity of the sampling sites to the coast where they receive more rainfall and the geochemical properties of the soils (e.g., organic matter content and mineral types) (Muramatsu et al., 2004; Hu et al., 2007).

Iodine exhibits a complicated biogeochemical behavior because it can exist in multiple physical states, as well as in multiple oxidation states ranging from -1 to +7, under environmentally relevant conditions. Figure 1 shows the simplified relationships of the major inorganic iodine species in Eh-pH diagram. Iodate ($IO_3^-$) is stable under very oxidized conditions across the range of natural pH values likely to be encountered. In the absence of natural organic matter, elemental iodine is stable at moderately oxidized and acidic conditions. Iodide ($I^-$) is the most stable form in reducing environments, but actually also over most of the range of natural conditions. The protonated acids HI and $HIO_3$ only exist under very low pH conditions. Thus, a simplified picture of the chemistry of iodine under natural conditions is presented in Figure 1. However, the biophilic properties of iodine, i.e., the ability of iodine to react with organic compounds, together with its hydrophilic and atmophilic characteristics, further complicate its speciation and transport properties in organic-rich environments,

which are not considered in the simplified thermodynamic diagram. Fuge and Johnson

(1986) studied 183 UK soils and found out that about 80% of these soils contained less

than 10% extractable inorganic iodine. In 15 U.S. surface soils with varying organic

carbon content of 0.01% to 28.1%, iodine is mostly (nearly 90% of total iodine) present

as organo-iodine, with appreciable amounts (~ 50% for most soils) being associated with

refractory organic matter (Hu et al., 2007).
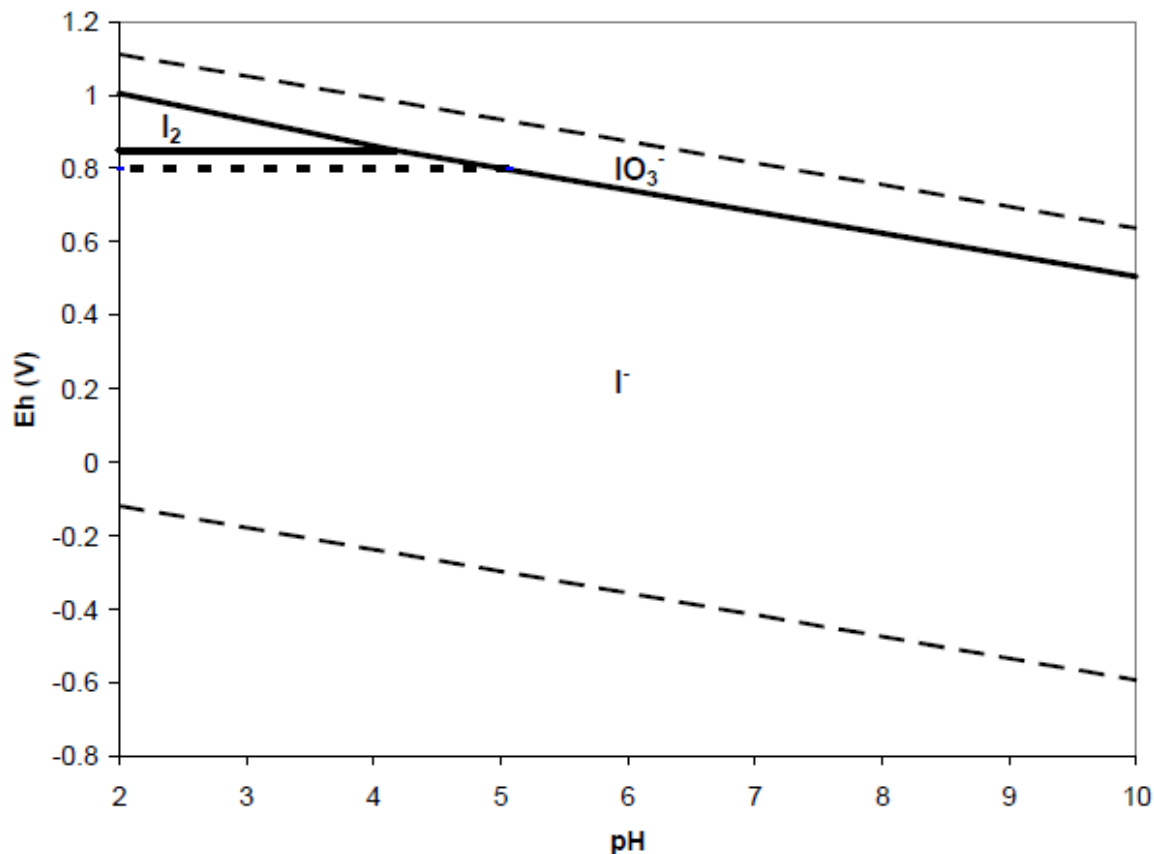


Fig. 1.1 Eh-pH diagram of aqueous iodine speciation; solid line= total iodine concentration of 1 μg/L, a typical groundwater concentration, dotted line= total iodine concentration of 58 μg/L, a typical seawater concentration (Fuge and Johnson, 1986); dashed lines are stability limits of water .

Furthermore, in freshwaters, enrichment (concentration) factors (or distribution coefficients) for $^{127}I$ and $^{129}I$ to natural colloidal organic matter were reported to be extremely high, e.g., (5-9) x $10^5$ L/kg (Oktay et al., 2001). The presence of organo-iodine species, however, has not been widely recognized due to non-quantitative analytical techniques and the limitations of the detection methods (Schwehr and Santschi, 2003, Zhang et al., 2010), and often it is still be assumed that iodate ($IO^{3-}$) and iodide ($I^-$) are the only species to be considered in aquatic environments. However, recent studies have now repeatedly recognized that organic iodine species in fresh, estuarine and surface ocean water as well as some groundwaters are more important than previously thought (Krupp and Aumann, 1999; Szidat, 2000; Oktay et al., 2001; Wong and Cheng, 2001; Santschi and Schwehr, 2004; Schwehr and Santschi, 2003; Schwehr et al., 2009; Hou et al., 2009, Zhang et al., 2010, 2011). For example, Schwehr and Santschi (2003) reported that about 30% of all iodine in freshwater and seawater, including some groundwater samples, exist as organo-iodine. Furthermore, Yang et al. (2007) confirmed that 10-50% of all iodine exist as organo-iodine in groundwater samples they took from various geologic and hydrologic environments, using size exclusion chromatography-high performance liquid chromatography-inductively coupled plasma-mass spectrometry (SEC-ICP-MS) for analysis. Groundwater sampled from a well adjacent to the nuclear waste seepage basin of the SRS, which contained 177.96 pCi/L $^{129}I$, was largely composed of iodide, yet it contained surprisingly large amounts of organo-iodine species (12.7%). In comparison, the iodine speciation in another well a few hundred meters from the seepage basin and approximately 10 m from the wetland

edge, was very different, consisting of no detectable iodide, 93.4% of iodate, and 6.6% of organo-iodine (Kaplan et al., 2010). In another investigation from the same site, Otosaka et al. (2011) found that organo-iodine was present in a dozen wells spatially distributed down gradient from the $^{129}$I-iodide source region along the plume area to the wetland area, varying from 8% to 82%, with an average value of 37% of the total iodine.

While it is commonly believed that the content of organic matter has a dominant influence on total iodine content in the soil or groundwater (Fuge and Johnson, 1986; Schwehr et al., 2009; Kaplan et al., 2010; Zhang et al., 2010, 2011; Otosaka et al., 2011), the composition of the mineral phases can also affect speciation and the resulting mobility of iodine in the environment, especially in organic-deplete or organic-poor soils. For example, total iodine content in 154 samples collected from a subsurface (>10 cm depth) of 18 soil profiles was well correlated with oxalate-soluble Al but not with oxalate-soluble Fe or organic matter (Whitehead, 1978). In the same investigation, the total iodine content of five acidic soils was found to be positively correlated with Fe instead of Al. Thus overall, Hu et al. (2007) concluded that organic matter, clays and sesquioxide (Fe and Al oxides) play important roles in sequestering iodine in soils.


**1.1.1.3 Iodine mobility (sorption/uptake vs. desorption/release) in the soil and groundwater**

Laboratory approaches to study iodine transport in the soil and groundwater are usually through batch and column experiments. Iodate was generally found to be retarded in the soils and sediments to a significantly greater degree than iodide, with a

distribution coefficient (Kd, the ratio of the concentration in the solid phase to that in the aqueous phase) in the range of $1\text{-}10^3$ cm$^3$/g, compared to that of iodide, which ranges from $\leq 1$ to 10 cm$^3$/g (Sheppard and Thibault 1991; Yoshida et al., 1998; Hu et al., 2005; Schwehr et al., 2009; Zhang et al, 2011), partially due to its interaction with mineral phases. As discussed by Kaplan et al. (2000), the cause for the difference in the sorptive behavior of I$^-$ and IO$_3^-$ is due to the harder base nature of IO$_3^-$, as compared to I$^-$, which would favor weaker hard-hard interactions with the hard acid sites on the mineral surfaces.

Abiotic and biotic interactions between iodate and organic matter through the formation of covalent C-I bonds, mostly likely in the aromatic region, are regarded as another mechanism to explain iodate retardation in soils (Schlegel et al., 2006). Similarly, iodide can also be incorporated into the soil organic matter through microbial activity, including enzymatic catalysis (Christensen and Carlsen, 1991) and cellular accumulation (Li et al., 2011), or through abiotic reactions (Yamaguchi et al., 2010).

Almost all studies of sorption (used here in the broadest sense) in shallow soils that contain organic matter (OM) indicate that the OM is a primary control on soil and sediment uptake of iodine species, of which the approaches and results can be summarized: 1) By comparing the sorption of iodine between untreated soils and treated soils after the removal of OM, it was demonstrated that sorption of iodine was substantially decreased when OM was destroyed (Whitehead, 1973; Muramatsu et al., 1990). 2) By comparing the uptake of iodine with soil samples of various organic matter contents, it was demonstrated by Bors et al. (1988) that in a single soil profile uptake of

iodine correlated with organic carbon content. In another case, Sheppard and Thibault (1991) measured Kd values that were 1-2 orders of magnitude higher in the organic-rich soils (6.8% OC) relative to organic-poor soils (0.2% OC). 3) Comparison of sorption onto individual components that comprise the soil, for example, the individual high surface area inorganic phases that make up most of volcanic soils sorb iodide poorly, relative to bulk soils (Yu et al., 1996). In contrast, Fukui et al. (1996) found a ten-time higher partitioning coefficient of iodine onto pure humic material, compared to that of the bulk soil.

Though sorption of inorganic iodine species is relatively low in the organic-poor soils, when compared to uptake in the organic-rich soils, Um et al. (2004) noted that sorption to these soils was partially irreversible, with much higher desorption Kd values(1.4 ml/g, residual iodide that remained sorbed to the solid phase after contacting iodine-free water and could not be released in the solution phase) than the sorption Kd (0.2 ml/g), indicating some kinetic limitations. Yoshida et al. (1992) concluded that iodide sorption was likely through electrostatic attraction to the positively-charged mineral surfaces, while iodate sorption also involved chemical interactions with the mineral allophone or with sesquioxides. However, Fukui et al. (1996) hypothesized that iodide sorption was more complicate than simple ion exchange with surface sites, and might be enhanced by molecular diffusion into the inner pore spaces of soil particles.

Most importantly, iodide and iodate can be interconverted in the presence of oxidizing or reducing metal oxide phases, resulting in different transport behavior for these species. For example, in a series of column experiments, Hu et al. (2005) observed

the reduction of iodate to iodide by both the Savannah River Site aquifer sediment and Hanford sediment, possibly caused by the presence of structural Fe (II). Results from a field tracer test through sandy sediments using high concentrations of iodide show that $I^-$ was oxidized to $I_2$ (up to 46%) and $IO_3^-$ (up to 6%) in the oxic zone, with a concurrent pulse of dissolved Mn released from the sediment, suggesting that Mn oxides were responsible for $I^-$ oxidation. The newly-formed $IO_3^-$ was retarded compared to the conservative tracer ($Br^-$) downgradient from the injection spot (Fox et al., 2009, 2010). $IO_3^-$ was quickly reduced to $I^-$ without any observed production of intermediate species (i.e., $I_2$) in a Fe-reducing zone. About 60% of the injected iodate was reduced to $I^-$ within 1 m of transport, with complete reduction occurring after 3 m of transport, observed by the same authors (Fox et al., 2009, 2010).

Only a few studies have so far investigated the migration of organo-iodine species through soils or groundwaters (Hu et al., 2005; Schwehr et al., 2009; Zhang et al., 2011; Otosaka et al., 2011). This is mainly due to the complexity of the various organo-iodine species that could occur, and the analytical difficulty for their determination (Hou et al., 2009). This makes the direct measurement of organo-iodine-129 even more difficult. Hu et al. (2005) used 4-iodoaniline as a representative nonvolatile organo-iodine species to study its transport through a soil and aquifer sediment collected from two DOE sites. Transport of 4-iodoaniline was quite different from that of inorganic iodine species in that it was greatly retarded (by more than 20 times compared to that of $I^-$) in the SRS surface soil which contained 2.3% OC, while it was eluted very quickly through the organic poor SRS subsoil and aquifer sediment, in which the transport of inorganic

iodine were retarded somehow due to anion sorption. Thus a good understanding of the interconversion of iodine species, especially the uptake of inorganic iodine species into natural organic matter, and the resulting geochemical behavior and mobility of different organo-iodine species in terrestrial systems, is still lacking.

**1.1.1.4 Isotopic equilibrium/disequilibrium of $^{129}$I and $^{127}$I in the environment and the application of $^{129}$I/$^{127}$I as tracer kinetic processes in the environment**

Due to slow kinetics, recently introduced anthropogenic $^{129}$I may not have isotopically equilibrated with natural $^{127}$I in surface environmental compartments, especially for organic $^{129}$I species. For example, Santschi and Schwehr (2004) documented the different equilibration times of $^{129}$I (and $^{127}$I) in European and North American soils and drainage basins, which they attributed to different climatic conditions. Furthermore, Hou et al. (2009) observed significant different speciation distributions for $^{129}$I and $^{127}$I when comparing the respective $IO_3^-/I^-$ ratios of these two isotopes along the European continent. Schmitz and Aumann (1995) also found different $^{129}$I distributions among different soil extracts, compared to those of $^{127}$I, which they ascribed to different sources of these two isotopes and their different contact times with the soils. It is generally accepted that chemical equilibrium between $^{129}$I and $^{127}$I within the soil environment can take a long time and results in a different species distribution among different components. Hu et al. (2007) suggest that $^{127}$I probably preferentially occupies the thermodynamically favorable sorption sites of environmental compartments, due to its longer interaction times (thousands of years) and the higher

concentrations, compared to those of $^{129}$I, thus $^{129}$I is less strongly bound to binding sites than $^{127}$I, on the time scale of anthropogenic $^{129}$I inputs, rendering $^{129}$I more mobile and bioavailable characteristics than $^{127}$I.

If certain conditions are met, $^{129}$I or $^{129}$I/$^{127}$I ratios could be used as a new environmental radioactive tracer and geochronometer in environmental archives. For example, $^{129}$I has been used as a tracer for recent North Atlantic water circulation and ocean mixing (Santschi et al., 1996; Raisbeck and Yiou, 1999); sedimentation (Oktay et al., 2000); evapotranspiration in a large watershed (Oktay et al., 2001), a tracer and dating tool of spreading of infiltrating river water in the near-surface infiltration zone (Santschi et al., 1999; Schwehr and Santschi 2003); a source tracer and geochronometer for terrestrial organic matter with ages of 50 years or less (Santschi and Schwehr, 2004). Thus, a better characterization of equilibration times in soil/water systems will greatly contribute to successful environmental tracer applications of $^{129}$I/$^{127}$I.

## 1.1.2 Interactions between iodine and soil organic matter and their transport in relation to the physical-chemical properties in the terrestrial systems

Natural organic matter (NOM) in the terrestrial environment is a complex mixture of thousands of molecules, and a large portion of the terrestrial NOM is present as humic substances (HS), which are dark colored, have variable composition, are heterogeneous, amorphous and composed of high molecular weight materials, including humic acid (HA, the fraction that is soluble under alkaline conditions but not acidic condition, generally pH<2), fulvic acid (FA, the fraction that is soluble under all pH conditions)

and humin (the insoluble fraction). The non-HS organic compounds in soils include macromolecular hydrophilic acids and more identifiable and less degraded organic molecules such as polysaccharides, proteins, lignin, lipids, nucleic acids, etc. The classical definitions of HS are operational only (see above) and based on the solubility in those aqueous solutions used as soil extractants or the technology applied to separate them from the soil or groundwater matrix and purify them, but the boundaries between these fractions are not firm in chemical terms. For example, HS extracted from soils can contain recognizable biomolecules such as carbohydrates, amino acids, lipids, etc. that have been specifically excluded from traditional definitions of HS. Piccolo et al. (2001) concluded HS should be regarded as supramolecular association of self-assembling heterogenous and relatively small molecules derived from the degradation and decomposition of dead biological materials, stabilized predominantly by weak dispersive forces instead of covalent linkages. Hydrophobic (van der Waals, $\pi$-$\pi$, CH-$\pi$) and hydrogen bonding are responsible for the apparent large molecular size of humic acid (HA), with the hydrophobic forces becoming more and more important with decreasing pH.  In addition, considerable evidence supports the notion that HA is a large, dynamic association of organic molecules capable of exhibiting micellar properties in aqueous solution, which cannot be simply explained by the traditional view of multivalent cation bridging formation (Sutton and Sposito, 2005). In contrast, the low hydrophobicity and high negative charge of fulvic acid (FA), compared to HA, would not favor the HA-like aggregates supported by largely hydrophobic and hydrogen bonded associations (Piccolo et al., 2001).

Numerous studies have demonstrated HS reacts with iodine to form iodinated organic matter (Christiansen and Carlsen, 1991; Warner et al., 2000; Steinberg et al., 2008), however, fewer studies have provided in-depth information about the physic-chemical aspects of the molecular environment of iodine in the NOM. X-ray absorption near-edge structure (XANES) can provide information on the oxidation state, electronic structure, and chemical environment of iodine (e.g., whether iodine is bound to aliphatic carbon or aromatic carbon) in natural organic matter, while the extended X-ray absorption fine structure (EXAFS) can provide insight into the nature and distance of neighboring atoms, provided that the iodine content is artificially increased to ease detection. Iodine K-edge XANES is usually applied to explore the molecular environment of iodine in crude soil and aqueous samples with a lower detection limit to avoid the disturbance from the abundant $Ca^{2+}$ present, while $L_{III}$-edge XANES can provide better resolution for purified iodinated natural organic matter. However, the above techniques can only tell whether iodine is in the form of organo-iodine in the crude soil or aqueous samples (Yamaguchi et al., 2010; Shimamoto et al., 2011) or indicate that iodine is bound to the aromatic carbon in purified iodinated humic substances by comparing its spectra to those of model compounds (Schlegel et al., 2006). By using electrospray ionization mass spectrometry (ESI-MS) techniques, one can compare the ESI spectrum of iodinated HS and that of unreacted compounds and produce structural assignments for the common "core" of iodo compounds. The measured masses of the precursor ions and their fragmentation patterns suggest that an aromatic substitution of the fulvic acid by iodine under investigation would have

occurred (Moulin et al., 2001). Preferred sites in the NOM for iodine to "attack" depend on the combined electronic and steric effects of the ring substituents. A substituent group of the aromatic ring will exert an influence on subsequent electrophilic substitution reactions, which is more complicated by more than two substituents. The activation or deactivation of the ring can be predicted more or less by the sum of the individual directing effects of all the existing substituents, as well as the steric hindrance of these same substituents. Electron-donating substituent groups are ortho/para-directing, while electon-withdrawing groups are meta-directing. Based on this, Moulin et al. (2001) proposed a possible structure of several iodo fragments of a fulvic acid and the potential sites that were substituted by iodine, in which iodination occurred in ortho positions not impeded by large site chains. Thus, further confirmation and elaborations for the exact iodine environment in NOM compounds is warranted.

### 1.1.3 Soil colloidal organic matter as the main [239, 240]Pu carrier in the Rocky Flats Envrionmental Technology Site (RFETS)

Surficial soils of the Rocky Flats Envrionmental Technology Site (RFETS), Colorado, USA, contain elevated [239,240]Pu due to dispersal of soil particles by wind and waters, contaminated in the 1960's by leaking drums stored on the 903 Pad. A wide range of work at RFETS has demonstrated that "particulate" forms ($\geq$0.45 $\mu$m, 40-90%) and colloidal forms (~2 nm or 3 kDa to 0.45 $\mu$m; 10-60%) of Pu make up the major fraction of actinides in surface waters and that particle transport is greatest during rainfall events (Santschi et al., 2002). Furthermore, controlled laboratory experiments

confirmed that most of the Pu in the 0.45 μm filter passing phase was in the colloidal phase (~80%) and the colloidal Pu is in the four-valent state and was mostly associated with a negatively charged ion-containing organic macromolecule with $pH_{IEF}$ of 3.1 and a molecular weight of 10-15 KDa, rather than with the more abundant inorganic (e.g. aluminosilicates) colloids. However, further molecular-level characterization of the composition and structures of this Pu-enriched colloidal fraction isolated by isoelectric focusing method was needed.

## 1.2 Hypotheses, objectives and experimental approaches

Hypothesis I: $^{129}I$ and $^{127}I$ are expected to have different behaviors and perhaps different chemical speciation since the recently introduced anthropogenic $^{129}I$ might have not isotopically equilibriated with natural $^{127}I$ in surface environmental compartments. This can be shown by investigating different fractions of soil organic matter, considering their different reactivity and turnover times of different organic compounds. For example, over time scales of months to years, iodine tends to bind in kinetically faster reactions to nitrogen-rich compounds (e.g., proteins), under the influence of microorganisms (phytoplankton and bacteria). Such microbially produced nitrogen-rich compounds are more labile, and might have a shorter life-time (days to weeks), before they are more slowly converted into more refractory compounds such as humic acid type molecules (Santschi and Schwehr, 2004). The specific objective is then to determine the concentrations of $^{129}I$ and $^{127}I$ in different organic fractions extracted from the soil based on solubility and molecular size. A novel method of directly and

simultaneously measuring $^{129}$I and $^{127}$I in both solid and liquid samples by combustion and GC-MS technique was recently developed and applied in this study (Zhang et al., 2010).

Hypothesis II: Physico-chemical properties of natural organic matter play an important role in the radionuclide ($^{129}$I and $^{239, 240}$Pu) biogeochemical cycle, by influencing their speciation and transport in the surface environment. Iodinated NOM with different mobility in soil and groundwater systems can either be part of the immobile soil organic matter or become incorporated into the mobile NOM fraction, depending on their composition and properties (e.g., relative hydrophobicity) of NOM. The specific objective is then to investigate the physico-chemical properties of natural organic matter extracted from the soils and groundwater of the contaminated sites and their variations in relation to iodine concentrations and isotopic ratios. In addition, those radionuclide-enriched organic fractions, isolated by electrophoresis (in the case of $^{239, 240}$Pu) or size fractionation (in the case of $^{129}$I) will be characterized at the molecular level by different state-of-the-art techniques, e.g., GC-MS, HPLC, ATR-FTIR, NMR, etc.

Hypothesis III: The interaction between iodine and NOM is dependent not only on abiotic but also on biotic processes. Most importantly, these processes must be investigated using environmentally relevant concentrations of iodine and organic carbon (moiety) concentrations. The specific objective is then to investigate the iodination of NOM extracted from the contaminated sites, under different conditions, for example, different starting species, $IO_3^-$ or $I^-$, NOM of different concentrations and compositions,

pH, in the presence or absence of metals (Fe (III and II), Mn (IV and II)), peroxide, enzyme, etc. $^{125}$I- and $^{125}$IO$_3^-$ can be used as analogues to track the reactions of naturally-occurring iodine species with NOM moieties, and the incorporated stable iodine can be determined using novel GC-MS methods.

## CHAPTER II

## IS SOIL NATURAL ORGANIC MATTER A SINK OR SOURCE FOR MOBILE

## RADIOIODINE ($^{129}$I) AT THE SAVANNAH RIVER SITE?

### 2.1 Overview

$^{129}$I is one of the three major radiation risk contributors to the public as a consequence of past nuclear processing activities at Department of Energy (DOE) facilities. Elevated levels of $^{129}$I are present in the surface soils of F-Area of Savannah River Site, which used to be an isotope separation facility for the production of nuclear weapons components. The $^{129}$I in soils is thought to be bound predominantly to soil organic matter (SOM). Measurements of stable $^{127}$I and radioactive $^{129}$I in humic acids (HAs) and fulvic acids (FAs) obtained by five successive alkaline, two glycerol and one citric acid-alkaline extraction, demonstrated that these extractable humic substances (HS) together account for 54-56% and 46% of the total $^{127}$I and $^{129}$I in the soil, respectively. The remainder was likely bound to residual SOM. The iodine content (µg-I/g-C) generally decreased with each subsequent extract, while $^{129}$I/$^{127}$I increased concurrently. The coincident variations in chemical compositions, aromaticity (estimated by UV spectroscopy), functional groups (e.g., aliphatic), degree of humification, relative migration in the hydrophobic interaction column, and molecular weight indicated that: 1) iodine in different HAs was bound to a small-size aromatic subunit (~10 kDa); 2) the large-size subunit (~90 kDa), which likely linked the small-size unit through some weak chemical forces (hydrogen bonds, hydrophobic or electrostatic interactions), determined

the relative mobility of iodine bound to organic matter; 3) from the strong correlation between iodine content and aromaticity in the HAs, we suggested that iodine incorporation into the SOM via covalent aromatic C-I bond is the key mechanism controlling iodine behavior in this system. However, this relationship is not universal for all fractions of organic matter as evidenced from the different slopes of this relationship at the two sampling sites, as well as from the different relationships for HAs and FAs, respectively.  These differences in iodination are due to different SOM molecular sizes, compositions, and availability of preferred iodination sites. $^{129}$I in the soil downstream from the contaminated site and near a wetland abruptly dropped below our detection limit (0.5 pCi-$^{129}$I/g-soil), which suggests that the high SOM in the plume soil around the $^{129}$I-contaminated F-Area might be a natural barrier to scavenge radioiodine released from the nuclear waste repository by forming organo-iodine compounds. Soil resuspension experiments showed that mobile $^{129}$I was mostly associated with a low average molecular weight amphiphilic organic carrier (13.5-15 kDa). SOM clearly behaves as a sink for iodine at the Savannah River Site F-Area. However, this work demonstrates that a small fraction of the SOM can also behave as a source, namely that a small fraction that may be readily dispersible under some environmental conditions and presumably release iodine in the organic-colloidal form. This radioiodinated organo-colloid likely can get into the groundwater through infiltration or surface runoff where it might migrate further into the wetlands. Results from this study provide the geochemical basis for future $^{129}$I migration controls, remediation, and/or land-groundwater management strategies.

## 2.2 Introduction

Iodine-129 is one of the key risk drivers that make a significant contribution to the overall long-term dose at nuclear waste depositories, such as the Savannah River Site in South Carolina. Due to its large inventories, longevity (half life=15.7 My) and high mobility, $^{129}I$ is considered to be weakly retained by natural or engineered barrier systems of the depositories (Kaplan et al., 2011). Another environmental concern results from its biophilic properties and bioaccumulation effect in human organs, especially the thyroid gland, through food chain magnification and transfer, or through inhalation. Thus the Maximum Contaminant Level, MCL, of $^{129}I$ in groundwater issued by EPA is the lowest among all radionuclides (1 pCi/L compared to 15 pCi/L for $^{239,240}Pu$, 200 pCi/L for $^{137}Cs$, 900 pCi/L for $^{99}Tc$, 2000 pCi/L for $^{14}C$ and 20,000 pCi/L for $^{3}H$).

Releases of $^{129}I$ from a nuclear waste depository occur through penetration into groundwaters, wet and/or dry deposition, and surface runoff, where the speciation of iodine is a key factor in determining its environmental mobility and fate. Major iodine species in soils include iodide ($I^-$), iodate ($IO_3^-$) and organo-iodine. Among these species, $I^-$ is the most mobile in soil due to its low affinity to soil minerals, while $IO_3^-$, formed under oxidizing conditions, is less mobile and significantly retained by sediment or soil (Fukui et al., 1996; Kaplan et al., 2000; Glaus et al., 2008). Though pH and redox potential of soil solution and soil mineral types are important parameters that affect iodine speciation and mobility, the existing literature indicates organic matter is a primary control on iodine retardation in soil systems. Kaplan (2003) compared iodide sorption between two soils in the Savannah River Site that were similar in grain-size, pH

and mineralogy, but had very different organic carbon contents (<200 vs. 1395 mg/kg), and he found that iodide was preferentially sorbed to organic-rich soils. Similar results were obtained in studies by Sheppard and Thibault (1991), Yoshida et al. (1992, 1998), Bird and Schwartz (1996), Sheppard et al. (1996), and Schwehr et al. (2009). Direct evidence for iodine sorption to soil organic matter, especially humic substances (HS), was also obtained as elevated partitioning coefficients (Kd) of HS over that of bulk soil by Fukui et al. (1996). Recently, Yamaguchi et al. (2010) using iodine K-edge X-ray absorption near-edge structure (XANES) reported soil organic matter (SOM) is capable of oxidizing $I^-$ or reducing $IO_3^-$ and subsequently binding iodine to reactive carbon sites. Even though it was apparently observed that a main reservoir for iodine can be the carbonate fraction in a Callovian-Oxfordian (Cox) clay rock, one needs to consider the fact that organic matter contents in these clay materials under investigation were mostly below 1% (Claret et al., 2010). Li et al (2011) provided indirect evidence that iodide was enzymatically transported into the soil bacterial cell and incorporated into cellular components via covalent binding. An investigation of organo-iodine formation by electrospray ionization (ESI) mass spectrometry (Moulin et al., 2001) revealed that under laboratory condition, iodine is covalently bound to fulvic acids via aromatic substitution, and the resulting iodo-derivative was fairly stable at room temperature and in the dark. By comparing the XANES spectra of several humic acids (HA) and fulvic acids (FA) and the simulated spectra of phenolic reference compounds, Schlegel et al. (2006) suggested iodine is bound covalently to carbon on aromatic rings in naturally iodinated HS extracted from the field.

Once iodine is incorporated into SOM, its transport and bioavailability largely depend on the differential mobility of the associated organic matter compounds. The heterogeneous nature of SOM (i.e., different chemical compositions, hydrophobicity, etc.) could then either prevent or favor the release of radioiodine from soils. Soil-bound organo-iodine flushed by surface or storm runoff could then be fractionated similarly to what occurs in a liquid chromatography system. Iodinated organic matter that is released into the mobile phase could become a radioiodine carrier, though overall migration would be retarded with respect to inorganic iodine (Hu et al., 2005; Zhang et al., 2011). Zhang et al. (2010) found substantial amounts of organo-iodine (24% of total iodine) in the groundwater of the Savannah River Site, which may mostly result from the surface inflow of iodinated SOM, or more likely, formed in-situ. In contrast to this, Fukui et al (1996) observed that soluble humic acid and other soluble organic compounds had little influence on uptake of iodine onto the fine sand and thus its mobility. But they observed the insoluble fraction of humic acid led to iodine species transformation and enhancement of uptake of iodine unto the sand, which they ascribed to the different anion exchange capability of humic acid. Insoluble and/or mineral-wrapped organic matter may act as iodine sink (Andersen et al., 2002; Bostock et al., 2003; Maillant et al., 2007).

In summary, there is no consensus on the role of organic matter on iodine mobility, i.e., whether organic matter will tend to trap iodine, or make it more mobile. Few have looked into the interactions between iodine as both $^{127}$I and $^{129}$I with humic acids both at the molecular level and under ambient conditions. The purpose of this study is therefore

to extract humic acid and fulvic acid of different solubility and thus mobility, as well as isolate a potentially mobile colloidal organic $^{129}$I (and $^{127}$I) carrier which could easily be transported by surface runoff, from both a $^{129}$I contaminated surface soil in the F-Area of the Savannah River Site and an uncontaminated surface soil downstream of the F-Area. Direct analysis on both the $^{127}$I and $^{129}$I contents of these HS and water extractable colloids (defined below) by a novel GC-MS technique (Zhang et al., 2010), and characterization of these iodinated organic moieties will help to understand the mobility, stability, and evolution of radioiodine-SOM and predict its behavior in the long-term stewardship of DOE remediation site. To the best of our knowledge, this is the first time where 1) the distribution of organically bound $^{129}$I and $^{127}$I in SOM fractions extracted based on a mild sequential extraction procedure and 2) the molecular level chemical composition of SOM related to the potential mobility of $^{129}$I and $^{127}$I was investigated.

## 2.3 Materials and methods

### 2.3.1 Study area and sampling protocols

The F-Area at the Savannah River Site was a separation facility for the production of nuclear weapon components between 1955 and 1988, during which time large amounts of radionuclides were processed and radioactive liquid waste was then discharged to seepage basins. Low levels of radioactive elements were released into the atmosphere and surface water during the years of operation and continuously after site closure. While site remediation is still going on, the contaminant plume contains $^{129}$I at concentrations well above the primary drinking water standard of 1 pCi/L (Kaplan et al.,

2011). The selected soil sampling sites were FSI18, in the path of the contaminant

groundwater plume, and a background site (named "4 Mile Creek"), close to the Four

Mile Branch where the contamination is regarded as minimal (Fig. 2.1). Both soils were

sampled to a depth of ~10-15 inches near the O-horizon boundary by removing the

debris at the surface and using a hand trowel. The soil sample was stored and shipped in

a zip lock bag under ice and immediately transferred to a refrigerator at 4 °C in the lab.
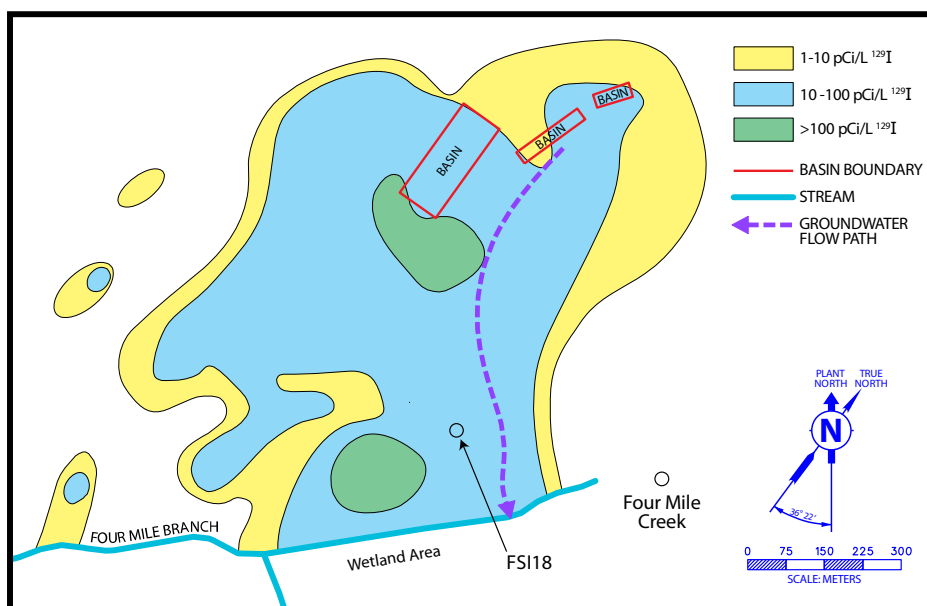


Fig. 2.1 Map of the Savannah River Site. The blue rectangle represents the Seepage Basin of F-Area. The red circles are representative sampling sites from the contaminated (FSI18) and uncontaminated (4 Mile creek) area.

## 2.3.2 Extraction of humic acids (HA) and fulvic acids (FA)

Five HA fractions were obtained by repeatedly extracting the soil five consecutive

times following a standard procedure recommended by IHSS (Swift, 1996; Fig. 2.2).
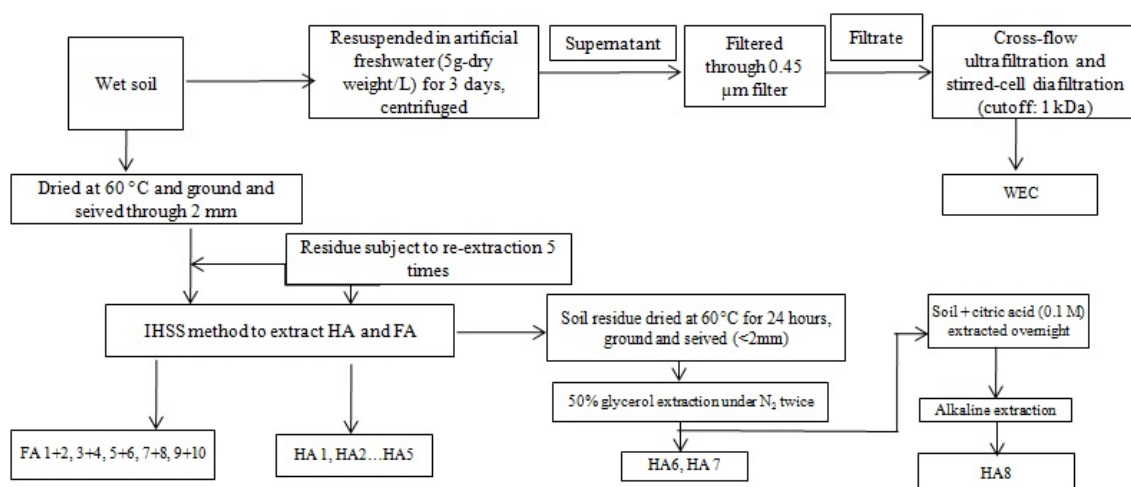
Fig. 2.2 Flow diagram for the extraction of water extractable colloid (WEC), fulvic acids (FAs) and humic acids (HAs).

Briefly, soil was dried in an oven of 50-60 °C after the removal of leaves and roots, gently and thoroughly homogenized with a mortar and pestle, and then sieved through a 2 mm sieve. A total of 100 g of the dried soil was partially dissolve in 1 L of 1 M HCl and shaken for 1 hr on a DS-500E orbital shaker (VWR). The acidic soil slurry (pH 1-2) was centrifuged at $3200 \times g$ and the supernatant was saved for fulvic acid extraction (FA1). Under $N_2$ atmosphere (to minimize the formation of carbonates), the soil pellet was neutralized with 1 M NaOH and then 0.1 M NaOH was added to make a final volume of 1 L. The alkaline suspension was shaken overnight in a $N_2$ atmosphere. The slurry was centrifuged to collect the supernatant. A 6 M HCl solution was added to the supernatant to achieve a pH= 1.0 and the suspension was allowed to stand for at least 12 hr. The suspension was centrifuged to separate the supernatant (FA2) and precipitate. The precipitate was redissolved by adding a minimum volume of 0.1 M KOH under $N_2$ purging and KCl was added to attain a concentration of 0.3 M $K^+$. The insoluble fraction

was removed by centrifugation. The supernatant (HA1) was re-precipitated at pH=1.0

using 6 M HCl and obtained by centrifugation.  The HA was then suspended in 0.1 M

HCl/ 0.3 M HF solution and stirred with a magnetic bar overnight. This step was

repeated another four times to minimize the ash content. After HF digestion, the HA was

washed repeatedly with Milli-Q water (18.2 $\Omega$) to minimize ions. The FA1 fraction (~1

L) was loaded onto a Knotes glass column (15mm ID, 100mm length, 18mL volume)

packed with ~15 mL XAD-8 resin, which was well conditioned according to Thurman

and Malcolm (1981) and back-eluted first with 0.1 M NaOH and then followed by Milli-

Q, with a peristaltic pump. The back eluted solutions (NaOH and Milli-Q wash) were

combined and immediately acidified to pH = 1.0 and HF was added to achieve a final

concentration of 0.3 M. The FA2 fraction was processed by the same method. The two

FA fractions were combined and purified again with a third XAD-8 column. The eluate

was passed through $H^+$-saturated cation exchange resins to remove the cation and named

"FA1+2". The same extraction was repeated five consecutive times for the same soil and

the HAs and FAs extracted were named HA1, HA2,…, HA5 and FA1+2, FA3+4, …,

FA9+10, respectively. For XAD-8 and cation-exchange resin cleaning, we followed the

method of Thurman and Malcolm (1981). Resin bleeding was minimal based on DOC

measurements and UV full spectrum scanning (200-800 nm) of the resin eluent extracted

by Milli-Q water with a 1:1 (v/v) ratio.

The soil residue, after five times of HA and FA extraction, and saturation with

NaOH, was dried overnight in an oven at 50-60 ºC, then homogenized by grinding.

Three more fractions were obtained, partially following the methods recommended by

Baglieri et al., 2007, yet to focus on further extracting residual organic matter after the alkaline/acid removal of HAs and FAs. The soil residue was re-dissolved in 800 mL 1:1 (v/v) glycerol in de-gassed Milli-Q water. The soil resuspension solution was disaggregated for 15 min by ultrasonic treatment, shaken for 20 h and then centrifuged to collect the supernatant, which was immediately subjected to acidification and purification steps described above for HA. The resulting sample was named "HA6". This entire procedure was repeated once to obtain HA7. After these two glycerol extractions, the soil residue was added to 400 mL of 0.5 M citric acid, disaggregated with an ultrasonic treatment for 15 min and shaken under $N_2$ for 20 h. The aqueous phase was separated from the soil by centrifugation, and discarded. It was assumed that citric acid complexes iron or other major cations, thus breaking HS-metal-clay complexes. The soil residue was washed once with Milli-Q water and subjected to NaOH extraction to obtain HA8, following the method of IHSS (Fig. 2.2). Hence the first five HAs and FAs probe the SOM that are loosely bound to the soil mineral and thus can be more easily released under alkaline/acid extraction conditions. Glycerol has the ability of penetrating into the interlayers of the phyllosilicates and thus releasing any HS still trapped in the interlayers; while combined citric acid-alkaline extraction was to release the HA that is more strongly fixed in the organic matter-mineral complexes.

### 2.3.3 Extraction of water extractable colloid (WEC)

The procedure use for collecting water extractable colloid (WEC) is diagramed in Fig. 2.2. After the removal of the undecomposed leaves and roots, a moist soil sampled

from the field was directly applied without drying, in a soil resuspension experiment to mimic the co-release of dissolved organic matter (DOM) and colloidal organic matter (COM) and radioiodine during a storm runoff event.  In order to investigate the yield of WEC based on the dry soil weight and make the radioiodine data comparable among bulk soil, HA, FA and WEC, the ratio of weight of oven-dried soil to that of original damp soil was calculated in a preliminary experiment. Moist soil was dispersed in 20 L artificial freshwater (ionic strength: ~1.7 mM) (Martin and Whitfield, 1983) to reach a final concentration of 5 g-dry soil/ L and shaken very gently at 150 rpm on an orbital shaker for three days. Later, the soil resuspension was centrifuged for 30 minutes at $3200 \times g$, and the supernatant was successively filtered through 10 μm and 0.45 μm cartridge filters. Filtration was followed by cross-flow ultrafiltration, utilizing a spiral-wound 1kDa SOC 1812 cartridge (Separation Engineering, Inc.), until 1L retentate remained.  The retentate was diafiltered against 20 L Milli-Q until it was concentrated to 1 L.  Then, the cartridge was rinsed with 250 mL Milli-Q water with the pump on for 30 min, and then the pump was turned off. The cartridge was allowed to soak for four hours or more.  The cartridge was consequently rinsed with another 250 mL of Milli-Q water, and the procedure was repeated twice or more until the rinse water became clear. The retentate and rinse solution were then subsequently combined and concentrated utilizing an Amicon 8400 stirred-cell ultrafiltration unit with a 1 kDa regenerated cellulose filter at 275 kPa.  The retentate was freeze-dried for further radioiodine analysis and chemical characterization (Xu et al., 2008).

## 2.3.4 Analysis of $^{127}$I and $^{129}$I

The determination of total iodine ($^{127}$I and $^{129}$I) in soils, HS and WEC followed the procedure of Zhang et al. (2010). Solid samples (~ 5 mg for soil and ~ 2.5 mg for HS and WEC) were covered with 150 mg of vanadium pentoxide ($V_2O_5$), which acted as a catalyst for rapid combustion, and were placed in a porcelain boat. $^{125}$I was added to the sample-$V_2O_5$ mixture as a tracer for the pyrolysis recovery. The boat with the sample and catalyst was gently pushed into the center of a quartz combustion tube and subjected to combustion on a tube furnace (Lindberg/Blue M Mini-Mite, Thermo Scientific). The temperature of the furnace was programmed as follows: the temperature was increased to 300 °C within one minute and then held constant for three minutes. After that, the temperature was increased to 850 °C over ten minutes and left there for an additional five minutes. In order to increase the combustion recovery, humid and warm oxygen gas (85 °C) was used as carrier gas at a constant flow rate of 113mL/min during the whole program. The iodine released by pyrolysis was collected into a pyrex glass tube containing 2 mL of Milli-Q water.  After the pyrolysis program was finished, carrier gas was switched from oxygen to nitrogen at a flow rate of 134 mL/min and allowed to purge the receiving water for 40 minutes. Total iodine was measured by Finnigan Trace GC and Polaris Q EI-MS from Thermo, after being derivatized to iodinated N, N-dimethylaniline. The receiving solution after the combustion step for each sample was split into two aliquots and iodate standard (final concentration: 5 ppb) was intentionally added to one aliquot to calculate the recovery rate of the derivatization step, thus eliminating any matrix interferences that might vary from sample to sample. Duplicate

(or replicate) solid samples were weighed, combusted and measured for iodine contents, and errors were well within 10%. Quantification of $^{127}$I and $^{129}$I was based on the different masses of their respective derivatives in the mass spectrum, which were used as the "screening filter" to distinguish their respective responses in the gas chromatograms.

**2.3.5 Chemical characterization of HA, FA and WEC**

The C, H and N contents of the original soil, and all HA, FA and WEC samples were determined with a Perkin Elmer CHNS 2400 analyzer. Acetanilide (71.09% C, 6.71% H, 10.36% N) was used as an analytical standard. Soils and WEC were acidified overnight under concentrated HCl fumes to remove inorganic C and then transferred to a 60 °C oven to remove the acid fumes. The HA/FA samples were previously determined to barely contain any inorganic carbon (due to the extensive HF digestion) and were therefore run without acidification. Ash content was determined after igniting the samples at 550 °C in a muffle furnace (Thermolyne 30400, Thermo Scientific, USA) for 24 hours.

Aromaticity, as defined as the peak area in the 110-160 ppm chemical shift band of quantitative $^{13}$C-NMR spectra, was estimated according to its distinct relationship with UV absorbance (Chin et al., 1994). Briefly, freeze-dried samples were re-dissolved in a phosphate buffer and passed through a 0.45 μm syringe filter. Total organic carbon was determined using a Shimadzu TOC-5000 analyzer and the errors of duplicate samples were <3%. UV absorbance (280nm) was determined using a Turner spectrometer, with the error well below 5% for duplicate measurements. Absorptivity (L/mole of OC/cm)

of eight IHSS humic substances was determined the same way and plotted against their aromaticity, which was obtained from IHSS website and determined by $^{13}$C-NMR. The resulting calibration equation (y=0.0694x-4.8619, $R^2$=0.97, n=7, x and y denote absorptivity and aromaticity, respectively) was used to estimate the sample aromaticity from its molar absorptivity. This UV spectroscopy estimated aromaticity was briefly named "aromaticity" below for the sake of brevity.

For total carbohydrate concentration analysis, the HA, FA and WEC samples were hydrolyzed with 0.1 N HCl at 120 °C for three hours (Xu et al., 2008) and the hydrolysable polysaccharides were determined applying the TPTZ (2, 4, 6-tripyridyl-s-triazine, Sigma) method (Hung et al., 2001), using glucose as the standard. Aliquots of the hydrolyzed solution were used for determination of uronic acid (glucuronic acid, mannuronic acid and galacturonic acid) with a HPLC procedure, using a CarboPac PA10-4 mm column (4 × 250 mm), an electrochemical detector with a gold working electrode, and an ISAAC reference electrode (Zhang et al., 2008).

Amino acids were analyzed by reverse-phase HPLC, using a modified pre-column O-phthaldialdehyde (OPA) derivatization technique (Duan and Bianchi, 2007). Briefly, a sample was mixed with 2 mL 6 N HCl (containing 0.5% phenol) was added, purged with $N_2$, sealed in a 10 mL glass ampoule, and hydrolyzed at 110 °C for 24 h. Then the hydrolysis solution was dried under a $N_2$ stream and the residue was re-dissolved in Milli-Q water. Before injection, the sample was filtered through a 0.2 μm sterile syringe filter. Then 20 μL of sample was mixed with 100 μL of OPA solution and vortexed for 2 minutes. Finally, 40 μL of the mixture was injected into an Alltech Alltima C18 column

(5 μm, 250 × 4.6 mm) at a flow rate of 0.80 mL/min using a Waters HPLC system,

consisting of a 600S gradient controller, a 626 non-metallic pump, a 200 μL sample

loop, a 717-plus autosampler coupled with a 474 scanning fluorescence detector

(excitation wavelength: 330 nm; emission wavelength: 418 nm). A binary gradient of

0.05 M sodium acetate with 5% tetrahydrofuran (pH adjusted to 5.5 with acetic acid)

(eluant A) and 80% HPLC grade methanol (eluant B) was used. The gradient began at

time zero with 30% B, ramped to 70% within 40 min and finally to 100% B at

60 minutes, where it remained isocratic for another 15 min. Then eluant B was decreased

to 30% and held for 15 minutes to re-equilibrate the column before the next injection.

Individual amino acids were identified and quantified on the basis of 17 individual

standards (Sigma).

### 2.3.6 Molecular weight distribution

The fractions of HA, FA, and WEC were dissolved in 0.05M Tris HCl /0.02M KCl

buffer at a concentration of 1mg/mL (Franke et al., 2004).  Samples were then allowed

to equilibrate overnight before being passed through a 0.2 μm syringe filter.  The

molecular weight distribution for the fractions was then determined using size exclusion

chromatography (SEC) on a Waters High Performance Liquid Chromatographic (HPLC)

system, using Waters Empower™ 2 software to operate, acquire, and integrate all

chromatograms.  The Waters System components used in this analysis are a 600S

gradient controller, a 626 non-metallic pump, a 200 μL sample loop, a 717-plus

autosampler, a 2417 refractive index (RI) detector. The RI detector was set at a

temperature of 30°C and a sensitivity of 4. The mobile phase was a solution of 0.05M

Tris HCl/ 0.02M KCl, maintained at a flow rate of 0.5 mL/min through Tosoh

Biosciences guard and analytical columns G3000 PWxl, 6 mm x 4 cm and 7.8 mm x 30

cm, respectively, particle size 7 μm. The injection volume was 150 μL.  Polystyrene

sulfonate molecular weight standards of 1.6, 4.3, 8, and 35 kDa, from Polysciences, Inc.,

were used to calibrate the samples.  These standard solutions were prepared in the same

manner and were run in series with the samples. The logarithm of the molecular weight

(MW) of standards were plotted against their respective retention times and the obtained

equation (y=-0.3183x +5.9554, $R^2$=0.9985, x, y denote retention time and log (MW))

was used to calculate the sample's MW based on its retention time.


**2.3.7 Degree of humification**

Humification is defined as the transformation of macromorphologically identifiable

compounds into amorphous matter or the changes that occur in soil organic matter or

vegetal residues (Piccolo, 2001). Information about the degree of humification, which is

defined here as the concentration of stable free radicals (semiquinone-type), of the

sequential HA and FA is important for gaining a deeper understanding of species

conversion, availability and transportation of radioiodine in the soil. Fluorescence

measurement, by integrating the emission spectrum area between 480-800 nm with 465

nm as the excitation wavelength,  although indirect, has been proven to be the most

reliable method to determine degree of humification of HS, as compared to electron

paramagenetic resonance (EPR) (Rosa et al., 2005). Therefore, high integrated area

indicates high degree of humification. Each HS or WEC sample was dissolved in 0.05 M

NaHCO$_3$ at a concentration of 20.000 mg/L, pH ~ 8.0. Samples were placed on an

orbital shaker in the dark overnight to achieve equilibrium and better dissolution. A

Shimadzu RF-5301 Spectrofluorophotometer was used with a medium scanning speed,

1.0 nm sampling interval, and 5 nm for both excitation and emission slit widths. The

shutter was set to auto mode, to protect the sample from photo-bleaching.

**2.3.8 Attenuated Total Reflectance Fourier Transform Infrared (ATR-FTIR)**

**Spectroscopy**

A Varian 3100 FTIR was accessorized with a three-reflection ATR crystal plate from

PIKE Technologies, Inc. (Madison, WI). A diamond plate was used as the internal

reflection element. Freeze-dried material was mounted at the surface of the diamond.

Close contact with the diamond surface to achieve the greatest sampling sensitivity was

accomplished by use of a pressure clamp. ATR-FTIR spectra employed the spectrum of

a clean diamond as the background, which was auto-subtracted from the spectra of the

sample. A sensitivity of 8, a resolution of 8 cm$^{-1}$, and a total scan of 50 were applied (Xu

et al., 2008). The absorbance spectrum from 650 to 4000 cm$^{-1}$ was collected. Spectra

were baseline corrected and submitted to a 5-point S-G quad-cubic function as the

smoothing filter (Savitzki and Golay, 1964). Bands within 2000-2400 cm$^{-1}$ were caused

by the interferences of the diamond interface, as stated in the manufacturer's

instructions. In order to enhance spectral resolution caused by peak overlapping or

broadening, band identification and integration were performed on the second derivative of the corresponding spectrum.

**2.3.9 Relative mobility of HA, FA and WEC as assessed by hydrophobic interaction chromatography (HIC)**

HIC is a technique to measure the distribution of solvent accessible hydrophobic patches (i.e., the exposed hydrophobic area) of complex three dimensional macromolecules, through the HPLC system coupled with two sequential octyl-Sepharose fast flow columns (Amersham, 0.7 ×2.5 cm; column volume: 1mL). Normal measurements employ higher salt concentrations (2.5-0.5 M), which is not realistic for soil solutions. In order to investigate the relative mobility of different HS and WEC under ambient ionic strength, isocratic runs were performed using 3 mM $(NH_4)_2SO_4$ as the eluting buffer, at a flow rate of 0.4 mL/min, and a Waters dual $\lambda$ absorbance spectrophotometer ($\lambda_1$=214 nm, $\lambda_2$=280 nm) as the detector. Samples were dissolved in the same buffer and shaken overnight in the dark for equilibrium and better dissolution. Retention times (RT) of different HS and WEC fractions indicates the combined effects of electrostatic interaction and hydrophobic adsorption with the ligand of the column polymer matrix control column mobility.

**2.3.10 Statistical analysis**

Data were first tested for normality using the Kolmogorov-Smirnov test ($\alpha$=0.05), in SPSS 11.0 (SPSS Inc., Chicago, IL 60606). Normally distributed data were further tested for a significant correlation using two-tailed, bivariate Pearson analysis ($\alpha$=0.05).

## 2.4 Results

### 2.4.1 [127]I and [129]I concentrations in HA, FA and WEC

Some clear trends in [127]I and [129]I distribution were noted in the various extractions and the WEC (Table 2.1). The yields of HAs resulted in concentrations that were one or two orders of magnitude greater than those of FA or WEC. Very limited amounts of FA were obtained for the second extraction of 4Mile Creek soil (uncontaminated site), thus the extraction was not performed for the later steps. However, even though FSI18 (contaminated site) soil was extracted five times for FA, the extracts after the second one were barely enough for all the analysis. WEC released by soil resuspension with synthetic fresh water accounted for 0.2-0.5% of the total soil weight and 0.4-0.7% of the total soil OC.

Table 2.1 [127]I and [129]I concentrations and [129]I /[127]I ratios of humic acid (HA), fulvic aci (FA) and water extractable colloid (WEC) in 4Mile Creek and FSI18 soils (HA1-HA5, alkaline extraction; HA6-HA7, glycerol extraction; HA8, citric acid-alkaline extraction).

| | 4Mile Creek [a] | | FSI18 | | | |
|---|---|---|---|---|---|---|
| | Yield (%, g-C in sample/g-C in soil) | [127]I/C (μg/g-C) | Yield (%, g-C in sample/g-C in soil) | [127]I/C (μg/g-C) | [129]I/C (μg/g-C) | [129]I /[127]I |
| HA1 | 25.7 | 70.13 | 16.5 | 112.30 | 6.74 | 0.059 |
| HA2 | 12.8 | 30.20 | 8.7 | 78.29 | 4.93 | 0.065 |
| HA3 | 5.7 | 27.57 | 3.0 | 61.85 | 4.76 | 0.075 |
| HA4 | 2.8 | 34.14 | 1.6 | 59.10 | 4.53 | 0.076 |
| HA5 | 1.7 | 40.91 | 1.1 | 26.98 | 2.98 | 0.110 |
| HA6 | 1.2 | 17.48 | 1.4 | 26.82 | 1.89 | 0.070 |
| HA7 | 0.5 | 58.10 | 0.4 | 34.23 | 3.69 | 0.106 |
| HA8 | 0.2 | 21.43 | 0.4 | 33.05 | 3.97 | 0.118 |
| FA1+2 | 1.9 | 44.73 | 1.4 | 603.56 | 44.12 | 0.072 |
| FA3+4 | n.d. | n.d. | 0.3 | 518.79 | 32.32 | 0.061 |
| SOIL | 1.0 | 47.70 | 1.0 | 72.85 | 5.55 | 0.074 |
| Mass balance [b] | 52.4 | 56% | 34.8 | 54% | 46% | |
| WEC | 0.4 | 196.27 | 0.7 | 1473.29 | 120.98 | 0.081 |
| Mass balance [c] | | 2% | | 14% | 15% | |

[a] [129]I and [127]I/[129]I of all samples extracted from 4 Mile Creek soil is below the detection limit, thus not displayed here;
[b] mass balance was calculated as sum of all [127]I or [129]I in the HAs and FAs over that in the soil;
[c] mass balance was calculated as sum of all [127]I or [129]I in the WEC over that in the soil; n.d.=not determined.

Each successive extraction of HA recovered lower OC concentrations, following a near-exponential decrease (Fig. 2.3). The first HA fraction amounted to 48-49% of the total extracted humic substances, on an organic carbon-normalized basis. The total extracted HA and FA fractions consisted of 34.8-52.4% of the total soil organic carbon (Table 2.1).
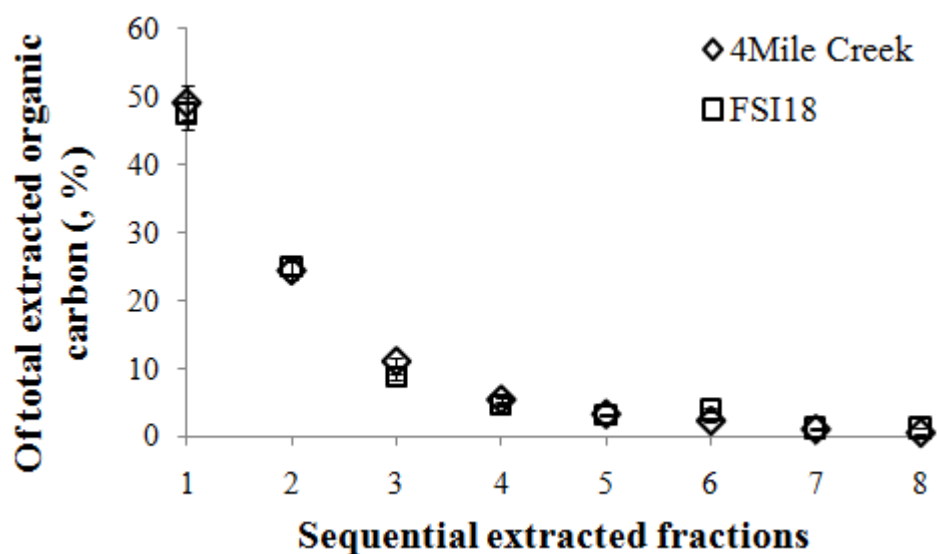
Fig. 2.3 Yield of humic acids (HAs) from sequential extraction experiments of surface soils from 4Mile Creek and FSI18 (HA1-HA5, alkaline extraction; HA6-HA7, glycerol extraction; HA8, citric acid-alkaline extraction).

Not surprisingly, the $^{129}$I concentrations in the uncontaminated soil sample, 4Mile Creek was below detection limits (0.5 pCi-$^{129}$I/g-soils or 3 ng-$^{129}$I/g-soils). $^{127}$I concentrations of HAs in this sample did not show a clear trend overall. For the contaminated soil sample (FSI18 soil), $^{127}$I and $^{129}$I concentrations of HAs generally decreased with each alkaline extraction but increased slightly in the later glycerol and citric acid-alkaline extractions, in particular, when iodine concentrations were normalized to organic carbon (OC) to correct for compositional differences (Fig. 2.4a). It is interesting to observe that in FSI18 soil, FA and WEC contained a much higher content of iodine to OC ratios than HA (Table 2.1). Furthermore, $^{129}$I/$^{127}$I ratios generally increased with each extraction suggesting that the anthropogenic $^{129}$I had not come to steady state with the stable $^{127}$I (Fig. 2.4b). In the contaminated soil resuspension

experiment with artificial freshwater (Section 3.3), there was no detectable organo-iodine found in the permeate (<1kDa) of the soil resuspension solution, where I⁻ and $IO_3^-$ were 162 and 273 μg-I/g-C, respectively. No detectable [129]I of any species (iodide, iodate or organo-iodine) was found in the permeate of the whole FSI18 soil since a large water to solid (200:1) was applied that lead to a dilution effect.
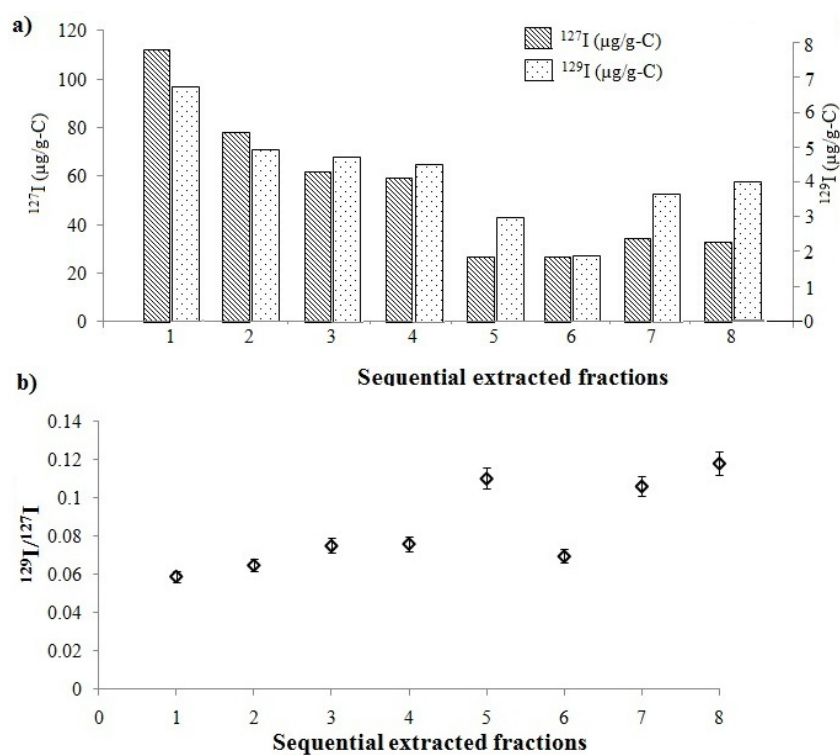


Fig. 2.4 a) FSI18 sample: a) [127]I and [129]I contents in sequentially extracted humic acids (HAs); b) [129]I/[127]I ratios in sequentially extracted HAs.

The elemental composition (C, N and H) results are listed in Table 2.2 for the 4Mile Creek and FSI18 soil samples.  For both sites, OC consistently increased up to the sixth fraction (the first glycerol extract after alkaline extraction, see Section 3.2) and then

decreased slightly in the later two fractions (Fig. 2.5a and b). There was no significant

trend for either H or N, except that the H and N are lower (or at the low end of the range)

for the FA and WEC extracts than for the HA extracts. The change in chemical

composition is also well depicted in C/N and H/C diagrams (Fig. 2.5 c-f). For the HA

fractions, the C/N ratios generally increased for both sites; H/C ratios slightly increase at

first, then decrease for 4Mile Creek, while they keep almost constant for the FSI18 top

soil. For the FA fractions, both the C/N and H/C ratios increased with extraction. WEC

for both stations was elementally different from all the HA and FA fractions. The ash

content accounted for about 5% of the dry weight of HS, but 22% and 39% of the WEC

of 4Mile Creek and FSI18, respectively.

**2.4.2 Aromaticity of HA, FA and WEC**

Aromaticity generally decreased with each extraction, with only a few exceptions

(HA6 and HA7 of 4Mile Creek soil) (Fig. 2.5 g, h and Table 2.2). Aromaticity of HA

was significantly higher than that of FA. WEC contains either a very similar aromatic

content (4Mile Creek) or a little bit lower content (FSI18 soil), compared to that of FA.

Table 2.2 Elemental composition of humic acid (HA), fulvic acid (FA) and water extractable colloid (WEC) of 4Mile Creek and FSI18 and comparison to that of the whole soil (HA1-HA5, alkaline extraction; HA6-HA7, glycerol extraction; HA8, citric acid-alkaline extraction).

| | 4Mile Creek (n=3) | | | | FSI18 (n=3) | | | |
|---|---|---|---|---|---|---|---|---|
| | C% | H% | N% | Aromaticity (%, OC) | C% | H% | N% | Aromaticity (%, OC) |
| HA1[a] | 54.4±0.6 | 5.3±0.2 | 3.1±0.0 | 40 | 54.0±0.1 | 6.3±0.2 | 4.0±0.0 | 30 |
| HA2 | 54.8±0.1 | 5.7±0.1 | 3.5±0.0 | 32 | 54.8±0.3 | 6.7±0.2 | 4.2±0.0 | 29 |
| HA3 | 56.5±0.2 | 6.2±0.0 | 3.3±0.0 | 30 | 55.4±0.6 | 6.6±0.0 | 4.0±0.1 | 25 |
| HA4 | 57.7±0.2 | 6.5±0.0 | 3.2±0.0 | 25 | 57.2±0.7 | 6.7±0.0 | 3.8±0.1 | 18 |
| HA5 | 57.8±0.1 | 6.5±0.1 | 3.1±0.0 | 21 | 57.5±0.1 | 6.6±0.1 | 3.3±0.0 | 22 |
| HA6 | 59.3±0.0 | 6.4±0.1 | 3.1±0.0 | 29 | 60.1±0.3 | 7.1±0.2 | 3.6±0.0 | 22 |
| HA7 | 55.9±0.4 | 5.9±0.1 | 2.6±0.0 | 39 | 59.9±0.1 | 6.9±0.0 | 3.4±0.0 | 19 |
| HA8 | 43.4±1.8 | 3.6±0.3 | 1.4±0.2 | 19 | 57.4±0.3 | 6.4±0.1 | 3.4±0.0 | 18 |
| FA1+2 | 45.1±2.3 | 3.9±0.1 | 1.3±0.1 | 26 | 46.2±0.4 | 4.4±0.1 | 2.3±0.1 | 19 |
| FA3+4 | 38.4±2.8 | 4.2±0.4 | 1.2±0.1 | 23 | 45.8±0.2 | 4.6±0.2 | 2.5±0.0 | 17 |
| FA5+6 | n.d. | n.d. | n.d. | n.d. | 38.7±0.4 | 5.1±0.0 | 1.7±0.0 | 15 |
| FA7+8 | n.d. | n.d. | n.d. | n.d. | 39.9±2.4 | 5.2±0.0 | 1.5±0.1 | 13 |
| FA9+10 | n.d. | n.d. | n.d. | n.d. | 36.0±3.8 | 5.5±0.6 | 1.2±0.2 | 14 |
| WEC | 21.4±2.1 | 3.6±0.2 | 1.6±0.1 | 26 | 34.7±0.4 | 4.6±0.1 | 2.3±0.2 | 16 |
| Whole Soil | 8.5±1.4 | 0.9±0.3 | 0.5±0.1 | n.d. | 24.1±1.1 | 3.14±0.5 | 1.5±0.1 | n.d. |
| Soil residue | 1.8±0.2 | 0.0±0.0 | 0.1±0.0 | n.d. | 10.6±0.2 | 1.3±0.0 | 0.4±0.0 | n.d. |

[a] n.d.=not determined
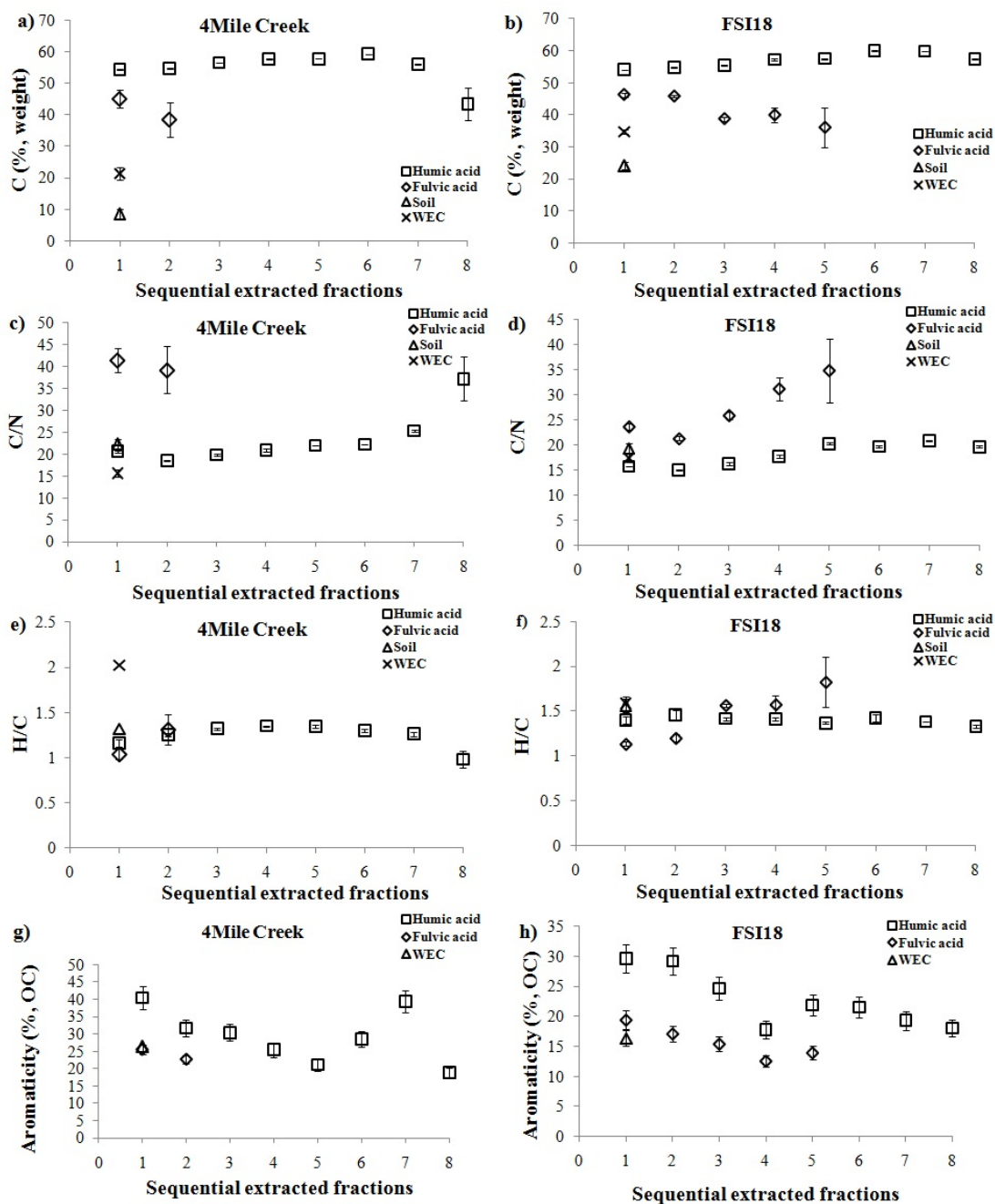
Fig. 2.5  a) OC of different humic acids (HAs), fulvic acids (FAs), soil and water extractable colloid (WEC) for 4Mile Creek; b) OC of samples for FSI18; c) C/N ratios for 4Mile Creek; d) H/C ratios for 4Mile Creek; e) C/N ratios for FSI18; f) H/C ratios for FSI18; g) aromaticity (%, OC) of samples for 4Mile Creek soil; h) aromaticity (%, OC) of samples for FSI18 soil. (HA1-HA5, alkaline extraction; HA6-HA7, glycerol extraction; HA8, citric acid-alkaline extraction).

**2.4.3 Total carbohydrates, uronic acid, and amino acid contents**

The total carbohydrates and uronic acids (the sum of galacturonic acid, glucuronic acid and mannuronic acid) generally decreased with each extraction, except in the last HA extract (HA8), which shows an abrupt increase (Fig. 2.6a, b). FA contains higher amounts of total carbohydrates but lower uronic acids than HA. WEC contains much higher total carbohydrates and uronic acids than the corresponding HAs or FAs from the same soil.

Glutamic acid (Glu), aspartic acid (Asp) and leucine (Leu) were the three dominant amino acids (Fig. 2.6c, d). Total amino acids concentrations stayed fairly constant with some variations ((139.1 ±16.1) mg-C in amino acid/g-C for 4Mile Creek HA and (152.6±27.1) mg-C in amino acid/g-C for FSI18) except the 8th HA of 4Mile Creek (63 mg-C in amino acid/g-C), which had a significant decrease in the total concentration. The two of the 17 amino acids with aromatic functional group, tyrosine and phenylanine, show a relative constant concentration in HAs ((19.1 ± 3.5) mg-C in amino acid/g-C) with extraction step rather than any significant pattern. Nevertheless, aromatic amino acid only accounts for 4.1-13.9% of the total aromaticity for HAs, 2.2-6.1% for FAs, and 6.8-7.0% for WEC, respectively (Table 2.3).
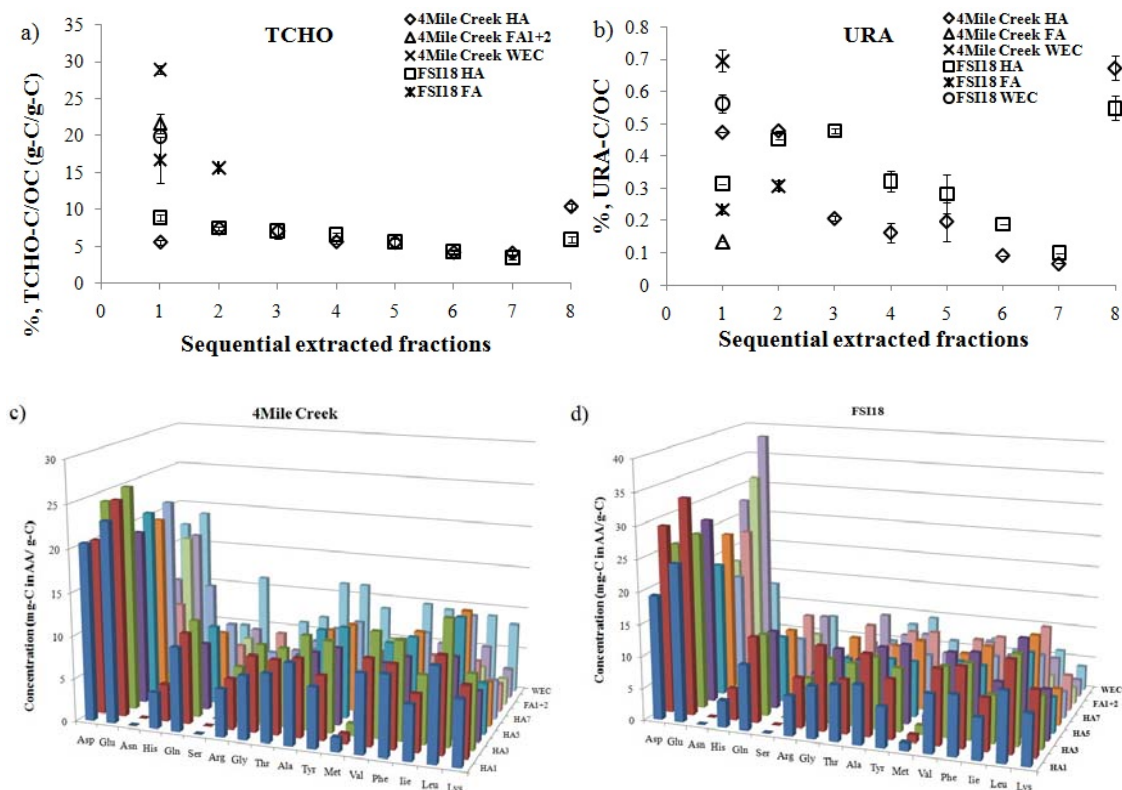
Fig. 2.6 a) Total carbohydrates (TCHO); b) uronic acid (URA) contents (both are normalized to organic carbon) of humic acids (HAs), fulvic acids (FAs) with each extraction and those of water extractable colloid (WEC); c) amino acid composition of samples from 4Mile Creek; d) amino acid composition of samples from FSI18 (Asp: aspatric acid; Glu: glutamic acid; Asn: asparagine; His: histidine; Ser: serine; Gln: glutamine; Arg: arginine; Gly: glycine; Thr: threonine; Ala: alanine; Tyr: tyrosine; Met: methionine; Val: valine; Phe: phenylamine; Iie: isoleucine; Leu: leucine; Lys: lysine; HA1-HA5, alkaline extraction; HA6-HA7, glycerol extraction; HA8, citric acid-alkaline extraction).

Table 2.3 Tyrosine (Tyr), phenylanine (Phe) and total amino acid (AA) concentrations of different humic acid (HA) extracts, fulvic acid (FA) extracts and water extractable colloid (WEC) extracted from the 4Mile Creek sample and the FSI18 sample.

| | 4Mile Creek | | | | | FSI18 | | | | |
|---|---|---|---|---|---|---|---|---|---|---|
| Sample | Tyr | Phe | (Tyr+Phe) | Total AA | (Tyr+Phe)/total aromaticity | Tyr | Phe | (Tyr+Phe) | Total AA | (Tyr+Phe)/total aromaticity |
| | (mg C in AA/g C) | (mg C in AA/g C) | (mg C in AA/g C) | (mg C in AA/g C) | (%) | (mg C in AA/g C) | (mg C in AA/g C) | (mg C in AA/g C) | (mg C in AA/g C) | (%) |
| HA1[a] | 7.0 | 9.4 | 16.39 | 140.1 | 4.05 | 6.3 | 9.3 | 15.61 | 141.5 | 5.27 |
| HA2 | 7.5 | 9.7 | 17.12 | 147.2 | 5.40 | 9.3 | 12.3 | 21.62 | 190.5 | 7.40 |
| HA3 | 10.6 | 11.5 | 22.10 | 169.4 | 7.27 | 9.8 | 11.8 | 21.64 | 173.1 | 8.77 |
| HA4 | 9.0 | 8.9 | 17.91 | 120.2 | 7.05 | 12.4 | 12.3 | 24.73 | 179.9 | 13.90 |
| HA5 | 10.7 | 10.3 | 21.02 | 137.5 | 9.97 | 8.7 | 9.3 | 17.98 | 132.4 | 8.21 |
| HA6 | 10.3 | 10.3 | 20.50 | 125.0 | 7.19 | 11.0 | 11.2 | 22.22 | 148.3 | 10.32 |
| HA7 | 9.8 | 9.4 | 19.22 | 134.5 | 4.88 | 7.7 | 8.6 | 16.29 | 107.9 | 8.43 |
| HA8 | 4.6 | 6.0 | 10.54 | 63.0 | 5.59 | 10.4 | 10.6 | 20.97 | 147.3 | 11.63 |
| FA1+2 | 3.1 | 2.6 | 5.70 | 73.7 | 2.23 | 2.5 | 3.5 | 6.04 | 99.0 | 3.11 |
| FA3+4 | 4.1 | 5.8 | 9.91 | 78.0 | 4.37 | 4.8 | 5.6 | 10.38 | 135.4 | 6.07 |
| FA5+6 | n.d. | n.d. | n.d. | n.d. | n.d. | 5.3 | 5.6 | n.d. | 103.6 | n.d. |
| FA7+8 | n.d. | n.d. | n.d. | n.d. | n.d. | 6.9 | 8.4 | n.d. | 113.4 | n.d. |
| FA9+10 | n.d. | n.d. | n.d. | n.d. | n.d. | 7.3 | 8.1 | n.d. | 110.3 | n.d. |
| WEC | 8.7 | 9.3 | 18.01 | 141.6 | 6.83 | 5.9 | 5.5 | 11.42 | 94.7 | 7.00 |

[a]HA1-HA5, alkaline extraction; HA6-HA7, glycerol extraction; HA8, citric acid-alkaline extraction; n.d.= not determined.

## 2.4.4 Degree of humification

The spectra obtained with excitation at 465 nm are nearly symmetric and the intensity generally decreased with each extraction for HA (Table 2.4, spectra shown in Fig. 2.7). The order of the integrated areas (emission wavelength: 480-800 nm) for 4Mile Creek was:

HA1>HA2>FA1+2>HA3>WEC>HA4>HA5>HA6≈HA7>HA8;

and for FSI18 is:

HA1>WEC>FA1+2>FA3+4>HA2>HA3>HA4>HA5>HA6>HA7≈HA8.
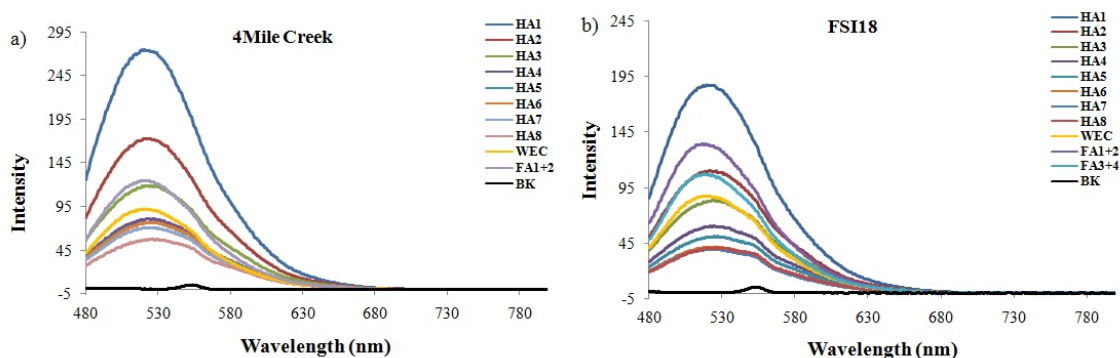


Fig. 2.7 Fluorescence emission spectrum of humic acids (HAs), fulvic acids (FAs) and water extractable colloid (WEC) obtained by excitation at 465 nm a) 4Mile Creek; b) FSI18. BK: blank (0.05 N NaHCO$_3$ solution) (HA1-HA5, alkaline extraction; HA6-HA7, glycerol extraction; HA8, citric acid-alkaline extraction).

Table 2.4 Integrated areas for fluorescence emission spectra (480-800 nm) obtained by excitation at 465 nm and relative aliphatic band area (normalization to amide I band) in the second derivative of ATR-FTIR spectra in humic acids (HAs), fulvic acids (FAs) and water extractable colloid (WEC).

| | 4Mile Creek | | FSI18 | |
|---|---|---|---|---|
| | Fluorescence integrated area | Aliphatic bands (normalized to amide I band) [a] | Fluorescence integrated area | Aliphatic bands (normalized to amide I band) [a] |
| HA1[b] | 11673 | 0.28 | 7993 | 0.20 |
| HA2 | 7229 | 0.61 | 4741 | 0.79 |
| HA3 | 4951 | 0.93 | 3540 | 0.88 |
| HA4 | 3389 | 1.45 | 2562 | 1.00 |
| HA5 | 3206 | 1.58 | 2181 | 1.32 |
| HA6 | 2966 | 1.48 | 1786 | 1.54 |
| HA7 | 2965 | 1.25 | 1652 | 1.86 |
| HA8 | 2426 | 1.19 | 1654 | 0.97 |
| FA1+2 | 5254 | 0.21 | 5573 | 0.25 |
| FA3+4 | n.d. | 0.14 | 4553 | 0.27 |
| FA5+6 | n.d. | n.d. | n.d. | 0.25 |
| FA7+8 | n.d. | n.d. | n.d. | 0.42 |
| FA9+10 | n.d. | n.d. | n.d. | 0.41 |
| WEC | 3890 | 0.24 | 6192 | 0.33 |

[a] Normalization to amide I band provides a relative abundance to sum or amino acids(protein), that remains relatively constant for most HA samples.
[b] HA1-HA5 = alkaline extraction; HA6-HA7 = glycerol extraction; HA8 = citric acid-alkaline extraction; n.d. = not determined; WEC= water extractable colloids.


## 2.4.5 ATR-FTIR spectra

The normal FT-IR spectra of all HA and FA fractions, as well as WEC and the whole

soil for both sites are shown in Fig. 2.8 a and b. Only the representative second

derivative spectrum of WEC extracted from FSI18 soil is shown in Fig. 2.8c and the

expanded region centering at amide I (1646 cm$^{-1}$) is shown in Fig. 2.8d. The band

assignment is shown in Table 2.5. The normal spectra include a very broad band around

3400 cm$^{-1}$ that can be attributed to OH stretching of carboxyl, hydroxyl and phenol

groups. The existence of NH groups (e.g., amino acidic compounds) may also contribute

to this absorption band. Superimposed on this band are doublet peaks between 2917 and

2848 cm$^{-1}$ (symmetric and asymmetric stretching variations of aliphatic C-H in $CH_2$ and

$CH_3$ groups) that increase in absorbance intensity with each extraction (HA1-HA8, see

discussion below). The 1725 and 1710 cm$^{-1}$ bands are more evident for FA fractions than

those of HA fractions, due to the occurrence of more aliphatic esters and carboxylic acid

groups in FA, respectively; whereas in the HA, they became weaker and thus

incorporated into the shoulder of amide I (1646 cm$^{-1}$). While bands between 1650-1600

responsible for aromatic C=C stretching and/or asymmetric C-O stretch in COO- might

overlap with the amide I band, they became well resolved in the second derivative

spectra (Fig. 2.8c and d). Bands between 1150 and 1000 cm$^{-1}$ could be related to C-O

stretching of polysaccharides except that 1033 cm$^{-1}$ caused by silicate impurities was

quite evident for WEC but not for any HA or FA, due to the fact that WEC was not

digested by HF.

Table 2.5 Assignment of ATR-FTIR absorption bands (Artz et al., 2008; Abdulla et al., 2010).

| Band (cm$^{-1}$) | Functional Group | Possible Compounds |
|---|---|---|
| 3600-3000 | OH stretching of carboxyl, hydroxyl and phenol groups and/or NH$_2$ in amino acid groups | Polysaccharides, protein and lignin phenol. |
| 2917, 2848 | Aliphatic CH$_3$ and CH$_2$ stretching | Lipids, fats, wax |
| 1729 | C=O stretching of COOR | Fatty esters |
| 1712 | C=O stretching of COOH | Fatty acids |
| 1646-1647 | -C=O stretching (Amide I) | Proteinaceous material |
| 1631 | Aromatic C=C stretching and/or asymmetric C-O stretching in COOR | Fatty esters and/or lignin and other aromatics |
| 1553 | -NH inplane bending and –CN stretching (Amide II) | Proteinaceous material |
| 1516 | Aromatic C=C stretching | Lignin and phenolic backbone |
| 1467 | CH$_3$ asymmetric deformation | Lignin, phenolic and aliphatic structure |
| 1453 | CH$_2$ scissoring | Lipids, fats, wax |
| 1415 | O-H bend in-plane and/or symmetric C-O stretching in COOR | Fatty acids and fatty esters |
| 1247-1206 | C-N amide III vibration or C-O asymmetric stretching of Ar-OH or C-O of aryl ethers and phenols, possibly P-O-aryl | Proteinaceous material or lignin, phenolic structure |
| 1033 | Si-O stretching and Si-O-Si | Clay minerals and silica |
| 1153-1006 | C-O-C and C-O stretching and O-H deformation | polysaccharide |
| 873-728 | C-H out of aromatic ring | Lignin and phenolic structure |
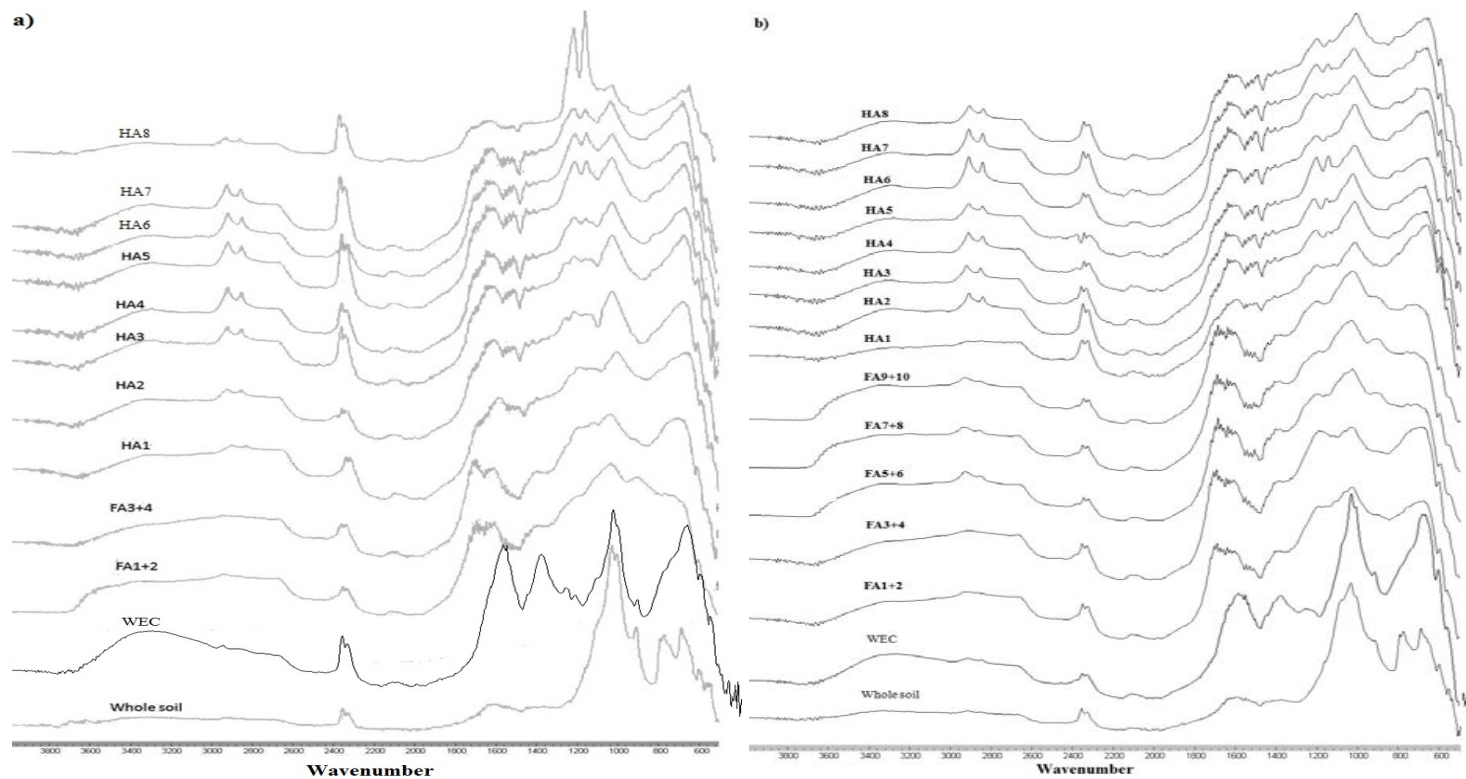
Fig. 2.8 a) ATR-FTIR spectra of humic acids (HAs), fulvic acids (FAs), water extractable colloid (WEC) and the crude soil of 4 Mile Creek; b) FSI18; c) representative second derivative ATR-FTIR spectrum of water extractable colloid from FSI18 soil; d) the zoomed-in spectrum of c) showing the amide I band and band area integration in gray.
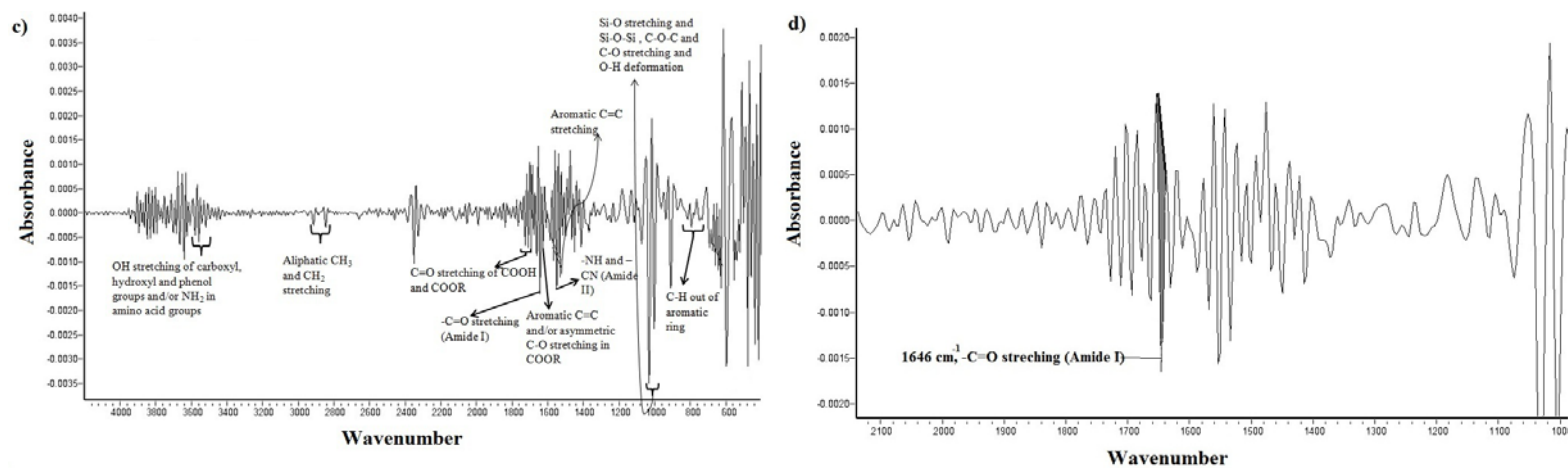
Fig. 2.8 continued.

In this study, ATR-FTIR shows better sensitivity for solid phase samples than samples in liquid form. However, using solid phase samples would make the quantification of the functional groups difficult because it is difficult to quantify how much sample is pressurized on the diamond crystal and out of this how much was actually probed by the penetrating infrared beam, i.e., the true sample size. By normalizing the ATR-FTIR spectra to a common and marked band in the second derivative spectra, e.g., the amide I band, the relative abundance of every functional group can be quantified (Table 2.5). This is based on the fact that the protein content, as represented by the sum of total amino acids independently measured using the HPLC method, was relatively constant for all HAs (Section 4.3, except HA8 of 4Mile Creek).

## 2.4.6 Molecular weight distribution

The chromatograms obtained from HPLC-SEC are shown in Fig. 2.9 a and b for HS and WEC extracted from 4Mile Creek and FSI18 soils. All HA similarly consisted of two fractions, a high molecular weight fraction around 90 kDa and a low molecular weight fraction around 10 kDa; all FA consisted of two subunits, one large-size around 3-4 kDa and the other small-size around 1 kDa. WEC was composed of two subunits, a large-size fraction of 105 kDa and a small-size fraction of about 4 kDa. In order to better illustrate the variations in molecular distribution of all HS, relative peak areas of the two subunits were calculated for each HA or FA. Interestingly, the large-size fraction of the HA appeared progressively more abundant with each alkaline extraction (ranging from 26.9-67.4% for 4Mile Creek and 28.5-75.6% for FSI18) and then followed different

patterns for the later non-NaOH extractions, yet still resulting in a general increase in the average molecular weight (29.8-74.7 kDa for 4Mile Creek and 31.4-78.4 kDa for FSI18). The opposite pattern was observed for FA, of which the 3-4 kDa fraction became less and less abundant with each extraction (Table 2.6).
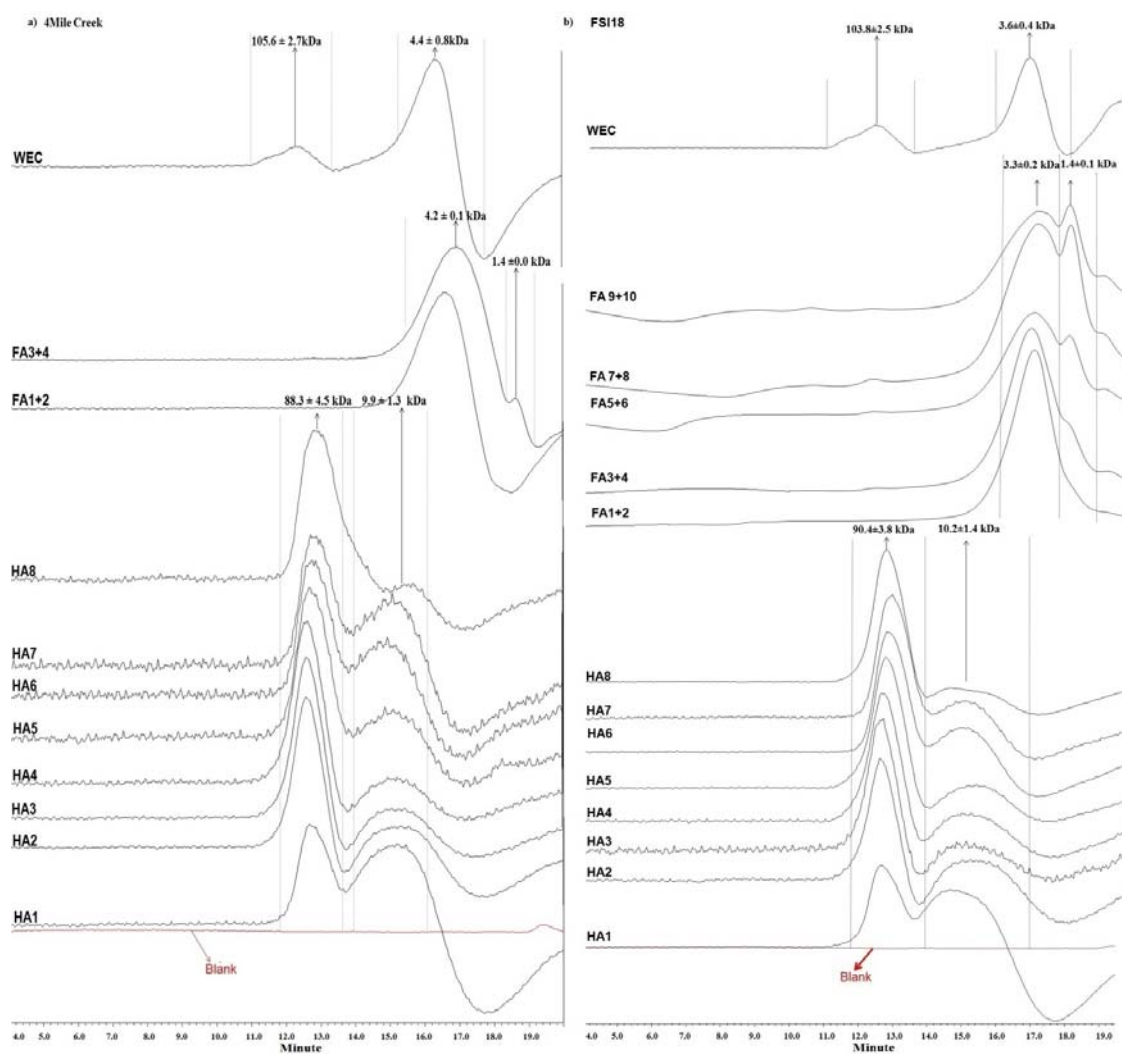


Fig. 2.9 Size exclusion chromatograms of humic acids (HAs), fulvic acids (FAs) and water extractable colloid (WEC) of a) 4Mile Creek; b) FSI18.

## 2.4.7 Relative hydrophobicity of HA, FA and WEC

All hydrophobic interaction chromatograms (HIC) obtained for HA, FA and WEC showed a single peak (Fig. 2.10). Though the change of elution volume was slight due to the small column volume (Fig. 2.11), the difference among samples was significant and reliable as indicated by the extremely low coefficient variation (~0.1%). HA was more and more retarded in HIC with each extraction step, as indicated by the greater elution volume. WEC was eluted either more quickly than its corresponding HA and FA (FSI18) or similar to the first extracts of HA and FA (4Mile Creek).

Table 2.6 Molecular weight distribution of humic acid (HA), fulvic acid (FA) and water extractable colloid (WEC) of SRS soils.

| | 4Mile Creek | | | | | FSI18 | | | | |
| | | Large-size HA | | Small-size HA | | | Large-size HA | | Small-size HA | |
| Extract[a] | Average MW (kDa) | MW (kDa) | Relative peak area (%) | MW (kDa) | Relative peak area (%) | Average MW (kDa) | MW (kDa) | Relative peak area (%) | MW (kDa) | Relative peak area (%) |
|---|---|---|---|---|---|---|---|---|---|---|
| HA1 | 29.8 | 88.1 | 26.9 | 8.3 | 73.1 | 31.4 | 89.2 | 28.5 | 8.3 | 71.5 |
| HA2 | 57.1 | 91.5 | 58.5 | 8.5 | 41.5 | 54.7 | 96.0 | 53.0 | 8.2 | 47.0 |
| HA3 | 67.9 | 93.6 | 69.5 | 9.3 | 30.5 | 66.7 | 93.5 | 68.1 | 9.4 | 31.9 |
| HA4 | 73.2 | 92.5 | 76.4 | 10.9 | 23.6 | 69.4 | 93.6 | 71.0 | 10.4 | 29.0 |
| HA5 | 64.3 | 90.2 | 67.4 | 10.7 | 32.6 | 70.7 | 90.2 | 75.6 | 10.1 | 24.4 |
| HA6 | 51.8 | 84.0 | 55.2 | 12.0 | 44.8 | 61.4 | 86.0 | 67.0 | 11.6 | 33.0 |
| HA7 | 47.2 | 86.0 | 48.8 | 10.2 | 51.2 | 66.4 | 84.9 | 74.6 | 12.2 | 25.4 |
| HA8 | 74.7 | 80.8 | 91.5 | 9.2 | 8.5 | 78.4 | 90.2 | 85.1 | 11.0 | 14.9 |
| FA1+2 | 4.0 | 4.1 | 99.7 | 1.5 | 0.3 | 3.1 | 3.1 | 99.9 | 1.2 | 0.1 |
| FA3+4 | 4.1 | 4.3 | 94.6 | 1.4 | 5.4 | 3.5 | 3.5 | 98.5 | 1.4 | 1.5 |
| FA5+6 | n.d. | n.d. | | n.d. | n.d. | 3.2 | 3.5 | 86.4 | 1.4 | 13.6 |
| FA7+8 | n.d. | n.d. | n.d. | n.d. | n.d. | 2.8 | 3.3 | 75.5 | 1.4 | 24.5 |
| FA9+10 | n.d. | n.d. | n.d. | n.d. | n.d. | 2.7 | 3.2 | 72.2 | 1.4 | 27.8 |
| WEC | 13.5 | 105.6 | 9.0 | 4.4 | 91.0 | 15.0 | 103.8 | 11.3 | 3.6 | 91.2 |

[a] HA1-HA5 = alkaline extraction; HA6-HA7 = glycerol extraction; HA8 = citric acid-alkaline extraction; n.d. = not determined; WEC = water extractable colloids.
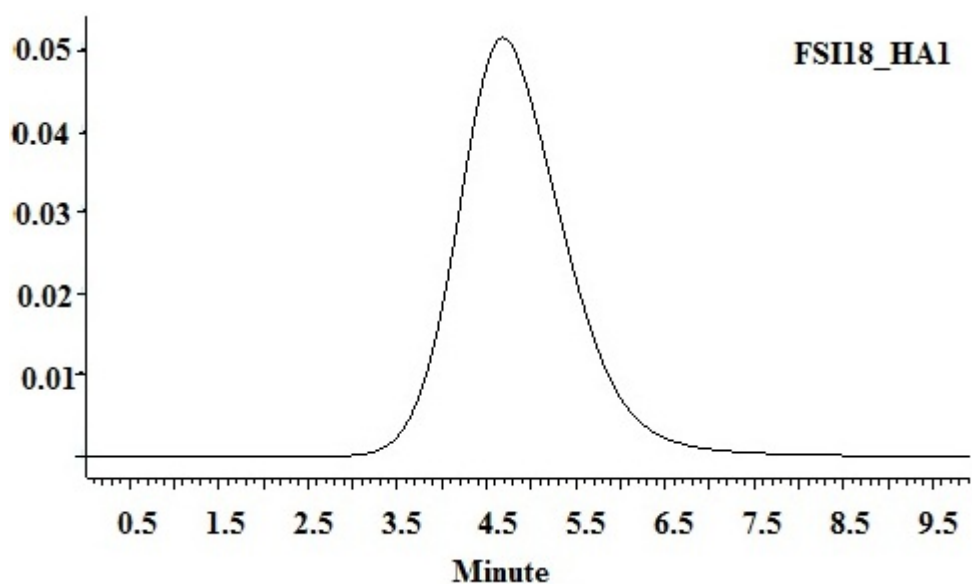
Fig. 2.10 Representative hydrophobic interaction chromatogram for the first HA extract (HA1) from FSI18 soil.
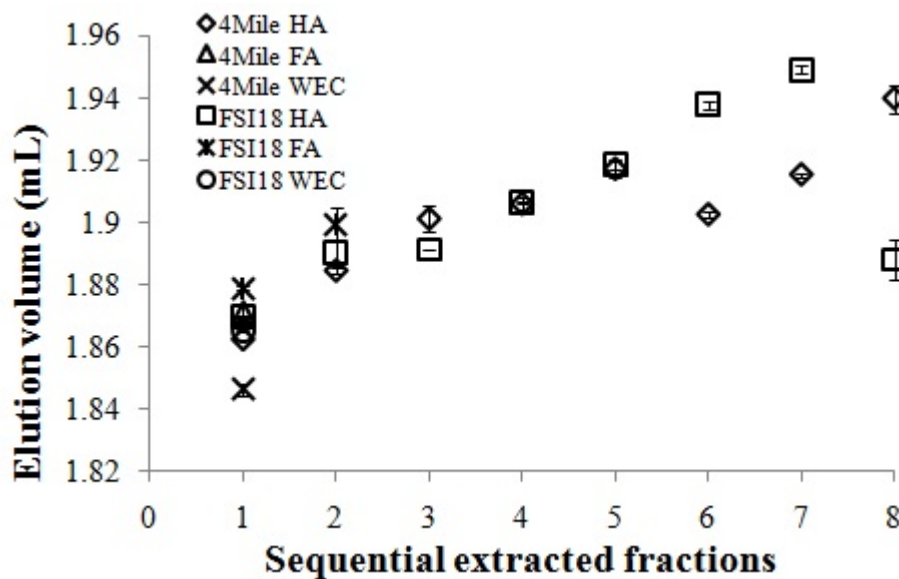


Fig. 2.11 Relative hydrophobicity of humic acids (HAs), fulvic acids (FAs) and water extractable colloid (WEC) extracted from 4Mile Creek and FSI18 soils, as expressed by its elution volume.

**2.5 Discussion**

**2.5.1 Chemical factors affecting the mobility of HS-bound $^{129}$I**

Together these various OC characterization parameters describe a complicated, but generally consistent description of the interaction of the OC with the radioiodine. The eight HA and five FA fractions, extracted based on their different solubility and accessibility to different extractants (i.e., water, NaOH, glycerol, and citric acid), are composed of two subunits of different molecular weight. The small-size fraction (vs. large-size) of HAs and FAs correlated well with a number of chemical parameters. For example, the relative abundance of the small-size fraction of HAs (calculated from peak area of the size exclusion chromatograms, Table 2.6) was found to correlate with their aromaticity, while the abundance of the large-size fraction of FAs shows a good and positive correlation with their aromaticity (Fig. 2.12a and b). Both of the large-size and small-size fractions of FA fell at the low end of the small-size range of HA. Furthermore, these large-size fractions of HAs seem to be more aliphatic, as shown by a significant correlation between their relative abundance and the relative area of aliphatic $CH_3$ and $CH_2$ stretching bands (2917, 2848 cm$^{-1}$), after normalization to amide I bands in the second derivative of the FTIR spectrum (Fig. 2.12c). The two subunits likely represent two end-members: one is large-size and has more aliphatic functional groups, while the other is small-size and contains more aromatic functional groups. As suggested by Li et al. (2003), the small-size and aromatic component is relatively more water soluble and more easily extractable than the large-size and more aliphatic component, with the abundance of the large-size subunit generally increasing with each subsequent

extraction step in the sequential extraction scheme. Therefore the apparent chemical heterogeneities as shown in elemental compositions, aromaticity, fluorescence, FTIR, organo-iodine, isotopic ratios of iodine, etc. might actually be caused by a different combination of these two end-members.

One might argue that the different HAs or FAs obtained by repetitive and sequential extraction could be operational artifacts. However, the single peak shown in the HIC analyses suggests that these two end-members must exist as aggregate or linked to each other by some weak chemical forces such as hydrogen bonds or electrostatic or hydrophobic interactions under environmental conditions (Sutton and Sposito 2005). For example, Allard (2006) found that HA of different origins were similarly composed of two main components: an aliphatic subfraction possibly from cutin- and suberin-derived moieties and an aromatic subfraction from lignin-derived methoxyphenols. Regardless, the order in which these HAs were extracted from alkaline, glycerol (after disruption of the interlayers of the phyllosilicates) and citric acid-alkaline (after disruption of humic acid-metal complexation) solutions indicate their relative mobility, i.e., the later extracts were more strongly trapped in the soil matrix, more difficult to be extracted and thus potentially more immobile. Molecular weight and hydrophobicity are factors that affect their mobility in the environment, of which both showed a general increase (Table 2.6, Fig. 2.9 and Fig. 2.11) with consecutive extractions. The increasing hydrophobicity of the HAs with extraction step might also be caused by the relative enrichment of the less polar (i.e., more aliphatic) and large-size component, as suggested by a strong correlation between their retardation in the hydrophobic interaction column and the

relative area of aliphatic $CH_3$ and $CH_2$ bands in the second derivative of FTIR spectra

(Fig. 2.12d).
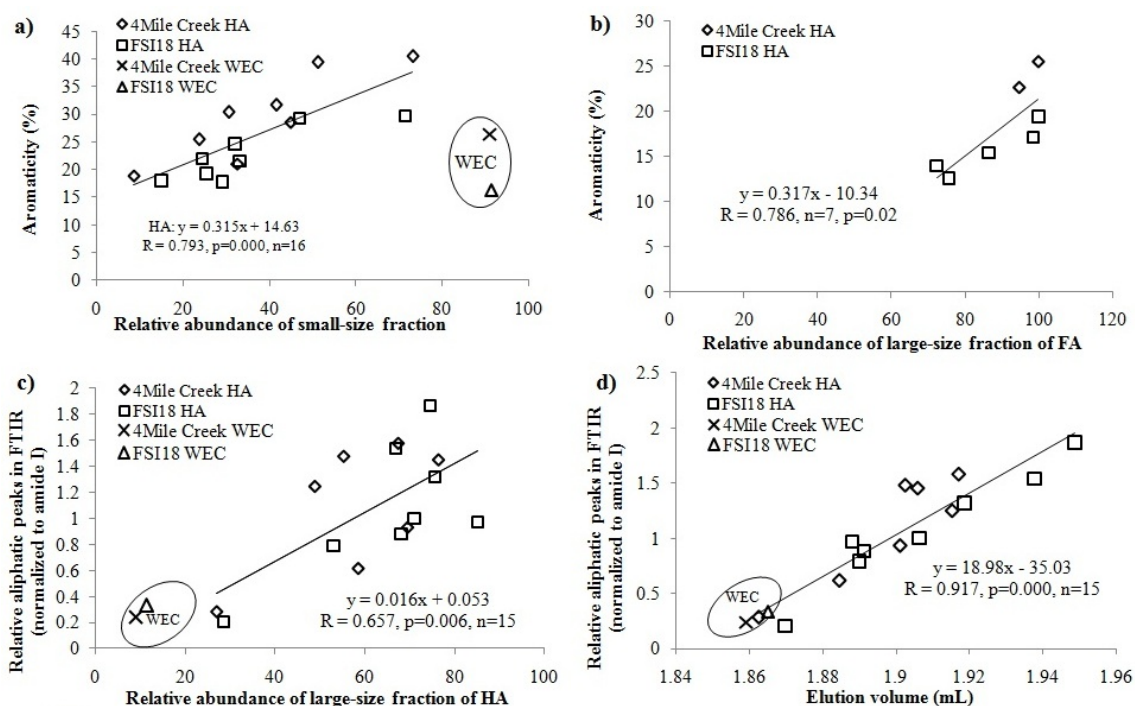


Fig. 2.12 Relationships between a) aromaticity (%, OC) and relative abundance of small-size fractions of humic acids (HAs) and water extractable colloid (WEC); b) aromaticity and relative abundance of large-size fractions of fulvic acids (FAs); c) relative aliphatic bands (normalization to amide I band) in the second derivative of ATR-FTIR spectra and relative abundance of large-size fractions of all HAs except the eighth HA extract of 4Mile Creek (HA8); d) relative aliphatic bands (normalization to amide I band) in the second derivative of ATR-FTIR spectra and the elution volume in hydrophobic interaction chromatography (HIC) of all HAs except HA8 of 4Mile Creek.

Interestingly, total carbohydrates and uronic acids as hydrophilic components in HAs

decrease dramatically with each extraction step (Fig. 2.6a and b), except in the last

extract, which might have been previously complexed with metal ions and got released

together with HA. This further strengthens the case that the later HA extracts are less mobile. FA is more mobile due to its small molecular weight (Table 2.6) and more polar characteristics as shown in the FTIR spectra (Fig. 2.8). This is also the reason why they had been suggested as carriers for trace metals and radionuclides in many soils (Warwick et al., 1993; Fujikawa et al., 1999; Generalova and Onoshko, 2006).

**2.5.2 Importance of soil organic matter as a radioiodine sink**

While there is still some debate on using C/N ratios as an index for humification (Rosa et al., 2005), the observation of an increase in C/N ratios and a decrease in fluorescence of HA with each extraction step agrees well with the fact that humification in the later extracts decreased (Fig. 2.5 c and d, Fig. 2.7 and Table 2.4). A significant positive correlation (Fig. 2.13a, R=0.961, p=0.000, n=8) was found between $^{127}$I content and integrated area of the fluorescence emission spectra (wavelength: 480-800 nm) for HA extracted from FSI18 soil, which was regarded as a reliable index for degree of humification (Section 3.7). Also significant correlation was found between $^{129}$I content and this index of humification (Fig. 2.13a, R=0.859, p=0.003, n=8). An investigation into the relationship between aromaticity and iodine content of HA shows that $^{127}$I contents were well correlated with aromatic functionalities (Fig. 2.13b, R=0.716, p=0.03, n=8 for 4Mile Creek; R=0.778, p=0.001, n=8 for FSI18) while this correlation was not as strong for $^{129}$I (figure not shown, R=0.60, p=0.088, n=8). The abundance of the small-size subunit is positively correlated with the $^{127}$I content of individual HA extracts (Fig. 2.14a). Thus, it is very likely that this small-size subunit is responsible for

the aromaticity and the bonding between aromatic C and iodine, or iodination, of the whole HA while the large-size subunit might affect its mobility. Though the aromatic structure of SOM could develop from its aromatic amino acids (Beyer et al., 1997), the relatively constant and low amount of aromatic amino acids in HAs with each sequential extraction (0.6-2.5% of OC and 4.1-13.9% of total aromaticity, see Table 2.2) suggests that other aromatic moieties (e.g., lignin-phenols) are mainly responsible for iodine binding.
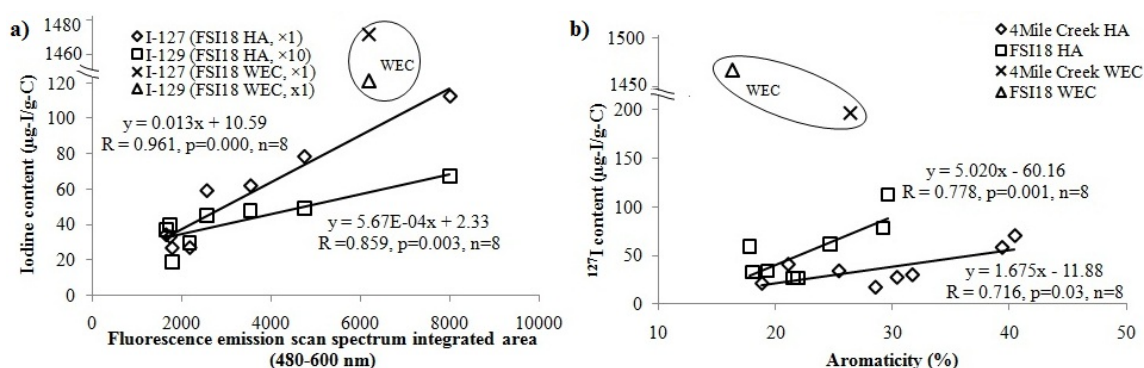


Fig. 2.13 a) Iodine content and fluorescence emission scan spectrum integrated area (480-800 nm) of eight HAs from FSI18 soil; b) $^{127}$I content and aromaticity of HAs and WEC.

A general increase in $^{129}$I/$^{127}$I with each extraction step (Fig. 2.4b) further suggests that these two isotopes have not reached equilibrium between the small-size and large-size subunits of HAs or among the eight HAs of different degree of humification. Surprisingly, a good correlation was found between $^{129}$I/$^{127}$I and the relative abundance of the large-size subunit in HAs (Fig. 2.14b). It is very likely that during recent years of

plant operation (1955-1988) and site remediation efforts during the last decade, iodine of

high $^{129}I/^{127}I$ ratios was intentionally or unintentionally introduced into the F-Area

environment through atmospheric deposition, pond water infiltration into groundwater,

and surface runoff, and continuously incorporated into the aromatic functional groups of

SOM.
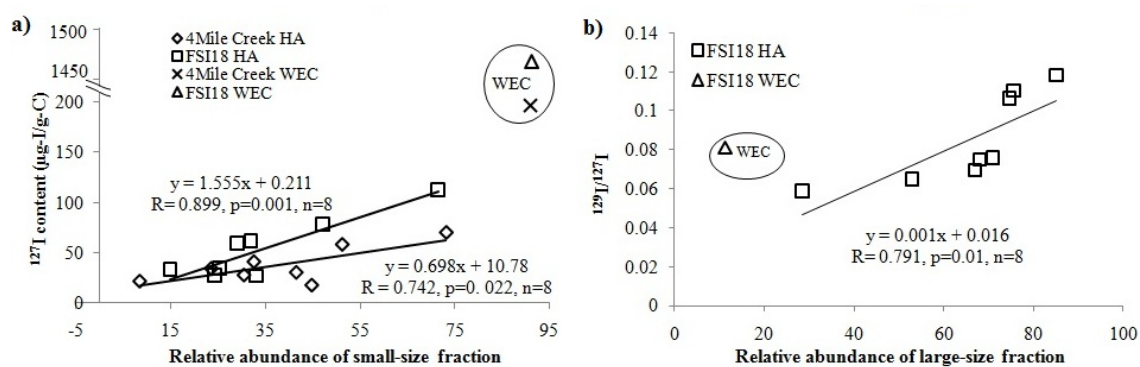


Fig. 2.14 a) $^{127}I$ contents and relative abundance of small-size fractions in HAs and
WEC; b) $^{129}I/^{127}I$ and relative abundance of large-size fractions of eight HAs from FSI18
(all correlations shown in the subplots are only for HAs).

Soil organic macromolecules also show increased degree of humification with time

as well as increased condensation conventionally assumed to produce more

polycondensated aromatic-ring structures (Hatcher and Spiker, 1988) that contain a

lower amount of aromatic C potentially available for iodination. This would have

decreased the possibility of iodination for recently input of iodine with high $^{129}I/^{127}I$, and

could have produced lower $^{129}I/^{127}I$ ratios, thus resulting in a decrease of this isotopic

ratio with an increase in the degree of humification. This is consistent with the theory

that iodination of organic matter occurs during an early stage of humification of fresh plant material (Keppler et al., 2004) and the observation by Price and Calvert (1977) that iodine is mostly associated with labile organic matter. Thus changes in $^{127}$I contents in different HA fractions of the same site are likely the result of changes in degree of humification rather than changes in the input whereas changes in $^{129}$I content are caused by both degree of humification and anthropogenic inputs.

Though FAs contain less aromatic functional groups than HA (Fig. 2.5g and h, Table 2.2), their iodine content is five to seven times higher than their corresponding HAs and 10 times higher than the rest of HAs in the case of FSI18. For FA1+2 extract of 4Mile Creek, the iodine content is much higher than that for HAs, except for HA1 and HA7 (Table 2.1). The iodine content and chemical composition in the later FA extracts were not measured due to limited sample amounts. Moulin et al. (2001) demonstrated that the optimal pH for iodination of FA was close to neutral. Besides, they also observed that iodinated FA was quite stable over a wide pH range through the comparison of their electrospray ionization (ESI) mass spectra. One mechanism to explain the higher iodine content of FA over that of HA is the smaller molecular masses of FAs in comparison to those of HAs, increased their accessibility to ions, and possibly resulted in higher iodination in the natural environment (Warner et al., 2000). This is also consistent with the observation of generally decreasing iodine content in HAs as their average molecular weight increased in this study. Another hypothetical mechanism is that FA contains more preferred sites for iodination, which depend on the combined electronic and steric effects of the aromatic ring substituents. For example, Rice and MacCarthy (1992) found

that in comparison to their corresponding HAs, FAs extracted from a peat and a stream

sediment sample contained more hydroxyl substituents, which are strongly activating

and *ortho*- and *para*-directing for iodination (Moulin et al., 2001). However, in

laboratory iodination experiments at elevated iodine concentrations (4.5-100 ppm),

higher iodination was observed for HA compared to the FA from a same origin (Reiller

et al., 2006). Even though HAs had a lower specific activity for radioiodine than FAs,

they are still regarded as the dominant pool for iodine fixation, due to the fact that HAs

had much greater yields than FAs (Table 2.1). Iodinated HS is quite stable, as the C-I

bond may only be broken by strong nucleophiles (e.g., dissolved sulfides or

thiosulfates). In addition, replacement of iodine only occurs in the presence of stronger

electrophiles (e.g., in the abiotic condition), thus little release of inorganic iodine should

be expected (Schlegel et al., 2006). The stability of iodinated HA and FA was also

supported in other studies (Carlsen et al., 1992; Moulin et al., 2001; Yamaguchi et al.,

2010). Therefore it is not likely that the employed extraction method would artificially

alter either the chemical characteristics or iodine distribution of the HS.

A mass balance calculation conducted by adding up all $^{127}$I and $^{129}$I contents

contributed by HA and FA and compared to the content in the bulk soil (Table 2.1)

indicates that about 54-56% of $^{127}$I and 46% of $^{129}$I in the soil comes from the extracted

HS, leaving the remainder for the inorganic fraction, or more likely, non-extractable

SOM. Hu et al (2005) suggested that some inorganic iodine ($I^-$ or $IO_3^-$) could be present

by sorption to the mineral phase, which possesses positively charged surfaces. While it

is possible that iodine (likely as iodate) can be trapped in the mineral pool such as

carbonate (Claret et al., 2010), this is not the case for the soils of this study, since barely any inorganic carbon was detected based on the difference between the total carbon and total organic carbon of the whole soils. Other minerals (quartz, kaolinite, goethite, etc.) cannot explain this missing part due to their low iodine partitioning coefficients (Kd) (usually <10 $cm^3$/g for $I^-$ and 1-1000 $cm^3$/g for $IO_3^-$) (Hu et al, 2007, Denham et al., 2009 and reference therein). Rather, the fact that the soil residue of 4 Mile Creek and FSI18 still contains 1.8% and 10.6% of organic carbon (Table 2.2) after the 8th extractions, compared to 8.5% and 24.1% of the total organic carbon in the initial whole soils, respectively, can be taken as a sign that iodine was very likely bound to the soil organic matter fraction that was not easily extractable in the methods we used, such as humin (Wang and Xing, 2005). Though the $^{129}I$ content in the 4Mile Creek soil is below the detection limit of our experimental method (0.5 pCi-$^{129}I$/g), taking a $^{129}I$/$^{127}I$ ratio of $10^{-10}$ (Santschi and Schwehr, 2004; Hou et al., 2009) as a representative value for the terrestrial environment, $^{129}I$ values would be about $10^8$ times more enriched in the FSI18 soil. While site remediation work is still ongoing, and different engineering materials (e.g., AgCl) are investigated in an effort to retard the transport of iodine (Denham et al., 2009), it is believed that the high SOM content in the plume soil around the F-Area might be a natural barrier to prevent further radioiodine migration.

**2.5.3 Colloidal organic macromolecules as a radioiodine source**

The WEC samples were collected to provide a measure of the water extractable

organic colloid fraction from the soil.  This fraction is only potentially mobile in this

system, as it reflects an operationally defined upper limit of the water-extractable

fraction in that the experimental procedure shakes the soil-water suspension prior to

extraction of the organic colloids. The introduction of kinetic energy only occurs in the

surface soils, and as such, less organic colloid may be expected in subsurface soils or

groundwater sediments. A high liquid to solid ratio (200:1) was applied in this study.

Fukui et al. (1996) suggested that different liquid to solid ratios can lead to different

partitioning coefficients (Kd) of iodine species, which is beyond the scope of this study.

Nevertheless, the intent was to extract all the potentially mobile soil colloids, which are

not necessarily leached into solution at any one time, but probably and potentially

leached out under the influence of soil erosion forces such as stormwater, surface runoff,

groundwater exifiltration, high winds, etc. in a long term, and thus it serves to provide

insight into the potential mobility of associated radioiodine. Iodine in the form of $IO_3^-$ is

more retarded and behaves very differently as indicated by elevated $K_d$ values (1-1000

mL/g) (Rechard, 1995; Kaplan et al., 2000; Schwehr et al., 2009; Kaplan et al., 2011).

The reduction of $IO_3^-$ to $I^-$ by SOM or partial convertion to organo-iodine was observed

in recent studies (Steinberg et al., 2008, Yamaguchi et al., 2010; Zhang et al., 2010,

2011). However, very few studies have tracked the chemical characteristics and mobility

of naturally occurring organo-radioiodine. The organic colloid (i.e., WEC) produced to

mimic the release organo-iodine from sediments during storm discharge or surface

runoff events contained highly elevated $^{127}$I and/or $^{129}$I compared to resident HAs or FAs from both soils (Table 2.1). WEC accounted for 14-15% of the total organo-iodine in the contaminated soil, though it only contained 16% of aromatic carbon, which is considerably lower than its corresponding HAs or FAs. Another notable fact is that WEC only accounts for <1% of the total OC in the soil (Section 4.1 and Table 2.1). Thus, the iodine in macromolecular colloids (WEC) is not only controlled by its aromaticity but also by the number of aromatic C sites that are available for iodination (e.g., its degree of humification) and its hydrophilicity, as is evident by the different relationships between aromaticity and iodine content among FAs, HAs and WEC, while each correlation among the different HAs of the same site was highly significant.

There are several features that could help WEC get re-mobilized from the soil: 1) it has a relatively small average molecular weight (13.5-15 kDa); 2) it contains less aliphatic functionalities as is evident from their small aliphatic to amide I ratios in FTIR spectra (Table 2.4); and 3) it contains much higher hydrophilic components (total carbohydrates and uronic acids, Fig. 2.6a and b).

In order to estimate the potential radioiodine discharge from the soil during a storm event based on the soil resuspension experiment, a calculation was carried out using the data from Table 2.1 as follows: $^{129}$I concentration in WEC ($1.2 \times 10^{-4}$ g-I/g-C WEC) × yield ($7 \times 10^{-3}$ g-C WEC/ g-C soil) × soil carbon content (0.24 g-C/g-soil) × soil to water ratio (5 g-soil/L) × $^{129}$I specific activity ($1.6 \times 10^{8}$ pCi/g), resulting in about 160 pCi/L of radioiodine, which is well above the MCL of 1pCi/L, regulated by EPA. Based on our detection limit (Zhang et al., 2010), potentially mobile radioiodine in the soil

resuspension solution was mainly in the colloidal organic fraction (~100%). The isotopic ratio of $^{129}$I/$^{127}$I as 0.081 was much higher than recently reported ones (~0.03) in the groundwater of Savannah River Site (Zhang et al., 2010), and organo-$^{129}$I concentrations were about three times higher than the same concentrations in the corresponding groundwater. Moreover, organo-iodine in the groundwater of the Savannah River Site was found to be associated primarily with low molecular weight organic moieties, consistent with the molecular size of the mobile iodine carrier reported here. Therefore, it is very likely that radioiodine in the soil, carried by the amphiphilic colloidal organic marcomolecules and potentially released during storm run-off or surface run-off events, could also infiltrate into the groundwater where it could equilibrate with stable $^{127}$I.

## 2.6 Conclusions

Riparian zone, organic-rich soils in the Savannah River Site have a high capacity to retain and store radioiodine by forming organo-iodine compounds, which could significantly affect the mobility and bioavailability of $^{129}$I in terrestrial ecosystems. For HAs, iodine was mainly associated with a small-size aromatic subunit, while the large-size aliphatic subunit is expected to have a greater impact on the immobilization potential of SOM due to its less polar and more hydrophobic nature. FAs and WEC have lower aromaticity than HAs but contain much higher radioiodine concentrations, suggesting that aromaticity is not the only predictor for potential iodination. Besides, even though there is significant correlation between aromaticity and iodine content for

HAs, this relationship is different from site to site (FSI18 vs. 4Mile Creek) (Fig. 2.12c and 2.14a), and thus, not universal.

A general increase in $^{129}I/^{127}I$ ratios of the different HAs with sequential extraction suggests that radioiodine was not fully equilibrated with its stable counterpart in the natural organic matter, and $^{129}I$ was more readily incorporated into the labile organic matter compounds having a lower degree of humification.

Though a major role of SOM is as a radioiodine scavenger, the sequestration of $^{129}I$ might be temporal and the chance that some of it could be re-mobilized during soil erosion and storm run-off, and seasonal redox changes cannot be overlooked. Unfortunately, $^{129}I$ is considered an extremely toxic substance, as implied by its low MCL of 1 pCi/L, and therefore the remobilization of only trace amounts of $^{129}I$ in the organic colloid form from resuspended contaminated soils can result in groundwater exceeding safe drinking water limits. A better understanding of this iodine organic carrier, which only makes up less than 1% of the total OC but ~15% of the total stable iodine and radioiodine in the soil, by NMR and ESI-MS analysis is warranted for predicting iodine biogeochemical behavior and remediating it in the environment. This study provided quantitative estimates of $^{129}I$ sequestration and potential mobilization in a soil system heavily contaminated by $^{129}I$. In addition, it provided insights into biogeochemical processes and mechanisms affecting the geochemical cycling of terrestrial $^{127}I$ and $^{129}I$ in the environment. Finally, it provided an important basis for risk assessment and site remediation of $^{129}I$ at a contaminated site.

# CHAPTER III

# SEQUESTRATION AND RE-MOBILIZATION OF RADIOIODINE ($^{129}$I) BY SOIL ORGANIC MATTER AND POSSIBLE CONSEQUENCES OF THE REMEDIAL ACTION AT SAVANNAH RIVER SITE

## 3.1 Overview

In order to investigate the distributions and speciation of $^{129}$I (& $^{127}$I) in a contaminated F-Area groundwater plume of the Savannah River Site that cannot be explained by simple transport models, soil resuspension experiments simulating surface runoff or stormflow and erosion events were conducted. Results showed that 72-77% of the newly-introduced I$^-$ or IO$_3^-$ were irreversibly sequestered into the organic-rich riparian soil, while the rest was transformed by the soil into colloidal and truly dissolved organo-iodine, resulting in $^{129}$I remobilization from the soil greatly exceeding the 1 pCi/L drinking water permit. This contradicts the conventional view that only considers I$^-$ or IO$_3^-$ as the mobile forms. Laboratory iodination experiments indicate that iodine likely covalently binds to aromatic structures of the soil organic matter (SOM). Under very acidic conditions, abiotic iodination of SOM was predominant, while under less acidic conditions (pH $\geq$5), microbial enzymatically-assisted iodination of SOM was predominant. The organic-rich soil in the vadose zone of F-Area thus acts primarily as a "sink," but may also behave as a potentially important vector for mobile radioiodine in an on-off "piggy-back" mechanism. Generally the riparian zone provides as a natural attenuation zone that greatly reduces radioiodine release.

## 3.2 Introduction

$^{129}$I has been recognized as a high risk radionuclide in groundwater at most low-level and high-level radionuclide disposal sites, including locations at Savannah River (SRS), Hanford, Idaho, and the former Yucca Mountain Repository (Denham et al., 2009). This high risk stems mainly from its long half-life (16 M years), relatively high mobility, the large inventory in these sites, and its biophilic properties to highly concentrate in human thyroid. Some of these factors have contributed to $^{129}$I having the lowest maximum contaminant level (MCL of 1 pCi L$^{-1}$) in groundwater among all radionuclides.

The F-Area at the SRS was a radionuclide separation facility for the production of nuclear weapons. During production at F-Area between 1955 and 1988, large amounts of radionuclides were disposed in an acidic aqueous form (pH 1.5-4) to an unlined, 27,200 m$^2$, seepage basin. Basin closure activities included adding limestone and blast furnace slag to the basin bottom and then covering it with a low permeability engineered barrier system to reduce groundwater infiltration. Since 2000, a funnel-and-gate groundwater remediation effort has been underway that involves the installation of a low permeability barrier wall and the annual injection of base solution at the "gate" (WSRC-RP-2006-4011, 2006). Below the base injection point, the concentrations of several radionuclides and metals have decreased, including $^{90}$Sr and $^{238}$U.

A key factor that determines the mobility of iodine in the environment is its chemical form. In terrestrial system, iodine mainly exists as iodide (I$^-$), iodate (IO$_3^-$) and organo-iodine (OI), of which the inter-conversion is primarily dependent on a number of factors, e.g., redox potential, pH, the presence of organic matter and/or iron and manganese

oxide, as well as microbial enzymatic activity (Denham et al., 2009). Recent investigations showed that [129]I released from the seepage basin into the adjacent groundwater has increased from 200 pCi/L to 800 pCi/L in 17 years after the site remediation action, while essentially all other radionuclide and metal pollutants have decreased (Kaplan et al., 2010). The increase in groundwater [129]I concentrations are consistent with groundwater pH increase of ~0.7 units over the same period time that could be attributed to the mentioned basin closure activities (Kaplan et al., 2010).

Along a groundwater flow path between the basins and a wetland area ~800 m away, a general increase of pH (from 3.2 to 6.8) and a steady decrease in Eh (< 800 mV) was measured within the contaminant plume, which was coupled with a dramatic change in iodine speciation: significant amounts of iodate (~31%) and organo-iodine (~35%) were found in 12 wells spatially distributed in F-Area (Otosaka et al., 2011). The results from this field speciation study clearly did not support the conventional wisdom that dictates iodide should be the dominant species under these thermodynamic conditions. While it is likely that speciation of iodine is primarily driven by pH changes in this region, such a dramatic (~4-fold) increase in [129]I concentration was surprisingly not observed in the groundwater remediation zone (base-injected area) some 220 and 375 m downgradient from the recharge area, where pH values generally increased by ~1 and ~2 from 1989 to 2010, respectively (Kaplan et al., 2010). Thus immobilization and re-mobilization of iodine species did not seemingly follow a consistent pattern in this region, which adds to the complexity of site remediation action that is attempting to minimize the groundwater flux of multiple contaminants.

Elevated $^{129}$I concentrations should lead to elevated $^{129}$I/$^{127}$I ratios. Indeed, elevated $^{129}$I/$^{127}$I ratios (0.059-0.118) were recently reported in soil organic matter extracted from a contaminated soil of F-Area (Xu et al., 2011a), which were significantly higher than those found in the nearby groundwater (~0.03) (Zhang et al., 2010; Otosaka et al., 2011). $^{129}$I, incorporated into mobile soil organic matter, can enter the groundwater by infiltration or the wetland area downgradient from it through surface run-off or stormflow (Weng et al., 2002), and thus becomes a possible carrier and source of radioactive organo-iodine detected in the groundwater and wetland area. Through batch (Schwehr et al., 2009) and soil column (Zhang et al., 2011) experiments, organo-iodine formation was observed at ambient iodine input concentrations using soils or sediments collected from the contaminated sites. However, little is known about the chemical properties of this organic iodine carrier, the nature of iodine binding to it, and its relevance to iodine mobility. Up to now, except for the studies mentioned above (Schwehr et al., 2009; Zhang et al., 2011), laboratory investigations into the interactions between iodine and soil organic matter (SOM) were mostly carried out at elevated iodine concentrations for experimental convenience or different purposes (Christiansen and Carlsen, 1991; Moulin et al., 2001; Steinberg et al., 2008; Gallard et al., 2009; Yamaguchi et al., 2010).

Therefore, the objectives of our study were to 1) investigate the role of SOM in the F-Area soils and sediments in sequestering radioiodine released from the seepage basins and their potential for re-mobilization during surface runoff or stormflow events; and 2) resolve the multiple factors that control iodine behavior at the contaminated sites,

including pH, organic matter concentration and composition, oxidants (e.g., metal oxides, $H_2O_2$), and microbial enzymatic activity. Our approach was to use a recently developed GC-MS technique to determine the organo-iodine and its isotopic ratios (by simultaneously measuring $^{127}I$ and $^{129}I$) in both aqueous and solid phases (Zhang et al., 2010), which allowed us to compare the behavior of both isotopes in the same experiment. The intent of these studies is to apply the results for risk evaluation and planning of different remediation actions (e.g., base injection) at this DOE site.

## 3.3 Materials and methods

### 3.3.1 Study area and sampling protocols

The selected organic-rich soil sampling sites included site FSI18, in the path of the contaminated plume area, a background site (named "4Mile Creek"), close to the Four Mile Branch, where the contamination is regarded as minimal. A third organic-poor sandy soil was sampled to the north of the F-Area seepage basin (named "N Borrow"), where the surface soil had the same formation as that composed of the aquifer and regarded as "background" (Fig. 3.1). The soil samples were stored and shipped in a zip lock bag under ice and immediately transferred to a refrigerator at 4 °C in the lab. Information on soil composition information is provided in Table 3.1.
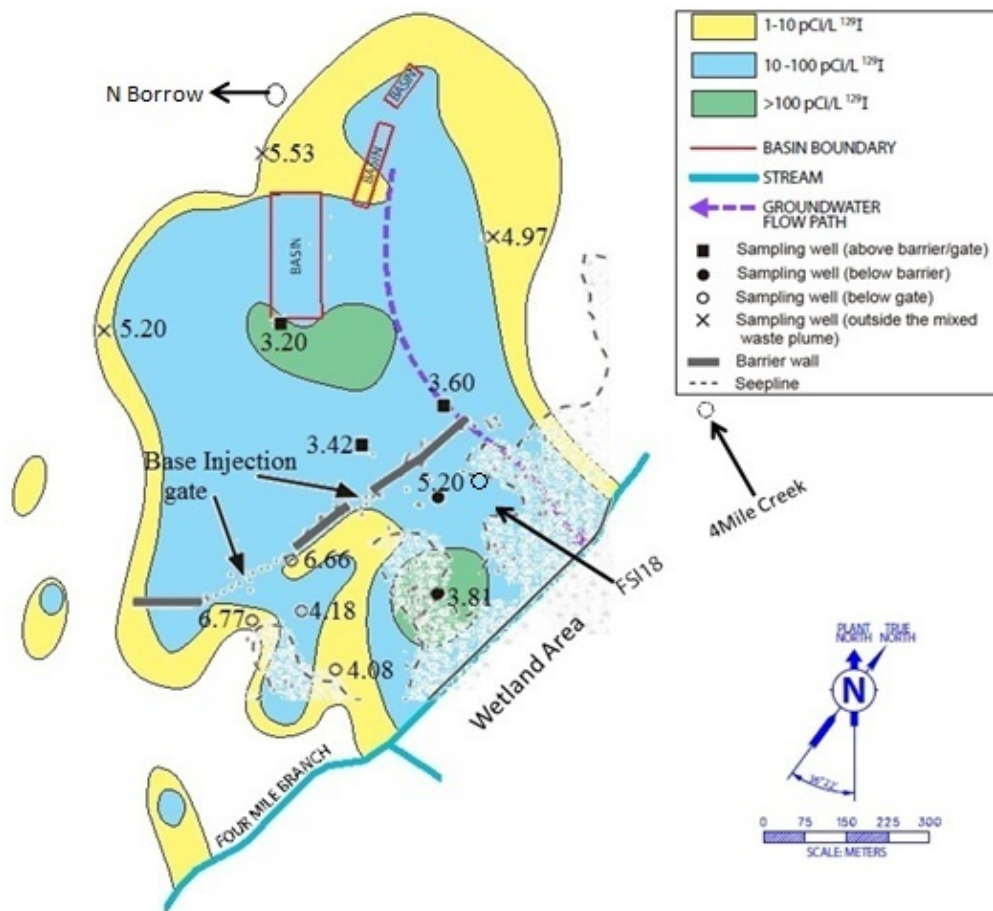
Fig. 3.1 Locations of sampling sites in F-Area of Savannah River Site. Numbers on this map denote the pH values of the local groundwater and adopted from Otosaka et al. (2011). FSI18 was located along the seepline where the grassland was abundant in organic matter (24% OC) but high amount of radioioidine was found in the local groundwater. It is a few hundred meters upward the wetland area.

Table 3.1 Soil characterization .

| Parameters | FSI18 | N Borrow | 4Mile Creek |
|---|---|---|---|
| pH | 5.63 ± 0.1 | 5.2 ± 0.1 | 4.1 ± 0.0 |
| OM,% | 24.1 | <0.01 | 7.9 |
| Sand/silt/clay (wt%) | 92.1/7.0/0.9 | N/A | 85.5/11.7/2.8 |
| $^{127}$I (µg/g) | 4.26 | N/A | 2.59 |
| $^{129}$I (µg/g) | 0.32 | N/A | BD |
| FeII/Fe(III), %/% | N/A | 1.9 / 98.1 | N/A |
| FeII/Fe(III), %/% | N/A | <2 />98 | N/A |
| Fe(III), Hematite, Goethite, % | N/A | 8, 28, 63 | N/A |
| Reduction Capacity, meq/kg | N/A | 2.88 ± 0.82 | N/A |
| Mineralogy (<53µm) | N/A | Kaolinite, goethite, hermatite, gibbsite, muscovite, rutile (no quartz; very slight 14Å) | Kaolinite, goethite, quartz, hermatite, muscovite/ 10 Å |
| DCB Al, <53µm (ppm) | N/A | 961.9 ± 78 | N/A |
| DCB Fe, <53µm (ppm) | N/A | 5346.3 ± 563 | 2.24 |
| DCB Mn, <53µm (ppm) | N/A | 8.8 ± 1 | N/A |

## 3.3.2 Iodine speciation analysis

Determination of iodide and iodate follows Zhang et al. (2010). Basically, iodide was oxidized by 2-iodosobenzoate to iodine, which then subsequently iodinated N,N-dimethylaniline to become 4-iodo-dimethylaniline. The resulting derivative was extracted by cyclohexane and detected either by GC-MS or liquid scintillation counter if $^{125}$I has been added. Iodate was converted to iodide first by sodium meta-bisulfite, followed the same reaction as iodide and calculated as the difference between total inorganic iodide and iodide. The presence of high organic matter "smeared" the

detection of inorganic iodine by interacting with the reagents, thus sample amended with known $I^-$ (or $IO_3^-$) was also measured and compared to the sample without the addition of standard, to calculate the recovery.

The determination of total iodine ($^{127}I$ and $^{129}I$) in aqueous solution followed the procedure of Zhang et al. (2010), with slight modification. 2mL of sample was mixed with 150 mg of vanadium pentoxide ($V_2O_5$), which acted as a catalyst for rapid combustion, and were placed in a porcelain boat. $^{125}I$ was added to the sample-$V_2O_5$ mixture as a tracer for the pyrolysis recovery. The boat with the sample and catalyst was gently pushed into the center of a quartz combustion tube and subjected to combustion on a tube furnace (Lindberg/Blue M Mini-Mite, Thermo Scientific). The temperature of the furnace was programmed as follows: the temperature was increased to 200 °C within one minute and then held constant for three minutes. After that, the temperature was increased to 900°C over ten minutes and left there for an additional 10 minutes. Oxygen was used as carrier gas at a constant flow rate of 113mL/min during the whole program. The iodine released by pyrolysis was collected into a pyrex glass tube containing 1 mL of Milli-Q water.  After the pyrolysis program was finished, carrier gas was switched from oxygen to nitrogen at a flow rate of 134 mL/min and allowed to purge the receiving water for 30 minutes. Total iodine was measured by Finnigan Trace GC and Polaris Q EI-MS from Thermo, after being derivatized to iodinated N, N-dimethylaniline. Quantification of $^{127}I$ and $^{129}I$ was based on the different masses of their respective derivatives in the mass spectrum, which were used as the "screening filter" to distinguish

their respective responses in the gas chromatograms. Organo-iodine was calculated as the difference between total iodine and total inorganic iodine.

### 3.3.3 $^{125}I^-$ and $^{125}IO_3^-$ sources and validation of their application for tracking stable iodine behaviors

Carrier-free $^{125}I$ was purchased in the form of NaI from MP Biomedical, USA. $^{125}IO_3^-$ was prepared from $^{125}I$ by combustion and oxidation of $Na^{125}I$. 0.5 mL of Milli-Q water and 5 µL of $Na^{125}I$ (45 µCi) was mixed with 100 mg $V_2O_5$ and combusted at high temperature (see above). Oxygen flow was adjusted to 100 ml/min to ensure the well-oxidation of iodide. Still, the conversion was only 50% (i.e., $I^-:IO_3^-$=1:1). Thus a Strata X_A 33u polymeric strong anion exchange column (Phenomenex, USA, Cat #: 8B-S123-EBJ) was used to separate $I^-$ from $IO_3^-$. The column was first conditioned with 2mL methanol and then Milli-Q water. 2mL of the solution after combustion and rinsing was loaded on the column and then eluted with 20 mM ammonium acetate. No $I^-$ was detected in the eluate according to the speciation analysis. The purpose of using combustion method instead of other chemical conversion (Takayanagi and Wong, 1986) is to minimize the interference during SOM iodination experiment.

Though the uptake of the inorganic iodine by the different soils used in this study was calculated based on a mass balance (activity of total added inorganic iodine-125 minus that of aqueous iodine-125), controls of only $^{127}I^-$ and $^{125}I^-$ (or $^{127}IO_3^-$ and $^{125}IO_3^-$) at two experimental concentrations (20 µM and 0.1 µM) shaken with artificial freshwater (Martin and Whitfield, 1983) for the same period of time and undergoing all

processing steps showed that the sorption of inorganic iodine species onto the experimental devices or release out of the system (e.g., in the form of $I_2$) to be negligible, with recoveries very close to 100%. In addition, the incorporated iodine-127 into the solid, colloidal and dissolved phases were also measured by combustion followed by GC-MS analysis and quantified by the difference between the amendment and control groups. The results based on the radiotracer ($^{125}I^-$ or $^{125}IO_3^-$) agreed well with those of the combustion and GC-MS analysis (error within 6%), and therefore validate the experimental approach of using radiotracer $^{125}I^-$ or $^{125}IO_3^-$ as spikes to track the behavior of stable iodine in the soil and groundwater.

### 3.3.4 Iodine uptake/transformation in soil resuspension experiment

Laboratory soil resuspension experiments were conducted using FSI18 (24.1% OC) and N Borrow (<0.01%) soils with contrasting organic matter contents, to mimic the co-release of truly dissolved organic matter ($DOM_{<3\,kDa}$), colloidal organic matter (COM) and their associated radioiodine from the soil during simulated surface runoff and stormflow events. Moist soil was mixed with artificial freshwater at a realistic solid to water ratio of 1:4 (Fukui et al., 1996), after the removal of the undecomposed leaves and roots. Uptake and transformation of inorganic iodine was observed in five treatments for each soil: 1) control (without any iodine addition), 2) 20 µM $I^-$ amendment, 3) 20 µM $IO_3^-$ amendment, 4) 0.1 µM $I^-$ amendment, and 5) 0.1 µM $IO_3^-$ amendment. Carrier free $^{125}I^-$ and $^{125}IO_3^-$ were well equilibrated with stable iodine before adding to treatments 2)-5), as an analogue for $^{129}I$. A series of 40 mL soil slurries were gently shaken with an

orbital shaker at ~160 rpm in 50 mL centrifuge tubes containing some headspace. Samples were then allowed to sit without caps for half an hour twice a day to exchange air with the atmosphere to avoid anoxic conditions. At each time point (the 4th, 10th, 17th, 24th and 30th day) two duplicate tubes were taken and processed for each treatment. Particles were allowed to settle by low-speed (~3200 $g$) centrifugation and the supernatant was immediately filtered by using sterile disposable vacuum filter/storage systems (Corning, USA). The filtrate (< 0.45 μm) was ultrafiltered through an Amicon Ultra-15 centrifugal device with a cut-off of 3 kDa. The soil pellet was exhaustively washed several times with 0.1 M KCl to measure exchangeable $I^-$ or $IO_3^-$ that was reversibly bound onto the solid phase, until no more activity was observed in the aqueous phase (<0.45 μm).

Total organic carbon concentration was determined with a Shimazu TOC-5000 analyzer. Particle-water partition or distribution coefficients, as ratios of concentrations in particles to those in freshwater solution, were empirically determined (uptake Kd). A desorption distribution coefficient, Kd', was determined using the ratio of the concentration of residually-sorbed iodine to that in the desorbing solution (0.1 N KCl). The Kd and Kd' construct is used here to quantify uptake of iodine from the aqueous phase by soils and not to imply a sorption mechanism.  Both irreversible uptake by natural organic matter (NOM) through forming covalent C-I bonds, as well as surface complexation are involved in producing a particular Kd value.

Aromaticity, as defined as the peak area in the 110-160 ppm chemical shift band of quantitative $^{13}$C-NMR spectra, was determined according to its relationship with UV

absorbance (Chin et al., 1994). Briefly, freeze-dried samples were re-dissolved in a phosphate buffer and passed through a 0.45 μm syringe filter.  Total organic carbon was determined using a Shimadzu TOC-5000 analyzer. UV absorbance (280nm) was determined using a Turner spectrometer.  Absorptivity (L/mole of OC/cm) of eight IHSS humic substances was determined the same way and plotted against their aromaticity, which was obtained from IHSS website and determined by $^{13}$C-NMR. The resulting calibration equation (y=0.063x-3.679, x and y denote absorptivity and aromaticity, respectively) was used to estimate aromaticity from sample molar absorptivity.

### 3.3.5 Extraction of HA, FA and WEC

Extraction of HA and WEC was described elsewhere (Xu et al., 2011a), but briefly mentioned here. Five HA fractions were obtained by repeatedly extracting the same soil five consecutive times following a standard procedure recommended by IHSS (Swift et al., 1996). The resulting HAs were named HA1, HA2,…, HA5. Two successive glycerol-extracted HA fractions and one alkaline extracted fraction (after the removal of metals by citric acid) were obtained from the soil residue after five times of HA extraction, by twice extracting the residue with 50% glycerol followed by removal of major cations (e.g., Fe) through complexation with 0.5 M citric acid, and extraction one additional time with 0.1 M NaOH (Baglieri et al., 2007). The three HA fractions were named as HA6, HA7 and HA8. Thus the first five HAs and FAs probe the SOM that are loosely bound to the soil mineral and thus can be more easily released under alkaline/acid extraction conditions. Glycerol has the ability of penetrating into the

interlayers of the phyllosilicates and thus releasing any HS still trapped in the interlayers.

Citric acid was used to complex iron or other major cations, which are involved in the

formation of HS-metal-clay complexes, and make the humic acid accessible to the

extraction solvent (NaOH). SRS soils commonly have high Fe-oxide contents.  For

example, in a sediment collected in an adjacent aquifer a the F-Area, Hixon et al. (Hixon

et al., 2010) used Mossbauer spectroscopy in a sediment containing 16,000 ppm Fe that

contained 34% hematite, 59% goethite, and 7% Fe in clay structures.

To collect water extractable colloid (WEC), the moist soil was dispersed in 20 L

artificial freshwater to reach a final concentration of 5 g-dry soil/ L and shaken very

gently at 150 rpm on an orbital shaker for three days (Xu et al., 2008). In order to

investigate the yield of WEC based on the dry soil weight and make the radioiodine data

comparable among bulk soil, HA, FA and WEC, the ratio of weight of oven-dried soil to

that of original damp soil was calculated in a preliminary experiment. Later, the soil

resuspension was centrifuged for 30 minutes at 3200 × g, and the supernatant was

successively filtered through 10 μm and 0.45 μm cartridge filters. Filtration was

followed by cross-flow ultrafiltration, utilizing a spiral-wound 1kDa SOC 1812 cartridge

(Separation Engineering, Inc.), until 1L retentate remained.  The retentate was diafiltered

against 20 L Milli-Q until it was concentrated to 1 L.  Then, the cartridge was rinsed

with 250 mL Milli-Q water with the pump on for 30 min, and then the pump was turned

off. The cartridge was allowed to soak for four hours or more.  The cartridge was

consequently rinsed with another 250 mL of Milli-Q water, and the procedure was

repeated twice or more until the rinse water became clear. The retentate and rinse

solution were then subsequently combined and concentrated utilizing an Amicon 8400

stirred-cell ultrafiltration unit with a 1 kDa regenerated cellulose filter at 275 kPa. The

retentate was freeze-dried for further radioiodine analysis and chemical characterization

(Xu et al., 2008).


### 3.3.6 Interaction of $I^-$ and $IO_3^-$ with SOM

HA and WEC samples were reacted with $I^-$ or $IO_3^-$ under different conditions. Briefly,

SOM samples were first dissolved in 20 mM Tris-HCl buffer to achieve maximum

dissolution (pH ~8, 1mg/mL), and diluted at a final concentration of 100 mg/L with

artificial freshwater. Different buffers were added to achieve the desired pH range of 3-9

(Table 3.2). The ionic strength of the final solution was maintained around 3-6 mM to

mimic that of the soil porewater. A final concentration of 0.1 μM of $^{127}I^-$ (or $^{127}IO_3^-$) and

0.9 μCi/L of $^{125}I^-$ (or $^{125}IO_3^-$) was added. The solution mixture was shaken in darkness to

reach equilibrium. Molecular weight of HA and WEC samples extracted from FSI18

and 4Mile Creek soils were determined to be larger than 3 kDa (Xu et al., 2011a), thus

Amicon Ultra-4 centrifugal filter units were applied to separate the un-bound $I^-$ or $IO_3^-$

from the iodinated HA or WEC fractions. The amounts of $I^-$ or $IO_3^-$ incorporated into

HA or WEC were determined by measuring the activity of the retentate with a LS 6500

Multi-Purpose Scintillation Counter (Beckman Coulter, USA). The amount of iodine

bound to HA or WEC was normalized to the initial total added concentration. Formation

of volatile iodine species (e.g., $I_2$ or methyl iodine) was estimated based on the mass-

balance comparison between the total iodine content (as $^{125}I$ activity or $^{127}I$ measured by

combustion and GC-MS analysis) in the reaction vessel at the time of collection and that of total initially added amount.

### 3.4 Results and discussion

### 3.4.1 Soil organic matter: the importance of a natural trap for radioiodine

The distribution of externally-amended iodide and iodate at high concentration (20 μM) in the solid, colloidal (0.45 μm- 3 kDa) and dissolved phases (<3 kDa) is shown in Fig. 3.2 a-b, and that at ambient concentration (0.1 μM) concentration in these three phases is shown in Fig. 3.3 a-b, for organic-rich soil (FSI18). The kinetics for $I^-$ and $IO_3^-$ uptake by the organic-rich soil was very similar. On the 17th day, both the uptake of $I^-$ and $IO_3^-$ by the organic-rich soil reached equilibrium (78.9% and 74.1% for $I^-$ and $IO_3^-$, respectively).

Table 3.2 Composition of solution for interaction between inorganic iodine ($I^-$ or $IO_3^-$) and SOM.

| pH | 0.2 ml | 1.475 mL | 0.3 mL buffer | 0.025 mL |
|---|---|---|---|---|
| 3 | 1mg/L HA/FA/WEC in 20 mM Tris-HCl) | Artificial freshwater | 0.05 M phosphate buffer, pH 2.46 | 20 μL 0.1 μM $^{127}I^-$ (or $^{127}IO_3^-$) + 5 μL 0.36 mCi/L $^{127}I^-$ (or $^{127}IO_3^-$) |
| 4 | | | 0.05 M acetate buffer, pH 3.8 | |
| 5 | | | 0.05 M acetate buffer, pH 4.75 | |
| 6 | | | 0.05 M acetate buffer, pH 4.75 and trace amount of NaOH | |
| 7 | | | 0.05 M phosphate buffer, pH 6.5 | |
| 8 | | | 0.05 M Tris-HCl buffer, pH 7.95 | |
| 9 | | | 0.05 M Tris-HCl buffer, pH 7.95 and trace amount of NaOH to the desired pH | |
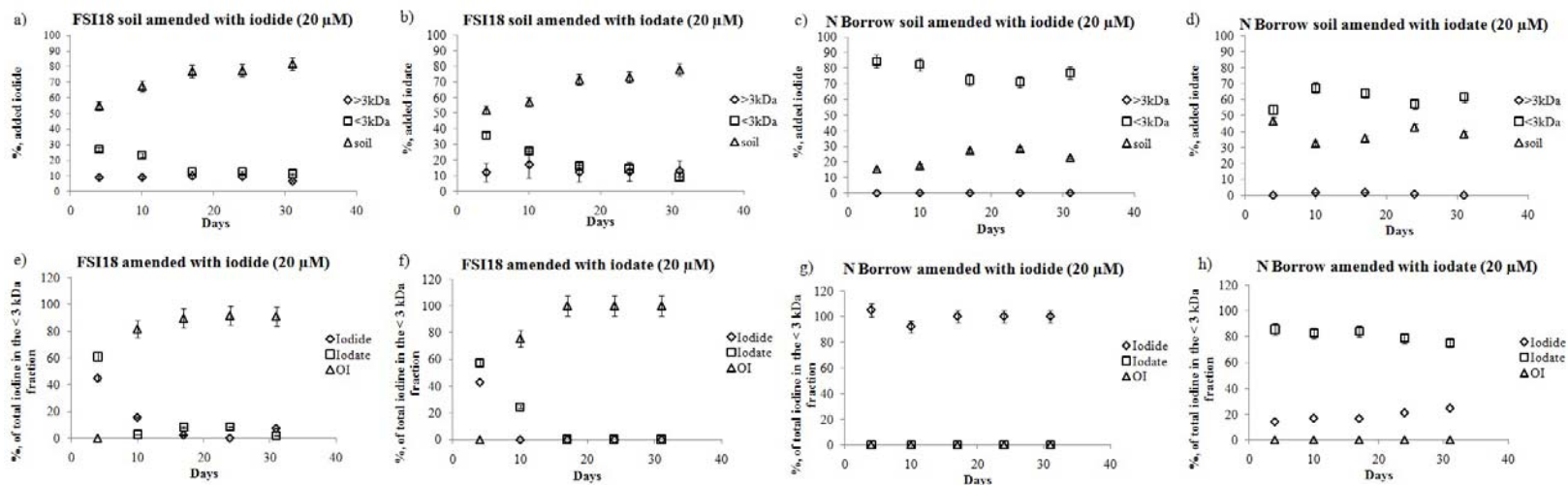
Fig. 3.2 Temporal partitioning of (a) iodide or (b) iodate at high concentration (20 µM) into the solid, colloidal and dissolved phases of the organic-rich (FSI18) soil resuspension and of (c) iodide or (d) iodate at 20 µM into the three phases of the organic-poor (N Borrow) soil resuspension. Temporal iodine speciation in the soil leachate truly dissolved phase (<3 kDa) in 20 µM (e) iodide or (f) iodate amendment groups for FSI 18 soil, and 20 µM (g) iodide or (h) iodate amendment groups for N Borrow soil (I⁻, IO₃⁻ or organo-iodine are normalized to the total iodine in the permeate). For experiments, final $^{125}$I or $^{125}$IO₃⁻: 0.9 µCi/L.

a) **FSI18 soil amended with iodide (0.1 μM)**

<3kDa 16%
>3kDa 5%
sorbed to the soil 79%

b) **FSI18 soil amended with iodate (0.1 μM)**

<3kDa 20%
>3kDa 0%
sorbed to the soil 80%

c) **N Borrow soil amended with iodide (0.1 μM)**

sorbed to the soil 13%
>3kDa 0%
<3kDa 87%

d) **N Borrow soil amended with iodate (0.1 μM)**

<3kDa 53%
sorbed to the soil 47%
>3kDa 0%
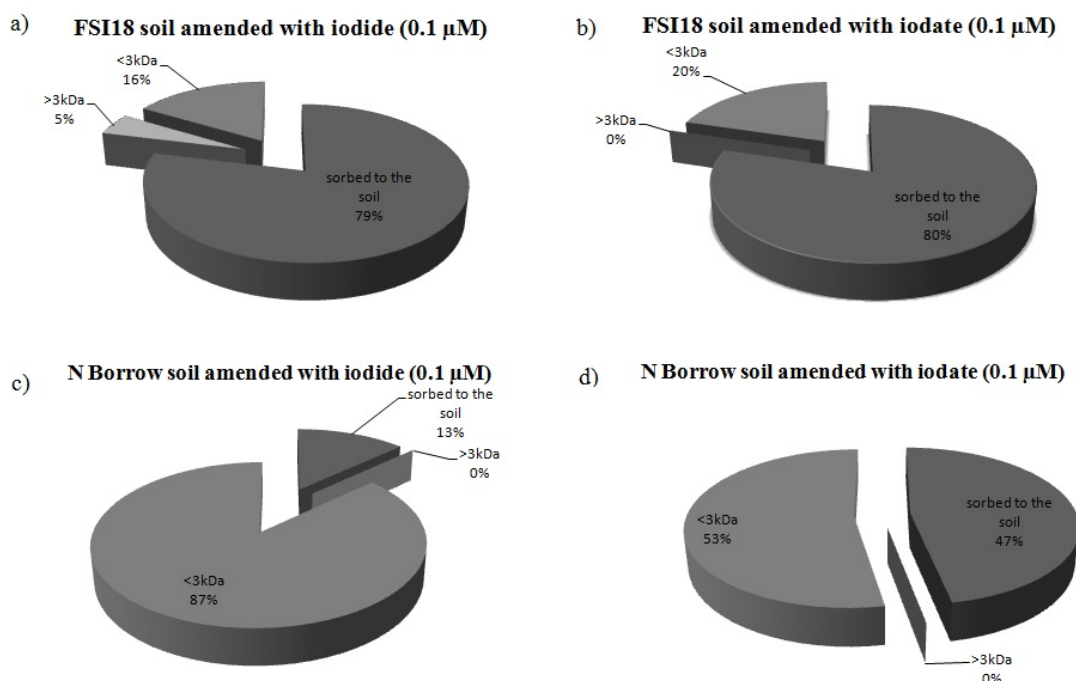
Fig. 3.3 Partitioning of (c) iodide or (d) iodate at ambient concentration (0.1 μM) into the three phases of this soil during a four-day resuspension. Temporal partitioning of (a) iodide or (b) iodate at high concentration (20 μM) into the solid, colloidal and dissolved phases of the organic-poor (N Borrow) soil resuspension. Partitioning of (c) iodide or (d) iodate at ambient concentration (0.1 μM) into the three phases of this soil during a four-day resuspension. Temporal iodine speciation in the soil leachate dissolved phase amended with 20 μM (e) iodide or (f) iodate ($I^-$, $IO_3^-$ or organo-iodine are normalized to the total iodine in the permeate). For experiments, final $^{125}I^-$ or $^{125}IO_3^-$: 0.9 μCi/L.

The slow and saturation kinetics for iodine species uptake was also observed previously for another soil sampled from the F-Area (OC, 8.4% wt) and amended with iodide (Schwehr et al., 2009), which was then ascribed to biotic reactions. It is interesting to note that uptake of iodate by the surface soil also followed a similar pattern and was not significantly higher than that of iodide. This is surprising, as many researchers report higher Kd values for iodate than for iodide (Fukui et al., 1996; Hu et al., 2005). However, Yamaguchi et al. (2010) also observed that the majority of the

iodide or iodate applied to several organic-rich soils from Japan were taken up by the solid phase in the form of organo-iodine, using iodine K-edge XANES. Furthermore, similar Kd values were also reported for both iodide and iodate of a wetland soil (OC, 7.9% wt) from the Savannah River Site (ref=3; Kd ~75 ml/g under oxidizing conditions). Thus it is likely that in the presence of sufficient amounts of organic matter, formation of organo-iodine is favorable in the oxic surface soils, and the equilibrium distribution does not depend on the oxidation state of the starting iodine species. At 200 times lower concentrations, 0.1 μM iodide or iodate partitioned similarly in the FSI18 soil suspension; however, appreciably greater soil uptake was detected compared to 20 μM system after 4 days.  For the 0.1 μM iodide treatment, 78% was taken up by the soil, 6% was associated with the >3kDa fraction, and   16% was associated with the <3kDa fraction (Fig. 3.3 a).   Almost identically for the 0.1 μM iodate treatment, 77% was taken up by the soil, 3% was associated with the >3kDa fraction, and   20% was associated with the <3kDa fraction (Fig. 3.3 b).

   The kinetics of iodide or iodate uptake by the organic-poor soil (N Borrow) is shown in Fig. 3.2c-d and 3.3 c-d, for 20 μM and 0.1 μM, respectively. The difference between the iodine partitioning demonstrates important speciation differences that the soil plays, and more specifically, the role SOM plays.  No significant iodine was found in the colloidal fraction due to the low OC content. Uptake of iodide increased steadily with time and reached equilibrium around the 17th day, while uptake of iodate attained equilibrium conditions more quickly (Fig. 3.2c-d).

Values for distribution coefficients (Kd) in the artificial freshwater and in the 0.1 N

KCl as the desorbing solution (Kd') are shown in Table 3.3. More inorganic iodine was

readily sorbed into both soils at ambient concentrations (0.1 μM), compared to the

elevated concentration (20 μM). Organic-poor soil showed much smaller values of Kd

and Kd' for both $I^-$ and $IO_3^-$ than the organic-rich soil, especially at ambient

concentrations. Both soils had higher values for desorption Kd' than uptake Kd,

indicating that uptake of inorganic iodine was mostly not reversible. The fractions

irreversibly taken up in organic-rich soil were much higher than those in the organic-

poor soil. Also, in the organic-poor soil, higher uptake Kd were observed for iodate than

for iodide, at both high and ambient concentrations; however, the desorption Kd' values

were about the same. Several mechanisms were suggested for the process of uptake of

iodine: 1) $I^-$ and $IO_3^-$ can be reversibly sorbed onto the positively-charged mineral

surface through electrostatic interactions primarily on the kaolinite, goethite and

hemetite; 2) they can also reversibly or irreversibly displace the inner-sphere anions of

the soil minerals through molecular diffusion; 3) formation of organo-iodine species.

The last mechanism is largely an irreversible uptake process, resulting in a strong

covalent bond between iodine and carbon in the SOM.

In the absence of organic matter, iodate sorbs more to the soil minerals than iodide,

presumably because the harder base nature of $IO_3^-$, compared to $I^-$, favoring hard-hard

interactions with the hard acid sites on the mineral surfaces (Hu et al., 2005); while more

of $I^-$ can sorb into intra-granular spaces which is more irreversible (Fukui et al., 1996).

From the much higher desorption Kd' values for the organic-rich soil compared to those

for the organic-poor soil, especially at ambient input concentrations, it can be inferred

that nearly 100% of the sorbed inorganic iodine (~72-77% of the total added iodine) was

irreversibly retained in the soil organic-mineral matrix, thus becoming immobile.

Table 3.3 Iodide and iodate uptake Kd (calculated as ratios of $I^-$ or $IO_3^-$ concentrations in particles to those in solution) and desorption Kd' (calculated as ratios of residual $I^-$ or $IO_3^-$ concentrations in particles to those released after KCl wash) values at two concentrations (20 µM and 0.1 µM) for organic-rich and organic-poor soils, during a four-day resuspension experiment. All fractions (%) are normalized to the total initial added amount (reported values represent averages of duplicates and standard deviation less than 10%).

| | Uptake (%, of total added) | | | | Desorption (%, of total added) | | | |
|---|---|---|---|---|---|---|---|---|
| | 20 µM | | 0.1 µM | | 20 µM | | 0.1 µM | |
| | $I^-$ | $IO_3^-$ | $I^-$ | $IO_3^-$ | $I^-$ | $IO_3^-$ | $I^-$ | $IO_3^-$ |
| FSI18N | 54.73 | 52.04 | 78.29 | 76.87 | 4.82 | 5.50 | 3.62 | 0.81 |
| Borrow | 25.86 | 46.45 | 12.51 | 50.78 | 6.09 | 18.86 | 2.16 | 20.62 |
| | 20 µM | | | | 0.1 µM | | | |
| | $I^-$ | | $IO_3^-$ | | $I^-$ | | $IO_3^-$ | |
| | Kd | Kd' | Kd | Kd' | Kd | Kd' | Kd | Kd' |
| FSI18N | 13.82 | 118.45 | 12.40 | 96.67 | 41.21 | 235.69 | 37.98 | 1077.11 |
| Borrow | 1.74 | 16.23 | 4.34 | 7.32 | 0.71 | 23.89 | 5.16 | 9.75 |

**3.4.2 Transformations of newly-introduced iodine species in the truly dissolved**

**phase**

The time-course of the release of colloidal organic carbon (COC) and truly dissolved

organic carbon ($DOC_{<3\ kDa}$) from the organic-rich soil and the changes in their

aromaticity are shown in Fig. 3.4.
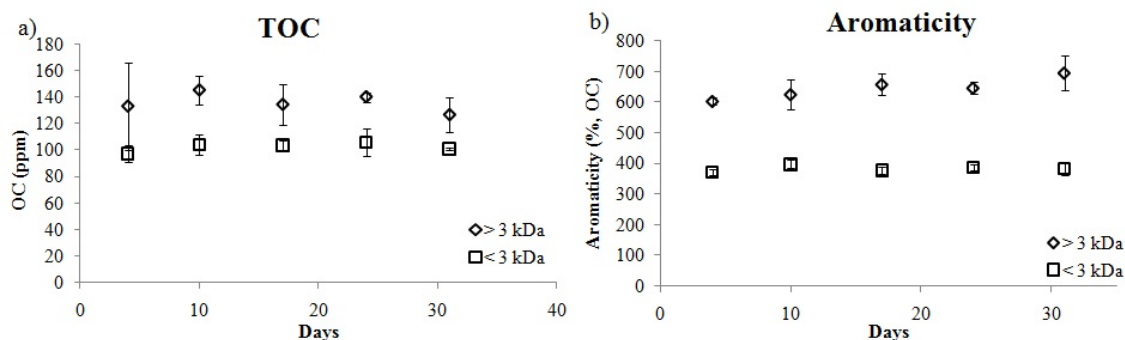
Fig. 3.4 Time-elapsed release of colloidal organic carbon (COC) and dissolved organic carbon (DOC) from the organic-rich soil and change of aromaticity. No significant difference in the organic matter characterization was found out among the control, $I^-$ amendment and $IO_3^-$ amendment groups, thus data were averaged from six samples for each time point (duplicates for each group).

Desorption of both colloidal and dissolved fractions reached equilibrium on the scale of 3-4 days, indicating that a normal storm event or groundwater exfiltration (upwelling with contaminated radioiodine, as occurs at F-Area wetlands) contacting the surface soil readily releases the potential mobile organic vectors and their associated contaminants. More importantly, the soil has changed the speciation of the radioiodine, from an inorganic form to an organic iodine moiety. The newly-introduced iodine, which was tracked by $^{125}I^-$ or $^{125}IO_3^-$ and thus can be distinguished from the "background" iodine, showed fast incorporation into the organic colloidal fraction (Fig. 3.2a-b and Fig. 3.3a-b, 9% or 13% of the total added $I^-$ or $IO_3^-$ at 20 μM, and 6% or 3% of the total added $I^-$ or $IO_3^-$ at 0.1 μM, respectively, after 4 days). Surprisingly, no matter what the starting

species is ($I^-$ or $IO_3^-$), organic-rich soil leachate permeate (< 3kDa) showed similar kinetics for the distribution of the different species. This may be the result of the stoichiometry of our system, such that we had an excess of SOM and trace levels of $I^-$ or $IO_3^-$. Nearly 100% of $I^-$ (or $IO_3^-$) was converted to organo-iodine in the <3 kDa fraction at the end of the observation period (Fig. 3.2e-f). In the FSI18 soil-iodide amendment, $I^-$ was partially (61% of the total iodine in the permeate) converted to $IO_3^-$ at the beginning but decreased dramatically to ~ 1.8% after 31 days, due to the conversion into organo-iodine. ~ 43% of total iodine in the < 3 kDa fraction was present as $I^-$ in the FSI18 soil-iodate amendment but dropped quickly to undetectable levels, indicating that FSI18 soil has both oxidizing and reducing capacity for $I^-$ and $IO_3^-$, converting them to reactive iodine species (e.g., $I_2$ or HOI) as intermediates, in order for the iodination of the SOM to occur. Organo-iodine appeared to be the favored form in the organic-rich soil leachate, no matter what the starting species was. In contrast, the organic-poor soil (N Borrow) exhibited only a reducing capacity for $IO_3^-$ (Fig. 3.2g-h). In the permeate of N Borrow soil amended with $I^-$, $I^-$ displayed a "pure" sorption behavior onto the solid phase; while a steady increase of $I^-$ was detected with time in the aqueous phase (14-25% of the total iodine in the permeate) of this soil amended with $IO_3^-$, thus a mixed sorption behavior of $I^-$ and $IO_3^-$ onto the solid phase was revealed.

### 3.4.3 [129]I transport facilitated by colloidal and truly dissolved soil organic matter carrier

While ^{125}I tracked the uptake and desorption of newly-introduced iodine with the surface soil during radioiodine-contaminated groundwater exfiltration, the control group without any iodine addition, when contacting the artificial freshwater, simulated the release of [129]I from the contaminated soil, under the influence of less contaminated (or "diluted") groundwater exfiltration or stormflow events. Co-release of [129]I with COC and $DOC_{<3\,kDa}$ from FSI18 soil reached equilibrium very quickly, with both fractions making up 61% and 39% of the total potentially mobile radioiodine (Fig. 3.4-5). The potentially mobile [129]I in the COC and $DOC_{<3\,kDa}$ fractions would result in activity concentrations of [129]I of 1015($\pm$129) and 639($\pm$64) pCi/L, respectively, much higher than the drinking water limit of 1 pCi/L. Interestingly, no inorganic iodine was detected in the permeate, similar to the observation in the $I^-$ or $IO_3^-$ amended groups where organo-iodine was identified as the only species (Fig. 3.2e-f). However, different amounts of remobilized colloidal organo-iodine but no detectable organo-iodine in the permeate were found when a low solid to liquid ratio (1:200) was applied (Xu et al., 2011a). This latter observation could be due to the fact that any species of iodine present in the permeate is too diluted for the method detection limit. In addition, a change of partitioning coefficient with different solid to liquid ratios might be expected (Fukui et al., 1996) but is beyond the scope of this study. Nevertheless, the conditions applied in this study are closer to the real situation and thus the results well represent the radioiodine carrier that can potentially be flushed out of soil and migrate downgradient

the wetland area after the surface soil is contacted by the exfiltrated groundwater (upwelled into the wetland) or stormwater in the vadose zone.
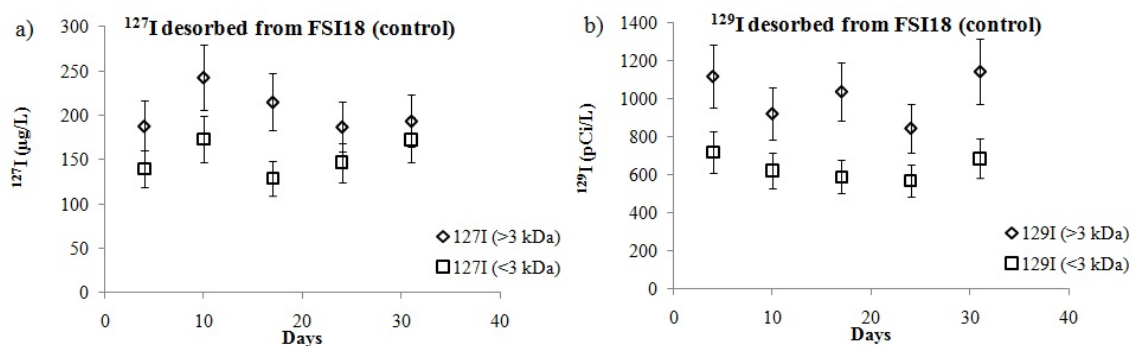


Fig. 3.5 Temporal desorption of a) $^{127}$I and b) $^{129}$I from an organic-rich soil (FSI18) of F-Area (soil resuspended in artificial freshwater).

The association of iodine with COC in aquatic systems was also reported in the Mississippi River (Oktay et al., 2001), as well as the groundwater of Savannah River Site (Zhang et al., 2010), but has not been described in the soil literature so far. The transformation of almost all inorganic iodine into particulate, colloidal and dissolved organo-iodine fractions by the organic-rich soil, and the resulting remobilization is unexpected, since the conventional view is that the mobile forms of iodine should be mostly $I^-$ (and, to some extent, $IO_3^-$) (Denham et al., 2009). The interaction between radioiodine and the organic-rich soil can be depicted as an on-off 'piggy-back' mechanism. First, the external inorganic radioiodine is picked up by the SOM through the formation of stoichiometrically outnumbered covalent C-I bonds, and thus, immobilized in this natural trap. However, some colloidal and dissolved organic matter either becoming iodinated by the newly-introduced radioiodine in solution, or being co-

released from solids with the early-bound radioiodine, would become an important mobile radioiodine source to any downgradient area. A relatively recent view of SOM is that they are a collection of diverse relatively low-molecular-mass component forming dynamic associations stabilized by hydrophobic interactions and hydrogen bonds (Sutton and Sposito, 2005). These quasi-temporal bonds can break resulting in the release of colloidal or complexed iodine species. The extractable humic substances obtained from the FSI18 soil was shown to be the predominant pool for iodine fixation (54% of the soil total $^{129}$I) (Xu et al., 2011a). The mobile iodine bound to COC and $DOC_{<3\ kDa}$ (when the solid to liquid ration was 1:4) amounted to ~9% of the soil total radioiodine, as can be seen from the following calculation:

((1015+639) pCi/L ($^{129}$I bound to COC and $DOC_{<3\ kDa}$) × 0.0225 L (total volume of the soil leachate due to pore water loss)) / (50.89 pCi/g (total $^{129}$I in the FSI18 soil) × 8g (total soil used in the resuspension experiment)) × 100%.

As the iodination of the natural "sink" in the immobile solid phase, and mobile "carrier" in the liquid phase, can be affected by recent site remediation actions, it is essential to define better the multiple factors that control the capability of soil systems to fix iodine under different environmental conditions, which will help to understand better the observed iodine transformations and distributions (Kaplan et al., 2010; Otosaka et al., 2011).

**3.4.4 Factors controlling iodination of purified radioiodine immobile "sinks" and mobile "carriers"**

The most critical parameter to consider is pH. Thus, reactions of iodide or iodate with WEC and HA in the pH range of 3-9, which covers the range of values that are seen in the groundwater at the F-Area, were investigated. As illustrated in Fig. 3.6a, in the presence of lactoperoxidase, iodide incorporation into the HA was significantly (3.5-12.5 times) elevated, compared to the reaction using only $H_2O_2$, $I^-$ and HA. At pH $\geq 5$, iodide uptake by HA reached a "plateau", whereas the formation of organo-iodine species decreased with increasing pH when the lactoperoxidase enzyme was absent. Peroxide is capable of oxidizing $I^-$ into electrophilic products (e.g., $I_2$ or hypoiodide, HOI), which readily react with organic molecules possessing electron-donor groups (Wong, 1980). The incorporation of iodide onto the WEC catalyzed by lactoperoxidase at pH 5, but with a much lower $H_2O_2$ concentration ($10^{-5}$ M) recommended by Christiansen and Calsen (1991), leveled off at higher concentrations of WEC, and followed a logarithmic curve (Fig. 3.6b), probably due to the complexation and deactivation of the enzyme by NOM at higher concentrations (Christiansen and Calsen, 1991), or the complete consumption of $H_2O_2$ by an enzyme-hypoiodous acid complex (Magnusson et al., 1984).
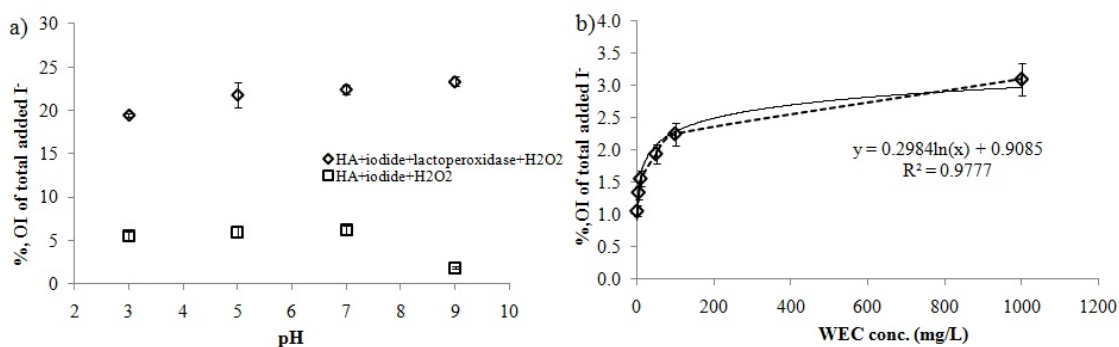
Fig. 3.6 a) pH-dependent lactoperoxidase catalyzed iodide incorporation into humic acid (HA) extracted from FSI18 soil. (HA, 100 mg/L; lactoperxidase, 20 µg/ml; $H_2O_2$: 5mM; reaction time, two hours; control group is with no lactoperoxidase addition); b) lactoperoxidase catalyzed iodide incorporation into the water extractable colloid (WEC) at pH 5 (lactoperoxidase, 20 µg/ml; $H_2O_2$: $10^{-5}$ M).

Results of the influence of metal oxides on the formation of organo-iodine starting from iodide are shown in Fig. 3.7 a-b. With the presence of $MnO_2$, iodination of HA and WEC under more acidic conditions (pH 3-4) sharply increased by a factor of 2 and 18, respectively, when compared to the control group with only iodide and NOM. When the pH reached up to 7 or higher, the amounts of iodinated NOM dramatically decreased and the enhancement by $MnO_2$ on iodination efficiency over the control group was barely detectable. The point of zero charge (pzc) of $MnO_2$ was reported as 1.5-2.5 (Tan et al., 2008) and that of soil NOM is ~3 (Xu et al., 2008), both of which are lower than the experimental pH range, thus resulting in a net negatively charged surface for both. Therefore, electrostatic repulsion between the inorganic iodine species and negatively-charged $MnO_2$ or NOM surfaces would be lowered at lower pH values, thus favoring the initial adsorption step of $I^-$. Besides, it might be noted that under acidic conditions (pH 3-4), iodide is probably converted to reactive iodine species by quinolic moieties (Yamguchi et al., 2010) or the free radicals of SOM (Shimamoto et al., 2011), and

sequestered into the SOM without enzymatic catalysis, peroxide or metal oxides, though the effect is less evident (Fig. 3.7). In contrast, though iron (III) oxide has a higher pzc (7.2) than $MnO_2$ (Baalousha, 2009), it did not remarkably enhance the iodination of the NOM as expected. It even slightly depressed the formation of iodinated NOM when the pH was $\geq 5$ (Fig. 3.7b). It is possible that $I^-$ was rapidly converted to $IO_3^-$ and partially irreversibly sorbed as inner sphere complexes of iron (III) oxide phases (Dai et al., 2004), thus not captured by the SOM.
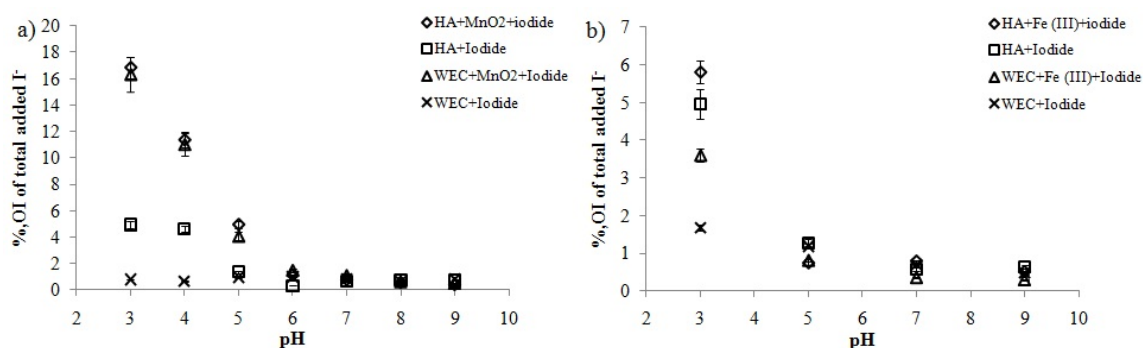


Fig. 3.7 a) pH-dependent iodide incorporation into HA or WEC at the presence of $MnO_2$ (HA or WEC, 100 mg/L; $MnO_2$, 0.5 g/L, Sigma Catalogue No., 217646, <5 µm, activated, ~85%; reaction time, 24 hours); b) pH-dependent iodide incorporation into HA or WEC at the presence of $Fe_2O_3$ (HA or WEC, 100 mg/L; $Fe_2O_3$, 0.5 g/L, Sigma Catalogue No., 217646, nanopowder, < 50 nm; reaction time, 24 hours).

In the presence of both metal oxides, volatile iodine species (e.g., $I_2$ or methyl iodine) were possibly formed under acidic conditions and escaped from the reaction vessel, which can be deduced from the fact that at pH 3-5, some ^{125}I was "missing" compared to the initially total added amount (Fig. 3.8). Though the ferrous ion was
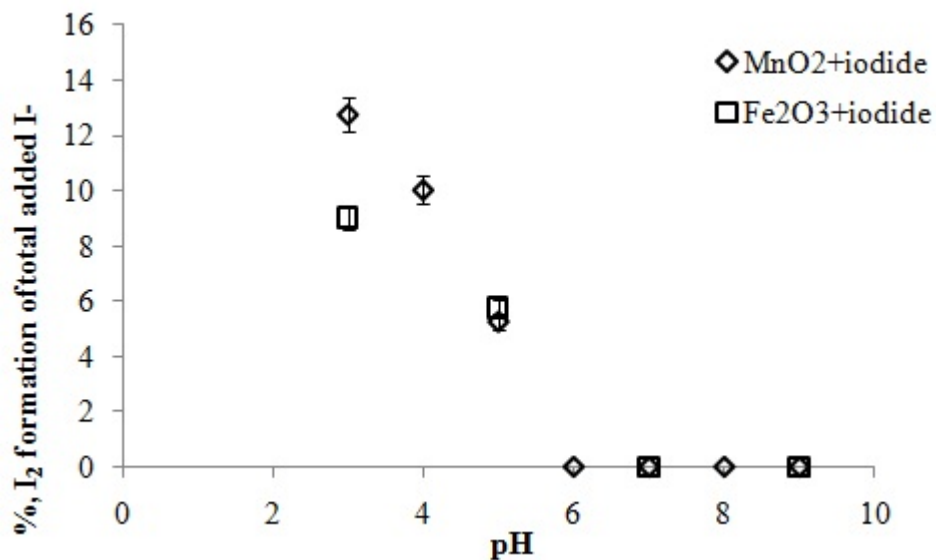
Fig. 3.8 pH-dependent formation of volatile iodine from iodide at the presence of $MnO_2$ or $Fe_2O_3$ (NOM, 0 mg/L; $MnO_2$ or $Fe_2O_3$, 0.5 g/L; reaction time, 24 hours).
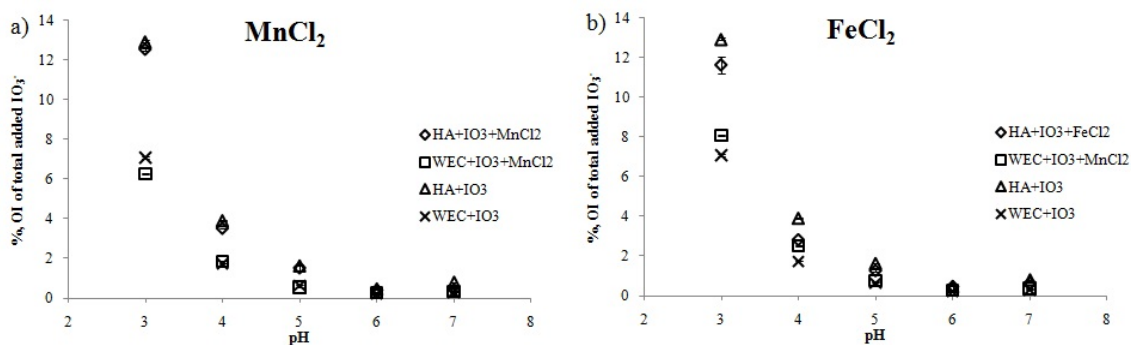


Fig. 3.9 a) pH-dependent iodate incorporation into HA or WEC at the presence of $MnCl_2$ (HA or WEC, 100 mg/L; $MnCl_2$, $10^{-5}$M; reaction time, 24 hours); d) pH-dependent iodate incorporation into HA or WEC at the presence of $FeCl_2$ (HA or WEC, 100 mg/L; $FeCl_2$, $10^{-5}$M; reaction time, 24 hours). All samples were performed in duplicates with the error < 1%.

previously reported to be capable of abiotically reducing iodate to iodide (Councell et al., 1997), iodination of HA or WEC starting from iodate under the presence of either $Fe^{2+}$ or $Mn^{2+}$ showed insignificant enhancement over the control group (without the addition of any metal ions, Fig. 3.9 a-b).

Similarly, the optimal uptake of iodate by WEC and HA occurred at pH 3 (Fig. 3.10a-b). Size-fractionation of the resulting iodinated HA or WEC products indicated that the high-molecular-weight (HMW, >50 kDa) subunit had much lower uptake of iodate than the low-molecular-weight (LMW, 3-50 kDa) subunit. Furthermore, the abiotic reaction at pH 5 between iodate and different NOM fractions (HAs from a sequential extraction of two soils and WECs) also showed a higher iodate uptake by the LMW subunit than by the HMW subunit (Fig. 3.10c-d). Thus, it is consistent with the previously reported observation that the naturally bound [127]I and [129]I in all those NOM fractions extracted from F-Area soils were positively correlated to the abundance of the LMW subunit (% OC of the NOM) (Xu et al., 2011a).
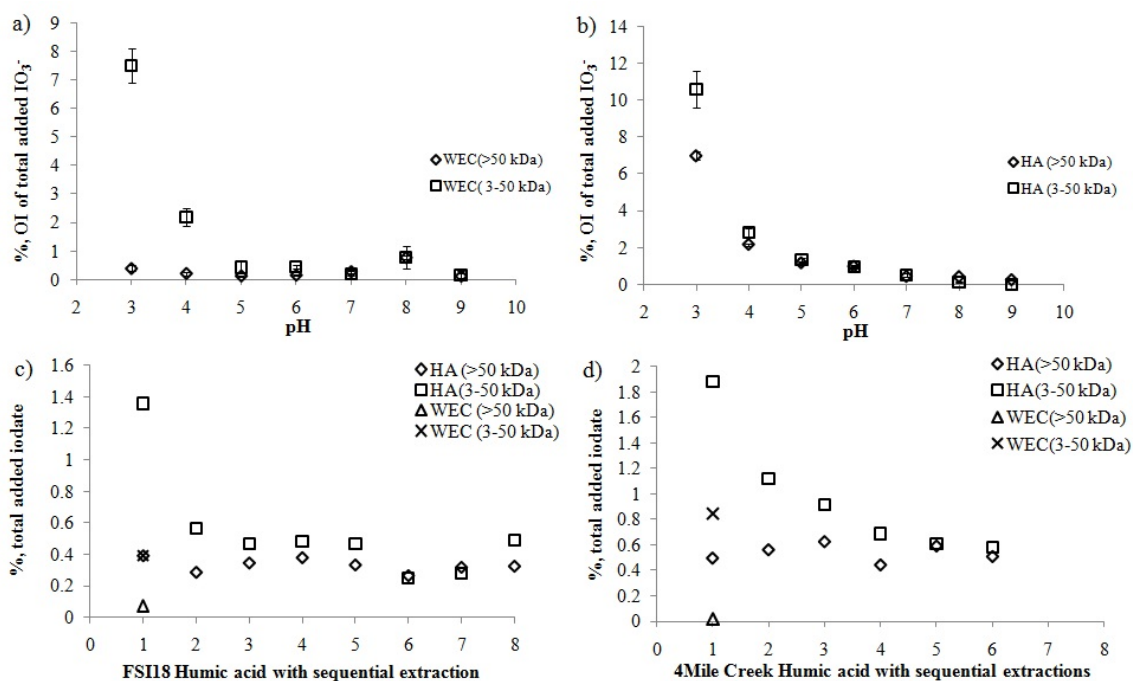
Fig. 3.10 a) pH-dependent iodate incorporation into WEC (WEC, 100 mg/L; reaction time, 72 hours); b) pH-dependent iodate incorporation into HA (HA, 100 mg/L; reaction time, 72 hours);  abiotic incorporation of iodate at pH 5 into humic acids (HAs) obtained by a sequential extraction method and water extractable colloid (WEC) of c) FSI18 soil; d) 4Mile Creek soil (NOM, 100 mg/L; $^{127}IO_3^-$, 0.1 µM; $^{125}IO_3^-$, 0.9 µCi/L, reaction time,72 hours).

As pH 5 is the average value, and the value that is most commonly seen in the groundwater of the F-Area, it was thus chosen for study of the enzymatic-catalyzed iodination between iodide and different HAs obtained by a sequential extraction procedure and WEC from both 4Mile Creek and FSI18 soils, as well as some HAs from IHSS. A significant correlation was found between the iodide uptake and the aromaticity of the different NOM samples (Fig. 3.11a). Laboratory organo-iodine formation starting from iodate was also positively correlated to the aromatic content of the NOM samples at pH 3 and 5 (Fig.3.11b-c). Moreover, naturally-occurring iodine content in these NOM fractions was strongly correlated with the overall aromaticity of the NOM (Xu et al.,

2011a), further strongly suggesting that a covalent aromatic C-I bond accounts for the organo-iodine species formation in the field.
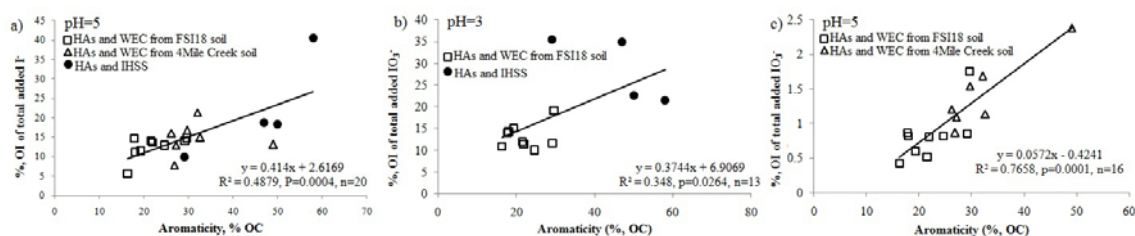


Fig. 3.11 a) pH-dependent iodate incorporation into WEC (HA, 100 mg/L; reaction time, 72 hours); b) relationship between enzymatic catalyzed iodination starting from iodide and aromaticity of NOM at pH 5 (NOM, 100 mg/L; lactoperxidase, 20 μg/ml; $H_2O_2$: 5mM; reaction time, two hours); c) relationship between abiotic iodination starting from iodate and aromaticity of NOM at pH 3 (NOM, 100 mg/L; reaction time, 72 hours); j) relationship between abiotic iodination starting from iodate and aromaticity of NOM at pH 5 (NOM, 100 mg/L; reaction time, 72 hours). For experiments, final [127]I⁻ or [127]$IO_3^-$: 0.1 μM; ^{125}I or [125]$IO_3^-$: 0.9 μCi/L.

**3.4.5 Possible consequences for in-situ site remediation**

Remarkable increases in groundwater [129]I concentrations near the seepage basins over 17 years were ascribed to its minor pH increase of 0.7 (Kaplan et al., 2010). However, [129]I concentrations in the long-term monitored wells downgradient from the seepage basins did not significantly increase in recent years, in contrast to a concurrent significant pH increase by 1-2.5 (Kaplan et al., 2010). One would expect that this pH change would have caused a dramatic [129]I increase in the downgradient groundwater based on desorption experiments described previously (Kaplan et al., 2010). One possible explanation for this discrepancy is that when this groundwater containing

elevated [129]I flows downgradient into the vadose zone and exfiltrates in the surface,

organic-rich soils "scavenge" and immobilize most (~80%, Fig. 3.2a-b and Fig. 3.3a-b)

of the iodine, as was the case for our results with FSI18 soil. In addition, the increase of

pH in groundwater would have made iodate a more favored species, with a much higher

desorption Kd' than that of iodide at ambient concentrations in the oxic organic-rich soil

(1077.11 ml/g vs. 235.69 ml/g, Table 3.3). Moreover, the installation of the barrier wall

increased the groundwater residence time (WRSC, 2006), thus would have increased the

soil-water contact time and allowed the iodine fixation in the soil in the form of organo-

iodine to approach equilibrium (Fig. 3.2a-b). More radioiodine in the permeate (<3 kDa)

would be also transformed into organo-iodine as the contact time increases (Fig. 3.2e-f).

Furthermore, the colloidal organic fraction of the soil leachate, which accounts for 61%

of the total potential mobile [129]I pool (Fig. 3.5), together with the organo-iodine in the

truly dissolved phase, probably altered the transport behavior of mobile iodine species

through the soil column, compared to the mobility of the inorganic iodine species (Hu et

al., 2005; Zhang et al., 2011).


### 3.5 Conclusions

In summary, laboratory iodination of the HA or WEC obtained from F-Area soils

indicates a preferential incorporation of inorganic iodine into NOM at acidic pH (3-4),

except for the iodination catalyzed by lactoperoxidase, which favors a relatively more

alkaline pH values (optimal pH $\geq$5, Fig. 3.6a). It is possible that haloperoxidase

catalyzed iodination can more effectively immobilize radioiodine in the groundwater

aquifers or soil-water systems, when the pH is less acidic (Morrison and Bayse, 1970), while those abiotic iodinations were favored at more acidic pH. The recent in-situ site remediation actions, i.e., soil and geosynthetic capping, base injection and barrier walls, in an effort of increasing the pH and decreasing the flow of the groundwater, has probably not exceeded the natural attenuation capacity toward radioiodine. The organic-rich soil in the vadose zone of F-Area thus acts as a natural "buffer" zone to largely reduce the radioiodine that can be released during remediation actions. As pilot scale new remediation technologies have been in progress, e.g., silver chloride injection into the existing base injection network, continuous assessment of the long-term impact on the iodine speciation and migration for sustainable environmental planning is warranted.

# CHAPTER IV

# THE MOLECULAR ENVIRONMENT OF IODINE IN NATURAL ORGANIC MATTER: EVIDENCE FROM NMR

## 4.1 Overview

$^{129}$I, which is a major by-product of nuclear fission and becomes one of the major radiation risk driver in the Department of Energy (DOE) sites, are present at elevated levels in the surface soils of F-Area of the Savannah River Sites and thought to be bound predominantly to soil organic matter (SOM). Naturally bound $^{127}$I and $^{129}$I of sequentially extracted humic acids (HAs), fulvic acids (FAs) and a water extractable colloid, of which the extraction procedure was to mimic the co-release of organic radioiodine carrier during stormwater or surface runoff events, were determined. Iodine uptake partitioning coefficients (Kd) of all these SOM samples at ambient iodine concentrations were also measured. Quantitative structure analysis by $^{13}$C DPMAS NMR and solution state $^{1}$H NMR on these humic substances indicate that iodine is closely related to the aromatic regions containing esterified products of phenolic and fomic acid or other aliphatic carboxylic acids, amide functionalities, quinone-like structure activated by electron-donating groups (e.g., $NH_2$), or hemicelluloses-lignin-like complex with phenyl-glycosidic linkage. The contrasting radioiodine contents among the three types of SOM (HAs, FAs and WEC), which cannot be solely explained by the difference in the amount of their reactive binding sites, indicate that the micro-molecular environment, such as the hydrophobic aliphatic periphery hindering the active aromatic cores and the

hydrophilic polysaccharides favoring its accessibility towards hydrophilic iodine species, play another key role in the interactions between iodine and SOM. This study by the means of NMR techniques, for the first time, reveals the nature of iodine binding to natural organic matter at ambient concentrations.

## 4.2 Introdution

Radioiodine, $^{129}$I, can be produced by the fission of $^{238}$U and released anthropogenically during bomb testing, nuclear fuel reprocessing or nuclear accidents (e.g., Chernobyl reactor). For example, from 1944 through 1972, the plutonium-production operation at the Hanford Site in Washington released about 266 kg of $^{129}$I into the air while the operation of production reactors in the Savannah River Site (SRS) in South Carolina released about 32 kg of $^{129}$I into the air from 1953 to 1990. Moreover, the geological depository for storing high-level nuclear waste at Yucca Mountain of Nevada will reach as much as 13,300 kg $^{129}$I based on the proposed storage of 70,000 tons of nuclear waste. By contrast, the man-made $^{129}$I release has overwhelmed the natural inventory (~100-260 kg) up to now (Schwehr et al., 2005). Its long half-life and high perceived mobility, the large inventory in some DOE sites (e.g., 26 Ci at the SRS), and its biophilic properties as an essential nutrient that concentrates in human thyroid, lead the maximum contaminant level, MCL, of $^{129}$I in groundwater to be the lowest among all radionuclides (1 pCi/L). Therefore, it has recently been recognized by the U.S. Department of Energy's Office of Environmental Management (DOE-EM) as a high risk radionuclide in groundwater at these DOE sites such as the SRS (Denham et al., 2009).

F-Area at the SRS was a radionuclide separation facility for the production of nuclear weapons between 1955 and 1988, during which large amounts of radionuclides were disposed, including $^{129}$I. Even though $^{129}$I makes up only a very small portion (~0.00002%) of the total radiological release from the site, it contributes 13% to the offsite population dose. This is a six orders magnitude higher risk than that of any other radionuclide (Kaplan et al., 2011). Thus, it needs to be considered not only as a major risk driver for DOE, but also as a potential threat to the environment and human health.

The dominant iodine species existing in the natural environment are iodide (I$^-$), iodate (IO$_3^-$) and organo-iodine (OI). Compelling evidence has shown the intimate relationship between iodine species and natural organic matter in the soil or aquatic systems (Francois, 1987; Keppler et al., 2004; Schlegel et al., 2006; Gallard et al., 2009; Schwehr et al., 2009; Yamaguchi et al., 2010; Xu et al., 2011a) which significantly alters its behavior and the resulting toxicity in the environment (Hu et al., 2005; Zhang et al., 2011; Otosaka et al., 2011; Xu et al., 2011b). On one hand, the transport of radioiodine was greatly retarded by the presence of organic matter in the soil or aquifer sediment (Hu et al., 2005; Schwehr et al., 2009; Zhang et al., 2011); while on the other hand, both field sampling and laboratory batch or column experiments discovered significant portion of the mobile radioiodine is in the form of organic species, contradicting to the conventional wisdom that only considers iodide (or iodate to some extent) as the mobile species (Xu et al., 2011 a,b). However, giving the challenge concerning the ananlysis of various organoiodine compounds, scarce studies up to date have provided in-depth information about the physic-chemical aspects of the molecular environment of iodine in

these iodinated organic moieties, addressing to questions such as why some organo-iodine species behave immobile and act as radioiodine "landfill" while some others can carry the radioiodine around under certain conditions (Hu et al., 2005; Zhang et al., 2011; Xu et al., 2011a,b). Recently, X-ray absorption near-edge structure (XANES) can provide information on the oxidation state, electronic structure, and chemical environment of iodine (e.g., whether iodine is bound to aliphatic carbon or aromatic carbon) in natural organic matter, while the extended X-ray absorption fine structure (EXAFS) can provide insight into the nature and distance of neighboring atoms, provided that the iodine content is artificially increased to ease detection. Iodine K-edge XANES is usually applied to explore the molecular environment of iodine in crude soil and aqueous samples with a lower detection limit to avoid the disturbance from the abundant $Ca^{2+}$ present, while $L_{III}$-edge XANES can provide better resolution for purified iodinated natural organic matter. Still, the above techniques can only generally tell whether iodine is in the form of organo-iodine in the crude soil or aqueous samples (Yamaguchi et al., 2010; Shimamoto et al., 2011) or indicate that iodine is bound to the aromatic carbon in purified iodinated humic substances by comparing its spectra to those of model compounds (Schlegel et al., 2006). Therefore, the objectives of this study are two-fold: 1) to chemically characterize and explore the molecular environment of radioiodine associated NOM extracted from the contaminated soil of the SRS, and 2) the relevance to their capability of incorporating iodine in the environment by the comparison between radioiodine organic "sink" and "carrier". Nuclear magnetic resonance spectroscopy (NMR) was applied to investigate the humic acids (HAs), fulvic

acids (FA) and water extractable colloid (WEC) that were obtained from a heavily-contaminated soil (FSI18) of F-Area in the SRS, and determined to contain various amounts of $^{127}$I and $^{129}$I previously (Xu et al., 2011a). Specifically, sequentially-extracted HAs as the major fraction of the soil organic matter (SOM) (~33% of the total organic carbon in the soil) accounts for ~40% and 33% of the total $^{127}$I and $^{129}$I pool in the soil, while sequentially-extracted FAs contributes ~14% and 13%, respectively, leaving the rest likely to be ascribed to soil residual organic matter (e.g., humin) or mineral phases. The WEC fraction was obtained by re-suspending the whole soil in artificial freshwater (Martin and Whitfield, 1983) and then size-fractioning the soil leachate by centrifugation, filtration and ultrafiltration steps to collect the 0.45 µm to 1 kDa fraction, of which the effort was to mimic the potentially co-releasing of radioiodine with colloidal organic matter during groundwater exfiltration (upwelling with contaminated radioiodine, as occurs at F-Area wetlands), surface runoff and stormflow events. $^{129}$I in the colloidal fraction of the soil leachate has greatly exceeded the drinking water limit issued by EPA (1015(±129) pCi/L vs. 1 pCi/L), and accounted for ~9-15% of the soil total $^{129}$I amount (Xu et al., 2011a, b). Thus unraveling these organo-iodine "sinks" and potential mobile "vector" will help to understand and predict better the biogeochemical cycle of radioiodine in those DOE sites and provide the basis for site remediation planning. To our best knowledge, this is the first time NMR techniques were employed to investigate these radioiodine associated SOM and to study the relevance of different organic mass components (or moieties) in affecting radioiodine binding at ambient

concentration level.

### 4.3 Materials and methods

### 4.3.1 Extraction of humic acids (HAs), fulvic acids (FAs) and water extractable colloid (WEC)

Sampling of the soil from the F-Area in the SRS and details for obtaining the HAs, Fas and WEC was described in Xu et al. (2011a). Briefly, Five HA fractions were obtained by repeatedly extracting the same soil five consecutive times following a standard procedure recommended by IHSS (Swift, 1996), and the HAs and Fas extracted were named HA1, HA2,…, HA5 and FA1+2, FA3+4, …, FA9+10, respectively. The soil residue, after five times of HA and FA extraction, and saturation with NaOH, was dried overnight in an oven at 50-60 ºC, then homogenized by grinding. Three more fractions were obtained by twice extracting the residue with 50% glycerol followed by removal of major cations (e.g., Fe) through complexation with 0.5 M citric acid, and extraction one additional time with 0.1 M NaOH (Baglieri et al., 2007). The three HA fractions were named as HA6, HA7 and HA8. Thus the first five HAs and Fas probe the SOM that are loosely bound to the soil mineral and thus can be more easily released under alkaline/acid extraction conditions. Glycerol has the ability of penetrating into the interlayers of the phyllosilicates and thus releasing any HS still trapped in the interlayers. Citric acid was used to complex iron or other major cations, which are involved in the formation of HS-metal-clay complexes, and make the HA accessible to the extraction solvent (NaOH).

To collect WEC, the moist soil was dispersed in artificial freshwater to reach a final concentration of 5 g-dry soil/ L and shaken very gently at 150 rpm on an orbital shaker for three days (Xu et al., 2008). Later, the soil resuspension was centrifuged for 30 minutes at $3200 \times$ g, and the supernatant was successively filtered through 10 μm and 0.45 μm cartridge filters. Filtration was followed by cross-flow ultrafiltration, utilizing a spiral-wound 1kDa SOC 1812 cartridge (Separation Engineering, Inc.), until 1L retentate remained. The retentate was diafiltered against 20 L Milli-Q until it was concentrated to 1 L. Then, the cartridge was rinsed with 250 mL Milli-Q water with the pump on for 30 min, and then the pump was turned off. The cartridge was allowed to soak for four hours or more. The cartridge was consequently rinsed with another 250 mL of Milli-Q water, and the procedure was repeated twice or more until the rinse water became clear. The retentate and rinse solution were then subsequently combined and concentrated utilizing an Amicon 8400 stirred-cell ultrafiltration unit with a 1 kDa regenerated cellulose filter. The retentate was freeze-dried for further radioiodine analysis and chemical characterization.

## 4.3.2 Laboratory iodination of the natural organic matter (NOM) obtained from the soil

HA, FA and WEC samples were reacted with $I^-$ or $IO_3^-$ under different conditions. Briefly, NOM samples were first dissolved in 20 mM Tris-HCl buffer to achieve maximum dissolution (pH ~8, 1mg/mL), and diluted at desired concentrations with artificial freshwater. Different buffers (e.g., phosphate buffer or acetic acid buffer) were

added to adjust the pH to 3 or 5 of the reaction systems for different purposes. The ionic

strength of the final solution was maintained around 3-6 mM to mimic that of the soil

porewater. $^{127}I^-$ (or $^{127}IO_3^-$) and 0.9 μCi/L of $^{125}I^-$ (or $^{125}IO_3^-$) were well mixed to achieve

good equilibrium and then added to the reaction vessels. The solution mixture was

shaken in darkness to reach equilibrium. Molecular weight of HA and WEC samples

extracted from FSI18 and 4Mile Creek soils were determined to be larger than 3 kDa

(Xu et al., 2011a), thus Amicon Ultra-4 centrifugal filter units with a cutoff size of 3 kDa

were applied to separate the un-bound $I^-$ or $IO_3^-$ from the iodinated HA or WEC fractions;

while the Microsep centrifugal device with a cutoff of 1 kDa (Pall Corporation, USA)

was applied for removal of free $I^-$ or $IO_3^-$ from iodinated FA. The amounts of $I^-$ or $IO_3^-$

incorporated into HA or WEC were determined by measuring the activity of the retentate

with a LS 6500 Multi-Purpose Scintillation Counter (Beckman Coulter, USA). The

amount of iodine bound to HA or WEC was normalized to the initial total added

concentration. Formation of volatile iodine species (e.g., $I_2$ or methyl iodine) was

estimated based on the mass-balance comparison between the total iodine content (as $^{125}I$

activity or $^{127}I$ measured by combustion and GC-MS analysis) in the reaction vessel at

the time of collection and that of total initially added amount.

### 4.3.3 Nuclear Magnetic Resonance (NMR) spectroscopy

### 4.3.3.1 Solution-state NMR analysis

The eight HAs, FA(1+2), FA(3+4) and WEC were dissolved at a concentration of

~36 mg/mL in 0.5 N NaOD/$D_2$O solution. Solution state $^1$H-NMR spectra were acquired

at Bruker Avance III 400 MHz NMR equipped with 5mm inverse probe (Bruker-biospin, Billerica, MA). Experiments were performed with a 90º pulse program with an acquisition time of 0.60 s, 640 scans and a relaxation delay of 2s. Complete water suppression was achieved by inserting a water-selective shaped pulse train during recycle delay and gradient-tailored excitation pulses before the data acquisition. Solution state gradient enhanced $^1$H-$^{13}$C Heteronuclear Single Quantum Coherence (HSQC) NMR was only acquired for HA1, FA(1+2) and WEC.

### 4.3.3.2 Solid-state NMR analysis

Direct-polarization 13-kHz magic-angle spinning (DPMAS) $^{13}$C NMR spectra were obtained on a Bruker Avance II 400 MHz NMR spectrometer (Bruker-biospin, Billerica, MA) using the following procedures and optimized parameters: samples were placed in a 4 mm rotor and spun at a frequency of 12.4 KHz at the magic angle (54.7º to the magnetic field); the spectra were acquired with the direct polarization pulse sequence; spectral width was 355 ppm; and line broadening was set to10 Hz. The chemical shifts were referenced to the carboxyl signal of glycine as an external standard (176.03 ppm).

## 4.4 Results and discussion

### 4.4.1 Iodine uptake partitioning coefficients

HA1, the first in the sequential extraction queue and most abundant HA of all humic substances extracted from the contaminated soil, scavenges ~25% and 20% of the total stable iodine and radioiodine in the soil, respectively, and accounts for ~ 17% of the total

carbon in the soil (data re-calculated from Xu et al. (2011a)). The iodine ($I^-$ or $IO_3^-$) uptake isotherm experiment conducted with HA1 showed increasing Kd values with decreasing concentrations of applied iodine (Fig. 4.1), which indicates either transformation of $I^-$ or $IO_3^-$ into reactive species or the following capture by the active sites in the SOM is the limiting step for organo-iodine formation. Consistent results were found in Schwehr et al. (2009), in which a linear regression was found between log Kd and the log of $I^-$ concentrations for a Savannah River Site subsurface sediment with an organic carbon of 8.4%. It was more likely related to the different rate constants of various reactive binding sites, since the preferred reactive binding sites for iodine to "attack" might become more and more limited when applied iodine concentration is increasing to the laboratory levels.

Based on the uptake Kd values of $I^-$ or $IO_3^-$ of the first HA and FA in the sequential extraction queue (and thus most abundant), as well as WEC (Fig. 4.2), the target humic materials can be arranged in the descending order: HA> WEC> FA for both iodide amendment through enzymatic iodination, and iodate through abiotic iodination. The factors contributing to the difference between the uptake partitioning coefficients for various SOM are probably directly related to the differences in chemical composition and state of aggregation, and also to the relative varying abundance of key subcomponents. Hence, establishing structure-iodine binding relationship through the molecular level spectroscopic methods is warranted.
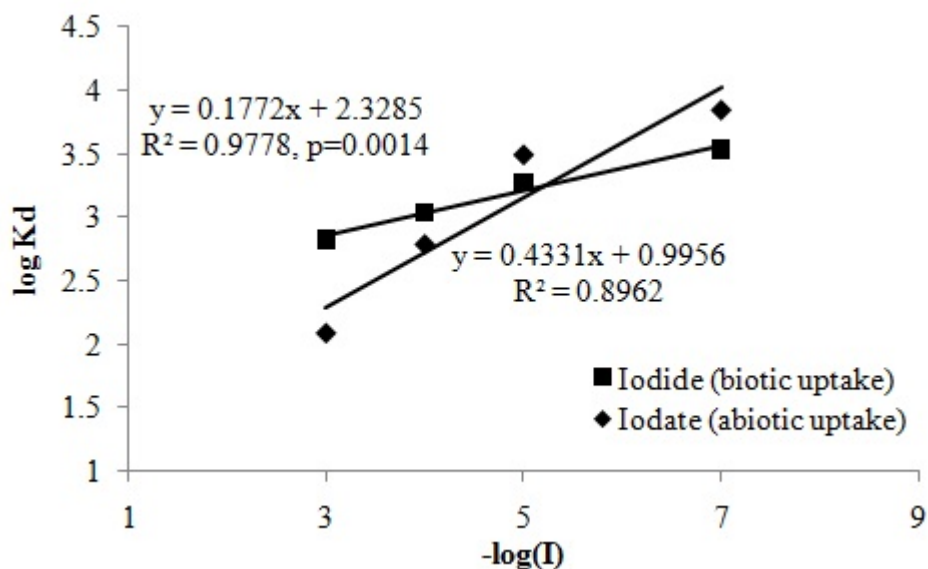
Fig. 4.1 Log Kd values of iodide or iodate uptaken by humic acid (HA1) extracted from Savannah River Site contaminated surface soil, as a function of concentrations of amended iodide or iodate. Black circle represents the ambient concentration ($10^{-7}$M). Duplicates for each concentration gradient are conducted and errors are less than 10%. For iodide amendment group, lactoperoxidase, 20 $\mu$g/ml, $H_2O_2$, 5mM; for iodate amendment group, no enzyme was added. HA concentration, 500 mg/L, $^{127}I^-$ or $^{127}IO_3^-$ in units of molarity; $^{125}I$ or $^{125}IO_3^-$: 0.9 $\mu$Ci/L, well equilibrated with stable iodine before addition. Reaction time for $I^-$ amendment group is 2 hours and for $IO_3^-$ amendment group is 72 hours.
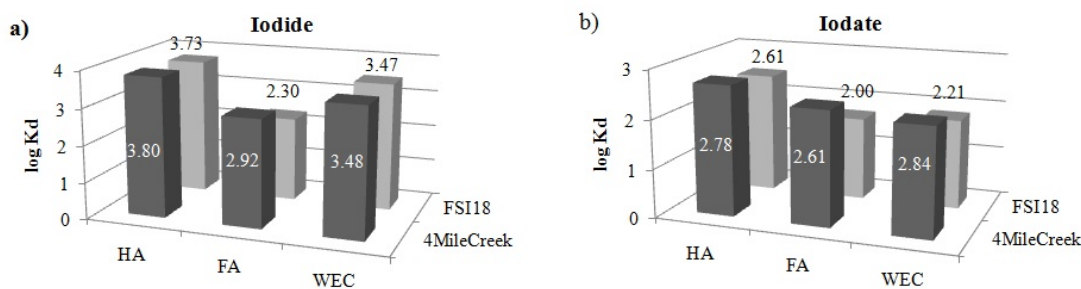
Fig. 4.2 Log Kd values of representative HA, FA and WEC extracted from the uncontaminated soil (4MileCreek) and the contaminated soil (FSI18) of F-Area in Savannah River Site. Replicates were conducted and the errors are mostly well within 1%, thus making the differences among groups significant. For iodide amendment group, lactoperoxidase, 20 µg/ml, $H_2O_2$, 5mM; for iodate amendment group, no enzyme was added. HA concentration, 100 mg/L, $^{127}I^-$ or $^{127}IO_3^-$ concentration, 0.1 µM; $^{125}I$ or $^{125}IO_3^-$: 0.9 µCi/L, well equilibrated with stable iodine before addition. Reaction time for $I^-$ amendment group is 2 hours and for $IO_3^-$ amendment group is 72 hours.

## 4.4.2 $^{13}$C solid state DPMAS NMR spectra and $^1$H solution state NMR spectra of sequential extracted HAs, FAs and WEC

DPMAS NMR spectra of the different HAs, FAs and WEC as well as the peak assignments were shown in Fig. 4.3. The estimated relative percentage of the peak areas are presented in Table 4.1. In general, the peak areas for DPMAS spectra can be divided into several main regions: aliphatic C ($C_{Alk-H,C}$, 0-60 ppm), hetero-aliphatic carbons primarily bonded to oxygens (60-96 ppm), anomeric carbon in carbohydrate (or aromatic carbon neighboring phenolic carbons, 96-108 ppm), aromatic carbon ($C_{Ar-H,C}$, 108-145 ppm), phenolic carbon ($C_{Ar-O}$, 145-162 ppm), carboxylic acid, ester, amide, quinone, and lactone carbon ($C_{COO}$, 162-190 ppm), and carbonyl carbon ($C_{CO}$, 190-220 ppm) primarily from ketone carbons with some overlap of quinone carbons. In the following

discussion, hetero-aliphatic carbons bonding to oxygens (60-96) and the anomeric

carbons were also sometimes combined as $C_{Alk-O}$.
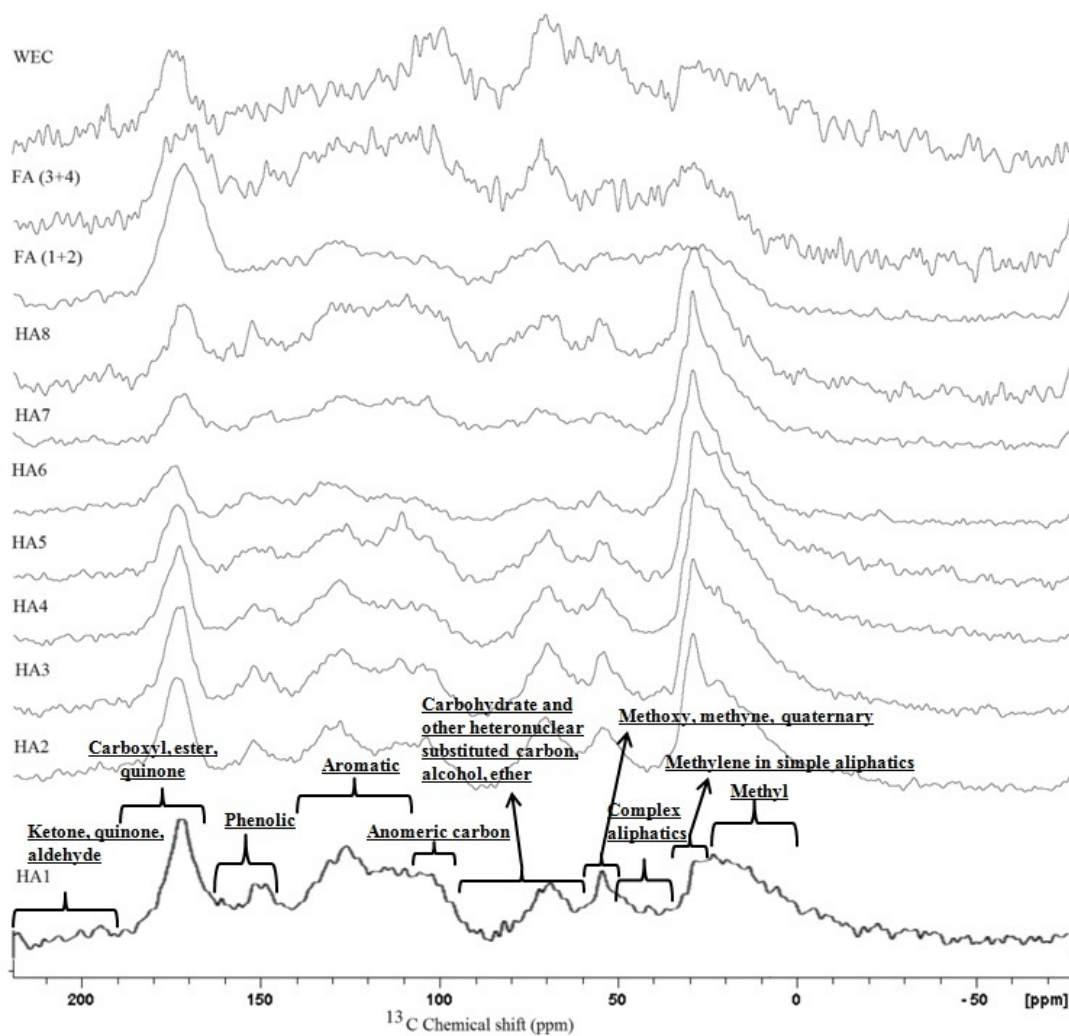


Fig. 4.3 DPMAS NMR spectra of sequentially extracted humic acids (HAs), fulvic acids (FAs) and water extractable colloid (WEC).

Table 4.1 DPMAS NMR spectral assignments and integration (%).

| Chemical shift (ppm) | 0-25 | 25-35 | 35-50 | 50-60 | 60-96 | 96-108 | 108-120 | 120-145 | 145-162 | 162-190 | 190-220 |
|---|---|---|---|---|---|---|---|---|---|---|---|
| | methyl | methylene in simple aliphatics | complex aliphatic | methoxy, methyne, quaternary | Saccharide alcohol ether | anomeric, aromatic carbon neighboring phenolic carbons | aromatic | aromatic | phenolic | carboxyl, ester, quinone | ketone, quinone, aldehyde |
| HA1 | 24.48 | 9.11 | 8.99 | 7.90 | 9.64 | 2.35 | 2.32 | 12.84 | 2.34 | 14.10 | 5.94 |
| HA2 | 26.53 | 15.48 | 7.62 | 8.03 | 13.55 | 1.49 | 1.90 | 8.15 | 2.59 | 9.65 | 5.03 |
| HA3 | 29.68 | 14.68 | 6.78 | 7.15 | 12.81 | 2.72 | 1.37 | 7.32 | 2.95 | 10.71 | 3.81 |
| HA4 | 29.93 | 14.12 | 4.92 | 6.33 | 14.19 | 2.47 | 2.41 | 6.31 | 4.15 | 9.79 | 5.38 |
| HA5 | 30.37 | 15.26 | 4.85 | 5.76 | 10.61 | 3.07 | 2.45 | 7.85 | 5.66 | 8.45 | 5.67 |
| HA6 | 25.51 | 23.22 | 7.05 | 5.56 | 9.77 | 2.00 | 2.62 | 4.34 | 3.31 | 8.55 | 8.07 |
| HA7 | 25.66 | 24.77 | 5.25 | 5.43 | 7.63 | 2.66 | 3.14 | 8.27 | 2.67 | 7.45 | 7.06 |
| HA8 | 19.50 | 20.46 | 9.49 | 9.16 | 9.38 | 3.14 | 4.02 | 9.14 | 2.38 | 9.68 | 3.64 |
| FA1+2 | 9.43 | 12.19 | 15.50 | 9.47 | 8.25 | 1.34 | 5.25 | 5.74 | 2.66 | 26.05 | 4.12 |
| FA3+4 | 11.16 | 14.32 | 14.23 | 10.47 | 9.90 | 5.61 | 2.21 | 12.30 | 2.17 | 11.58 | 6.03 |
| WEC | 11.55 | 5.13 | 7.12 | 5.97 | 20.32 | 7.81 | 6.03 | 10.80 | 5.94 | 11.58 | 7.75 |
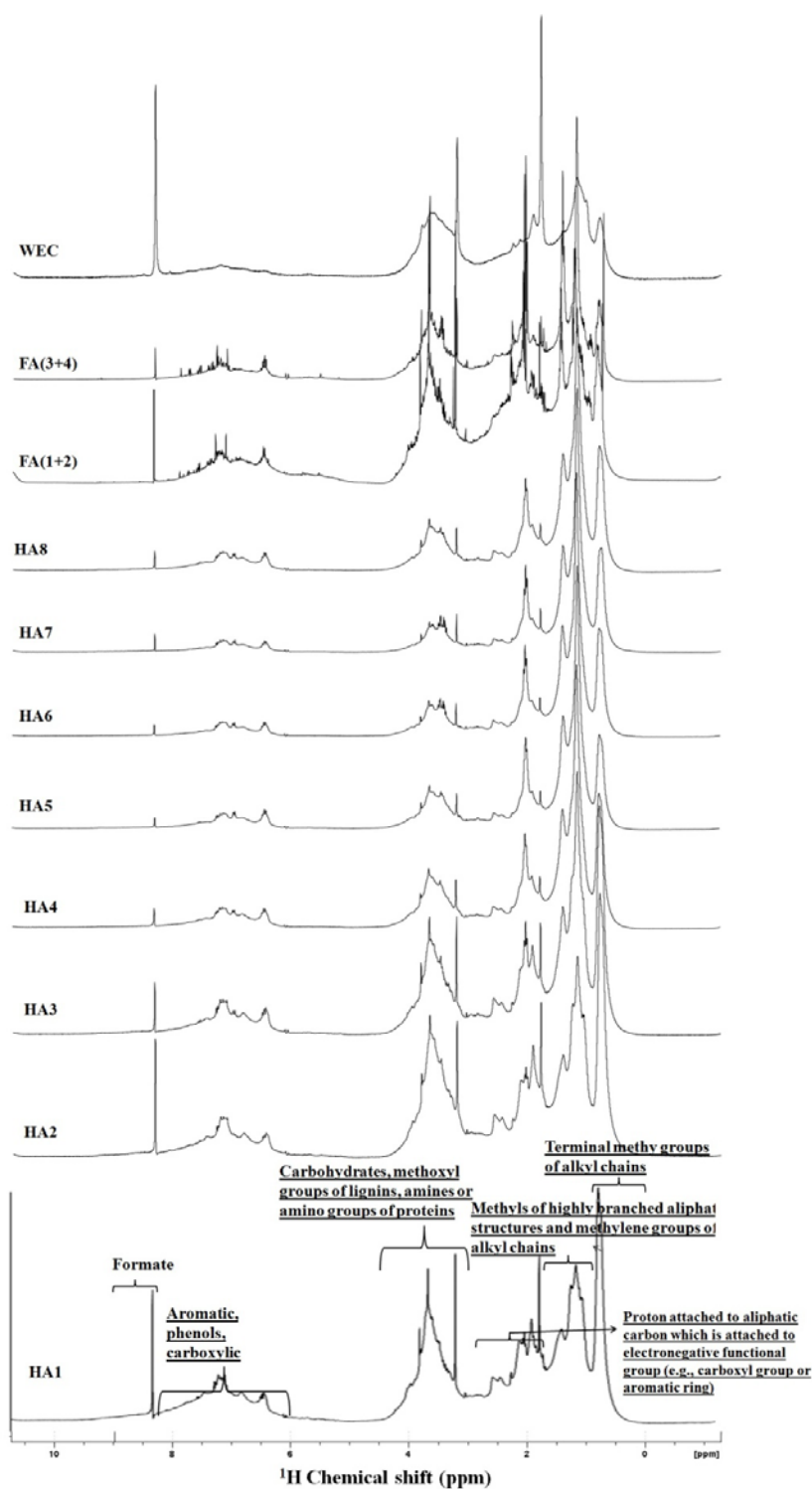
Fig. 4.4 Solution state 1D $^1$H NMR spectra of sequentially extracted humic acids (HAs), fulvic acids (FAs) and water extractable colloid (WEC).

Solution state $^1$H NMR spectra of different SOM and their estimated relative percentage by peak integration were shown in Fig. 4.3 and Table 4.2, respectively. The main proton functionalities can be grouped into: 1) aliphatic region ($H_I$, 0-1.67 ppm, also sub-grouped into 0-0.9 and 0.9-1.67ppm); 2) protons on carbon which is attached to electronegative functional group (e.g., carboxyl group or aromatic ring) ($H_{II}$, 1.67-3.0 ppm); 3) protons on carbon directly bonded to O, N, or carbohydrates ($H_{III}$, 3.0-4.5 ppm); 4) protons on aromatic rings ($H_{IV}$, 6.0-8.25 ppm); 5) protons in the formate ($H_V$, 8.25-9.0).

Table 4.2 Solution state 1D $^1$H NMR spectral assignment and integration.

| | 0-1.67 | | 1.67-3 | 3-4.5 | 6.0-8.25 | 8.25-9 |
|---|---|---|---|---|---|---|
| | I* | | II | III | IV | V |
| | 0-0.9 | 0.9-1.67 | | | | |
| HA1 | 23.35 | 17.61 | 10.75 | 26.26 | 20.62 | 1.40 |
| HA2 | 23.77 | 20.26 | 11.66 | 28.55 | 14.60 | 1.16 |
| HA3 | 21.79 | 28.69 | 10.27 | 24.24 | 14.50 | 0.51 |
| HA4 | 18.78 | 37.68 | 12.82 | 18.47 | 11.96 | 0.29 |
| HA5 | 16.33 | 42.65 | 12.45 | 16.33 | 12.04 | 0.20 |
| HA6 | 18.51 | 44.73 | 11.43 | 13.28 | 11.74 | 0.31 |
| HA7 | 18.71 | 47.18 | 12.14 | 13.25 | 8.59 | 0.14 |
| HA8 | 18.56 | 40.32 | 11.72 | 17.08 | 11.99 | 0.34 |
| FA(1+2) | 15.59 | 18.00 | 22.81 | 29.18 | 14.16 | 0.26 |
| FA(3+4) | 13.30 | 29.24 | 17.13 | 28.30 | 11.75 | 0.28 |
| WEC | 13.38 | 19.81 | 17.77 | 36.26 | 7.27 | 5.51 |

*$I_{0-0.9}$: Terminal methyl groups of alkyl chains; $I_{0.9-1.67}$: Methyls of highly branched aliphatic structures and methylene groups of alkyl chains: II: Proton on carbon which is attached to electronegative functional group (e.g., carboxyl group or aromatic ring): III: Carbohydrates, methoxyl groups of lignins, amines or amino groups of proteins; IV: Aromatic, phenols, carboxylic; V: formate.

Correlation with the naturally bound $^{127}$I and $^{129}$I, and laboratory determined uptake

Kd at ambient iodine concentration (0.1 μM) of the sequentially extracted HAs were

individually evaluated for different carbon functionalities as well as some combined

variables (Table 4.3 and 5.4). Those combined variables, suggested by Perminova et al.

(1999), are possibly better in revealing the interaction features within the chemical

structure of humic substances than individual variable. Only combined variable with

strong correlation was shown for brevity. Interestingly, naturally bound $^{127}$I, $^{129}$I and

laboratory uptake Kd were consistently negatively couple with the aliphatic carbon

abundance.  Aromatic moieties, which were thought to be the binding sites for iodine, do

not show any significant correlation, except for the laboratory uptake Kd values. This

can be explained by the decreasing signal-to-noise ratios and the loss of resolution in the

aromatic region of the $^{13}$C NMR spectra (108-162 ppm) with the latter extracted HA

fractions (Fig. 4.3), thus leading to inaccurate estimation about the aromatic carbon.

Moreover, compared to $^1$H NMR, $^{13}$C NMR tends to misrepresent potentially available

binding sites for iodine substitution due to the poly-condensated aromatic ring structure.

The degree of humification, measured by fluoresences emission scanning spectroscopy

(excitation at 465 nm) (Rosa et al., 2005), decreased with the extraction sequence and

confirmed these successively extracted humic material had different extents of

condensation (Xu et al., 2011a). It should be also noted that the region with a chemical

shift range of 3-4.5 ppm in the $^1$H NMR spectra was often regarded as resonance from

carbohydrate protons. Total carbohydrates measured by an acid hydrolysis and TPTZ

spectrophotometric method (Xu et al., 2011a) of the eight HAs, two FAs and WEC

samples have a significant correlation with the integrals in this region (Table 4.3, n=11,

$R^2$=0.78, p=0.000), whereas a lack of linear relationship between anomeric carbon and

the colormetrically measured values can be explained by the loss of resolution in the

anomeric carbon region in $^{13}C$ NMR spectra of the latter extracts. Among all the

individual and combined variables, the strongest correlations with naturally bound $^{127}I$,

$^{129}I$ and laboratory Kd were observed for carbon functionality with chemical shift of

162-190 ppm ($C_{COO}$) and the product of $C_{Ar-H,C}$ and $C_{COO}$.

Table 4.3 Naturally bound $^{127}I$, $^{129}I$ content, laboratory Kd of iodate, N/C ratios and total carbohydrates (%, OC) (Xu et al., 2011a) for different humic acids (HAs), fulvic acids (FAs) and water extractable colloid (WEC).

| | $^{127}I$/C | $^{129}I$/C | Kd | N/C | TCHO |
|---|---|---|---|---|---|
| | μg/g-C | μg/g-C | ml/g | $\times 10^{-2}$ | %, OC |
| HA1 | 112.30 | 6.74 | 406 | 6.33 | 8.93 |
| HA2 | 78.29 | 4.93 | 207 | 6.63 | 7.50 |
| HA3 | 61.85 | 4.76 | 196 | 6.11 | 7.14 |
| HA4 | 59.10 | 4.53 | 201 | 5.62 | 6.63 |
| HA5 | 26.98 | 2.98 | 186 | 4.92 | 5.65 |
| HA6 | 26.82 | 1.89 | 114 | 5.07 | 4.29 |
| HA7 | 34.23 | 3.69 | 133 | 4.79 | 3.52 |
| HA8 | 33.05 | 3.97 | 190 | 5.08 | 5.95 |
| FA1+2 | 603.56 | 44.12 | 99 | 4.22 | 16.69 |
| FA3+4 | 518.79 | 32.32 | 96 | 4.68 | 15.65 |
| WEC | 1473.29 | 120.98 | 163 | 5.95 | 22.33 |

Table 4.4 Correlations between the naturally bound $^{127}$I, $^{129}$I and laboratory determined uptake Kd (g/ml) of iodate at pH 5 (iodate concentration: 0.1 μM) and different individual or combined carbon functionalities for sequentially extracted humic acids.

| Functional group | Chemical shift (ppm) | $^{127}$I /C µg/g-C | | $^{129}$I/C µg/g-C | | | | Kd (g/ml) | |
|---|---|---|---|---|---|---|---|---|---|
| | | $R^2$ | P | $R^2$ | p | $R^2$ | p | | |
| $C_{Alk-H,C}$ | 0-60 | -0.610 | -* | -0.607 | - | -0.871 | - | | |
| $C_{Alk-O}$ | 60-108 | 0.055 | - | 0.053 | - | 0.003 | - | | |
| $\Sigma C_{Alk}$ | 0-96 | -0.289 | - | -0.339 | - | -0.715 | - | | |
| $C_{Ano}$ | 96-108 | -0.189 | - | -0.020 | - | -0.004 | - | | |
| $C_{Ar-H,C}$ | 108-145 | 0.226 | - | 0.420 | - | 0.523 | 0.028 | | |
| $C_{Ar-O}$ | 145-162 | -0.186 | - | -0.209 | - | -0.066 | - | | |
| $\Sigma C_{Ar}$ | 108-162 | 0.100 | - | 0.243 | - | 0.449 | 0.048 | | |
| $C_{COO}$ | 162-190 | 0.774 | 0.030 | 0.711 | - | 0.882 | 0.000 | | |
| $C_{C=O}$ | 190-220 | -0.043 | - | -0.196 | - | -0.056 | - | | |
| $C_{Ar-H,C} \times C_{COO}$ | (108-145)×(162-190) | 0.576 | 0.017 | 0.665 | 0.007 | 0.890 | 0.000 | | |

*"-"p values were not reported

In contrast, $^1$H NMR spectra provides more information with enhanced sensitivity (Fig. 4.4). Similarly, naturally bound iodine ($^{127}$I and $^{129}$I) and laboratory Kd negatively vary with aliphatic protons. Strong correlations were found between the three iodine parameters and aromatic protons, respectively. A sharp peak in the lower field ($H_V$) consistently occurring at 8.25-9.0 ppm and generally decreasing with the extraction sequence possibly arises from the proton of the formate functional group (H-COO⁻) (Gillam and Wilson, 1985). Interestingly, more significant correlation with the naturally bound iodine ($^{127}$I and $^{129}$I) was observed for the abundance of formate proton, than those for the aromatic protons; while with the laboratory determined uptake Kd, aromatic protons have a higher square of correlation coefficients ($R^2$) (Table 4.4).

While one might argue that the limited data points in this study possibly bias these comparisons (n=8), it is still believed that some reactive binding sites in these HAs are preferentially occupied by the naturally occurring iodine, leaving the secondary (or less) preferentially binding positions for the more recently introduced iodine.

The combined variable, $H_{III} \times H_{IV}$, was strongly and positively correlated to the three iodine parameters, might possibly have two-fold indications. One one hand, carbohydrate component connencting to aromatic ring likely increases the hydrophilicity of aromatics, which are supposed to be hydrophobic and thus not easily accessible to hydrophilic iodine species. One the other hand, iodine might be partially associated with the hemicelluloses-lignin like complexes, which were the degradation products that are commoly formed during woody terrestrial plants lignin deposition taking place in the hemicelluloses matrix of the cell walls (Wershaw, 2004). This is further confirmed by the strong correlation between the abundances of aromatic protons and carbohydrate protons from solution state NMR spectra ($R^2$=0.459, p=0.0155, n=11) as well as the correlation between the abundances of spectrophotometrically measured carbohydrates (Table 4.3) and aromatic protons obtained from NMR spectra ($R^2$=0.4729, p=0.0139, n=11).

Strongest statistical relevances to the three iodine parameters (naturally bound [127]I, [129]I and laboratory determined iodine uptake Kd) were observed for $H_{IV}/H_I$ ratios, which represent the relative prevalence of aromatic core over aliphatic periphery, or a hydrophilic-hydrophobic balance of the humic substances (Perminova et al., 1999).This can be indicative of accessibility of hydrophilic iodine species toward the active

aromatic sites which was controlled by the interaction of these two components. Humic

material was recently regarded as the aggregate of diverse, relatively low molecular

mass components forming dynamic assembly intimately stabilized by hydrogen bonding

and hydrophobic interactions, such that they are not easily and effectively separated by

chemical or physical methods. The different arrangement of these mass components,

e.g., hydrophobic aliphatic moieties versus hydrophilic aromatic moieties, plays a key

role in determining the covalent binding of iodine to SOM, besides the abundance of the

active aromatic sites.

Table 4.5 Correlations between the naturally bound $^{127}$I, $^{129}$I and laboratory determined uptake Kd (g/ml) of iodate at pH 5 (iodate concentration: 0.1 µM) and different individual or combined proton functionalities for sequentially extracted humic acids.
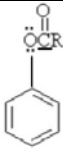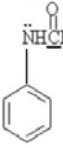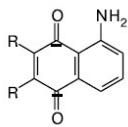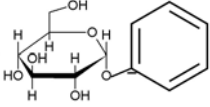
| Functional group | Chemical shift | $^{127}$I /C µg/g-C | | $^{129}$I/C µg/g-C | | Kd | |
|---|---|---|---|---|---|---|---|
| | ppm | $R^2$ | P | $R^2$ | p | $R^2$ | p |
| I | 0-1.67 | -0.853 | - | -0.714 | - | -0.660 | - |
| II | 1.67-3 | -0.219 | - | -0.160 | - | -0.152 | - |
| III | 3-4.5 | 0.741 | 0.003 | 0.650 | 0.009 | 0.452 | 0.047 |
| IV | 6.0-8.25 | 0.786 | 0.002 | 0.608 | 0.013 | 0.843 | 0.001 |
| V | 8.29-8.45 | 0.838 | 0.001 | 0.617 | 0.012 | 0.648 | 0.009 |
| $H_{III} \times H_{IV}$ | | 0.892 | <0.001 | 0.739 | 0.003 | 0.745 | 0.003 |
| $H_{IV}/H_I$ | | 0.883 | <0.001 | 0.701 | 0.005 | 0.848 | <0.001 |

The concurrent significant correlations with the three iodine parameters for both

carbon abundance in the 162-190 ppm region of $^{13}$C NMR spectra and the proton

abundance in the 6-8.25 ppm or 8.25-9.0 ppm region of $^1$H NMR spectra suggest that

iodine might be closely associated with the esterified product of phenolic and formic

acid or other aliphatic carboxylic acids in the aromatic region of HAs. 162-190 ppm was regarded as signals mostly contributed by carboxylic acid, ester, amide and quinone functionalities, of which the former two are electron-withdrawing or deactivating groups when the carbon in the COOR or COOH were directly connected to the aromatic ring, thus not favorable for iodine binding. But if they are connected to the aromatic ring through C-O bond via esterification, they become moderately electron donating or activating group. Amide functional group (-NHCOR), as another strongly activating substituent, can also account for resonance occurring in this region. However, amide functionalities were not observable in the $^1$H NMR run with NaOD/D$_2$O as the solvent due to proton exchange. Indirect evidence for their effect on iodine binding affinity towards these humic substances can be found in the significant correlations between the three iodine parameters and N/C ratios (n=8, $R^2$=0.771 for $^{127}$I/C, p=0.002; $R^2$=0.587 for $^{129}$I/C, p=0.002; n=11, $R^2$= 0.453  for Kd, p=0.014),  if assuming that most of the nitrogen is present as NH$_2$ or NH groups (structures that are equally ring-activating) (Reckhow et al., 1990). In addition, the possible presence of quinone-like structure in this region, though difficult for iodine to substitute due to the deactivating effect of the two electron-withdrawing carbonyl groups, can be compensated by introducing  the strong electon-donating amino group (NH$_2$) (Ivashkina et al., 2005). The product of C$_{COO}$ and C$_{Ar-H,C}$, being strongly correlated to the three iodine parameters (Table 4.4), also suggest the above carbon functionalities with the chemical shift of 162-190 ppm being the  electron-donating group to substitute aromatic proton, render the p system of the aromatic ring more nucleophilic for iodine to bind to the humic substances (Table

4.5). Moreover, as mentioned before, iodine is also possibly associated with the hemicellulose-lignin-like complexes, in which the connenction between hemicelluloses polymers and lignin polymers in the form of phenyl glycosidic linkage is favorable for iodine electrophilic substitution. Very likely iodine preferentially substitutes proton at the ortho/para position to the electron-donating group of the aromatic ring (Moulin et al., 2001). Moreover, simulated both $^{13}$CNMR and $^{1}$HNMR spectra obtained by running ACD/Labs (Version: 12.01) with the hypothesized structures also show the similar chemical shifts (Table 4.6, spectra not shown for brevity).

Table 4.6 Proposed active aromatic structures in the humic acids (HAs) for naturally bound iodine and laboratory iodination at ambient concentrations (iodine is preferentially incorporated into the ortho/para position to these functionalities).

| Proposed active aromatic ring for iodine binding* | $^{13}$C (ppm) | $^{1}$H (ppm) |
|---|---|---|
|  | 173.0 | 7.06-7.41 |
|  | 171.4 | 7.08-7.58 |
|  | 185.2-188.2 | 7.17-7.65 |
|  | 160.2 | 7.17-7.36, 8.29 |
|  | 158.6 | 7.03-7.38 |

*$^{13}$C chemical shift is for the carbon (with underlines) of the electron-donating group (not the aromatic carbon); $^{1}$H chemical shift is for the aromatic and formate protons; R denotes any other functionalities, such as aliphatic methylene.

Aromatic ring substituted with methyl and methylene groups were proposed previously to increase the electron density of the p system of the aromatic ring (Perminova et al., 1999), thus likely favorable for iodination. However, poor correlation was found between the product of $C_{Ar-H,R}$ amd $C_{Alk}$, or $H_{Ar}$ and $H_{Alk}$ (data not shown), for naturally bound iodine or laboratory uptake Kd at ambient concentrations. In any case, this observation that methyl and methylene substituents did not favor iodine binding to HAs, when the aromatic rings were substituted with carboxylate esters or amides, still follows the order of their overall electron-donating effects (Warner et al., 2000), especially when this study considers only the naturally bound iodine ($^{127}I$ and $^{129}I$) and laboratory iodination at ambient concentrations. As 57% is the average carbon content of these HAs (Xu et al., 2011a), and 14% C as contribution from the aromaticity (the average of integrals including the chemical shift 108-162 ppm regions), and if one out of six aromatic carbons is possibly available for formation of C-I bond only taking stoichiometric consideration, it will yield 0.25 g-I/ g-C (Equation 1), which is a few orders of magnitude higher than any naturally bound iodine or laboratory iodine dose used in this study (Table 4.1).

$$\left(\frac{1}{6}\right) \times \frac{1\,(g-HA) \times 0.57\,(g-C/g-HA) \times 0.14\,(g-aromatic\,C/g-C) \times 127\,(g-l/mol)}{12\,(g-C/mol) \times [1\,(g-HA) \times 0.57\,(g-C/g-HA)]}$$
(Eq. 1)

This calculation is just to give an idea that the iodine binding sites of the SOM must be ample compared to the ambient iodine that is already incorporated. Hence, iodine at ambient concentrations likely binds to those primarily preferential binding sites as discussed above. Again, the aliphatic methyl or methylene chains rather act like a

hydrophobic periphery "surrounding" the aromatic cores, thus regulate the aggregation state of the humic substances and the exposure of the active binding sites for iodine to attack. Hydrophilic biomacromolecules such as polysaccharides, can also jointly influence the aggregation-disaggregation of humic substances, thus either enhance or decrease the accessibility of active aromatic core towards radionucldies in the environment, as evidenced from their statistical relevance to the three iodine parameters, especially naturally bound iodine (Table 4.4).

It is not quite clear why FAs and WEC, with a relatively comparable aromatic carbon to HAs (Table 4.1), contain at least 5-6 times higher amount of naturally bound iodine than the HAs. A comparison of $^{13}$C NMR and $^1$H NMRspectra of the representative HA1, FA (1+2) and WEC showed FA (1+2) contains almost twice amount of electron-donating groups in the 162-190 ppm (Fig. 4.3 and Table 4.1), compared to HA1. $^1$H NMR spectra indicated that WEC contains much higher (~4 times) amount of –O–(C=O)– H functional group, compared to HA1. Nevertheless, the quantitative data still could not account for the large discrepancy in the naturally bound iodine among these three types of organic matter. However, laboratory uptake Kds of HA1, no matter what the starting iodine species are ($I^-$ or $IO_3^-$), are significantly higher than either those of FA(1+2) or WEC (Fig. 4.2). An examination of the Kd values of all the 11 samples obtained revealed a good correlation with their proton-estimated aromaticity (n=11, R2=0.523, p=0.008). It is very likely that the molecular arrangement of the three types of organic matter, or the radioiodine sink (HAs and FAs) versus carrier (WEC), is one of the most important determinant factors for the "exposure" of the active binding sites towards

iodine in the environment. For example, FAs and WEC are reported as small molecules (3-4 kDa for FA and 15 kDa for WEC), while HAs have an average molecular weight ranging from 31-78 kDa (Xu et al., 2011a). Both $^{13}$C NMR and $^1$H NMR consistently demonstrate that HAs contains much higher aliphatic content than FAs and WEC, which might act like a barrier preventing iodine from contacting the active binding sites. Last, higher contents of carbohydrates were detected in the WEC (Table 4.2 and 4.3), likely resulting in increase of its overall hydrophilicity and thus increase in accessibility by radioiodine, over its counterpart, HAs.

### 4.5 Conclusions

The aim of this study was to provide information on the relationships between quantitative structures and naturally bound iodine binding sites at ambient concentrations. This is of great environmental importance, as the molecular environment of natural organic matter binding sites determines the physico-chemical properties of the radio-iodine carrier, and thus, its relative mobility. In this study, it has been demonstrated that interactions between iodine species (I⁻ or $IO_3^-$) and SOM are iodine-concentration dependent (Fig. 4.1). Thus, when previous studies used elevated iodine concentrations, they might have overlooked the fact that iodine binding sites are dependent on the trace-level concentrations of radioiodine, with different rate constants for the different binding sites. At ambient concentrations, iodine might be preferentially incorporated into the aromatic regions containing esterified products of phenolic and formic acid or other aliphatic carboxylic acids, amide functionalities, quinone-like

structure activated by electron-donating groups (e.g., $NH_2$) or hemicelluloses-lignin-like complex with phenyl-glycosidic linkage. These most preferred SOM sites for iodination to occur largely depend on the combined steric and electronic effects on the organic binding molecule. However, the contrasting radioiodine contents among the three types of SOM (HAs, FAs and WEC) cannot only be explained by the difference in the amount of their reactive binding sites. Rather, the results indicate that the overall micro-molecular environment, such as the relative hydrophobic aliphatic periphery that is hindering the active aromatic cores, as well as the hydrophilic polysaccharides favoring the accessibility of the hydrophilic iodine species, also play key roles in the interactions between iodine and SOM. Since environmental processes such as soil erosion, rainfall, surface runoff, etc., as well as anthropogenic site remediation actions, can dramatically change soil physics and chemistry, knowing this nature of the physico-chemical interactions controlling the binding of iodine to SOM can help to better predict the environmental behavior of $^{129}$I.

# CHAPTER V

# COLLOIDAL CUTIN-LIKE SUBSTANCES CROSS-LINKED TO SIDEROPHORE DECOMPOSITION PRODUCTS MOBILIZING PLUTONIUM FROM CONTAMINATED SOILS*

## 5.1 Overview

Relatively recently, inorganic colloids have been invoked to reconcile the apparent contradictions between expectations based on classical dissolved-phase Pu transport and field observations of 'enhanced' Pu mobility (Kersting et al., 1999). A new paradigm for Pu transport is mobilization and transport via biologically-produced ligands. This study for the first time reports a new finding of Pu being transported, at sub-pM concentrations, by a cutin-like natural substance containing siderophore-like moieties and virtually all mobile Pu. Most likely, Pu is complexed by chelating groups derived from siderophores that are covalently bound to a backbone of cutin-derived soil degradation products, thus revealing the history of initial exposure to Pu. Features such as amphiphilicity and small size make this macromolecule an ideal collector for actinides and other metals and a vector for their dispersal. Cross-linking to the hydrophobic domains (e.g., by polysaccharides) gives this macromolecule high mobility and a means of enhancing Pu transport. This finding provides a new mechanism

_____

*Reprinted with permission from "Colloidal cutin-like substances cross-linked to siderophore decomposition products mobilizing plutonium from contaminated soils" by Xu, C., Santschi, P.H., Zhong, J.Y. , Hatcher, P.G., Francis, A.J., Dodge, C.J., Roberts, K.A., Hung, C.-C., Honeyman, B.D. (2008) Environ. Sci and Technol., 42(22), 8211-8217.

for Pu transport through environmental systems that would not have been predicted by

Pu transport models.

## 5.2 Introduction

Plutonium's low solubility and high particle reactivity led to the conventional

wisdom that it is essentially immobile in the subsurface environment. Classically, Pu

distribution throughout the environment has been considered to be primarily the

consequence of wind and water erosion of particles from surficial soils and sediments.

Confounding this expectation are observations of Pu concentrations approaching or

exceeding the drinking water limit of $10^{-12}$ M at substantial distances from known source

zones (Dai et al., 2002). It has recently been shown that colloids rich in Al-silicates

(Kersting et al., 1999), organic carbon (Santschi et al., 2002), or iron (Novikov et al.,

2006) are capable of facilitating transport of Pu from contaminated sites, possibly over

distances of many kilometers. Under most surface soil conditions, and with few

exceptions (Boukhalfa et al.2007a; Francis et al., 2007), +4 is the dominant Pu oxidation

state (Choppin, 2001); a state that has the ability to form complexes with a range of

environmental ligands (e.g., metal oxides, organic macromolecules, cell walls)

(Choppin, 2001; Runde, 2000). However, few studies (Santschi et al., 2002) have shown

that the mobile environmental form of Pu is Pu-organic ligand complexes.

The Rocky Flats Nuclear Weapons Plant manufactured components for nuclear

weapons for the Nation's defense until 1989. Surficial soils at RFETS contain elevated

$^{239,240}$Pu concentrations due to soil contamination in the 1960's by leaking drums stored

on the 903 Pad area whereby Pu-contaminated soil particles were later dispersed by wind and water. Although environmental remediation activities were completed in 2006, residual Pu remains in grassland soils of the site (Clark et al., 2006). Field studies of storm runoff and pond discharge samples from this site (Santschi et al., 2002), collected before remediation, demonstrated that off-site transport of the $^{239,240}$Pu occurred in the particulate ($\geq$0.45 μm; 40-90%) and colloidal (~2 nm or 3 KDa to 0.45 μm; 10-60%) size classes, amounting to an annual flux, estimated from flow and concentration data, of about 1-10 μCi of Pu away from the site. Controlled laboratory experiments (Santschi et al., 2002) further confirmed that $\geq$80% of dissolved Pu (<0.45 μm) in surface waters was present in the colloidal phase. Most importantly, isoelectric focusing (IEF) experiments conducted with this aqueous leachate material revealed that colloidal Pu, in the tetra-valent (IV) state, as determined by analogy to Th(IV) (Santschi et al., 2002), was mostly associated with a negatively-charged iron-containing organic macromolecule with an isoelectric point ($pH_{IEF}$) of 3.1 and a molecular weight of 6 kDa, rather than with inorganic (e.g., aluminosilicates) colloids. However, previous studies lacked the molecular level characterization needed to elucidate the composition and structure of this Pu-enriched colloidal organic carrier. This study fully describes for the first time an amphiphilic, organic colloidal class of compounds that contains much higher Pu concentration than either the ambient soil or bulk colloid, and can be easily leached out from the natural soil by rainwater in vadose and saturated zones as well as waste stream areas. This finding is of great environmental implication since it reveals one of the

possible pathways how "man-made" Pu can become mobile, and transported long distance.

## 5.3 Materials and methods

### 5.3.1 Sample collection

The RFETS soil was collected in 2004 from the upper 15 cm at a grass-covered hill slope, in the drainage of the neighboring creeks (Fig.5.1). The surficial geology in the study area consists of Quaternary alluvium, colluvium and slump deposits along with artificial fill, soil and debris deposits, and disturbed soils. The surficial deposits overlie bedrock which consists of weathered claystone and minor bedrock sandstones of the Cretaceous Arapahoe and Laramie Formations. Surficial deposits consist of sandy clay and clayey gravel. Soil developed over the alluvium is rocky and sandy in contrast to the clayey soils developed over the claystone bedrock.

During the summer of 2004, approximately 150 lb. of Pu-contaminated surface soil (0-15cm) from the 903 'lip area' of the Rocky Flats Environmental Technology Site were collected for use of this project. The bulk fraction received was air-dried and sieved. The less-than 1.00 mm fraction was homogenized and stored in freezer until use. This fraction was characterized for pH, moisture content, total organic carbon (TOC), particle size analysis ($d_{10}$ and $d_{60}$), particle density ($\rho$), oxalate extractable Fe and citrate-bicarbonate-dithionite (CBD) extractable Fe. Table 5.1 summarizes these basic soil properties.
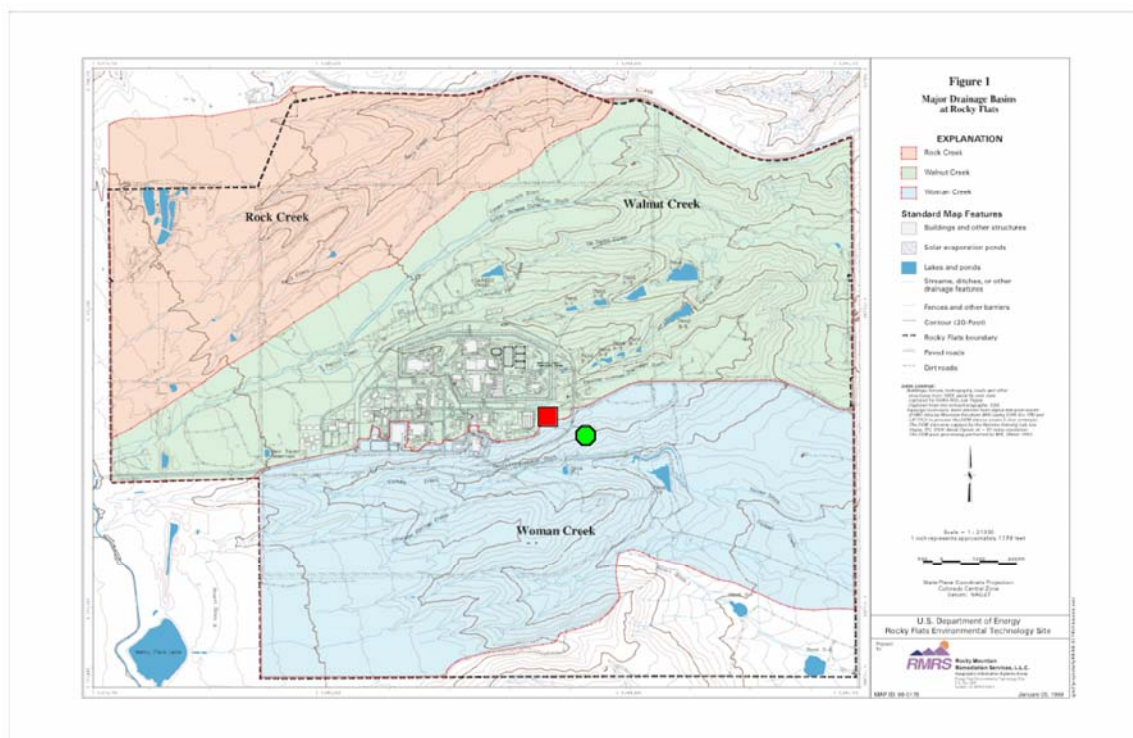
Fig. 5.1 The map of Rocky Flats Environmental Site. The red square is the former 903 Pad that was heavily contaminated by Pu, and green circle is the soil sampling site downhill from there on a grass-covered hill slope.

Table 5.1  Summary of Rocky Flats Soil Properties.

| Property | Average | Standard Deviation |
|---|---|---|
| pH (in Water) | 7.82 | 0.02 |
| pH (in 0.01M CaCl$_2$) | 7.31 | 0.08 |
| d$_{10}$ (µm) | 50 | 0 |
| d$_{60}$ (µm) | 613 | 36 |
| Total C (%) | 2.61 | 0.06 |
| $\rho_{particle}$ (g/cm$^3$) | 1.87 | 0.12 |
| Moisture Content (%) | 3.12 | 0.47 |
| Carbonate content(C%) | 0.66 | 0.32 |
| Oxalate extractable Fe (mg/g) | 0.19 | 0.02 |
| Citrate-bicarbonate-dithionite extractable Fe (mg/g) | 5.22 | 0.52 |

Sieved soil (<1 mm) was resuspended to a point of equilibrium in filtered tap water (<0.45 µm) overnight to: 1) simulate the release of mobile colloidal matter by storm and erosion events; and 2) to protect the structure and conformation of water-dispersible colloids from any traditional harsh chemical treatment. A mobile colloidal fraction (3 kDa-0.45 µm) was obtained from this slurry by re-suspension, followed by filtration and diafiltration (Fig. 5.2). This colloidal material, containing ambient $^{239,240}$Pu and to which $^{234}$Th was added as a proxy tracer, was called the "water extract" and was subsequently fractionated using isoelectric focusing gel electrophoresis.
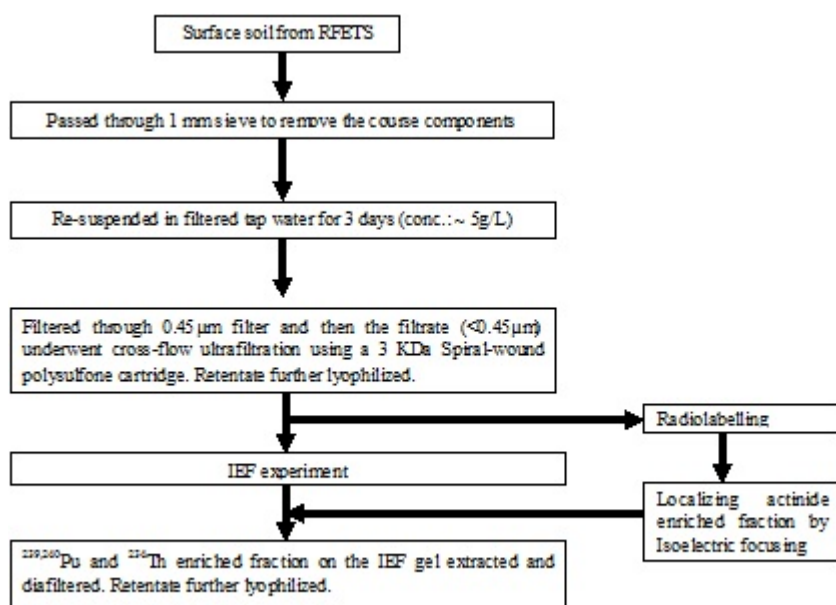


Fig. 5.2 A schematic graph of the isolation procedure for Pu-enriched colloidal IEF extract from RFETS soil.

### 5.3.2 Isoelectric focusing electrophoresis (IEF)

IEF is performed under denaturing conditions by mixing the sample with a rehydration solution, to make sure that each polymer is present only in one configuration and aggregation and molecular interactions are minimal (Quigley et al., 2002). For each IEF run, dry material (~11 mg) was dissolved in 1.1 mL of nanopure water (18.2 Ω) and mixed thoroughly with 1.54 mL of the rehydration solution. Exactly 240 μL of this solution (equivalent to 100μL sample and 140μL rehydration solution) was loaded in each Immobiline IPG Dry Strip (Amersham Biosciences, pH 3-10, 11 cm, Cat. No: 18-1016-61). Blank gels were loaded with 100μL nanopure water and 140μL rehydration solution, and run parallel with the sample gels in the electrophoresis apparatus (Amersham Biosciences, Multiphor II Electrophoresis System) for 17.5 hours with a manufacturer recommended current program (Quigley et al., 2002).

At the end of the program, pH values were measured immediately at every centimeter of each strip by a benchtop pH/mv/temperature meter (pH/Ion 510 series, OAKLON Instrument, USA). Strips were carefully cut evenly into 11 fractions, and the same fraction of every strip was pooled and extracted in 1% SDS for 24 hours. The fractions were further analyzed for either $^{234}$Th(IV) or $^{239,240}$Pu activity respectively. For $^{234}$Th activity, a liquid scintillation cocktail (Ecolume, ICN) was added to the SDS solution and the vials were capped. The solution was then vigorously shaken, loaded into a Beckman Model 8100 Liquid Scintillation Counter (LSC) and counted for 10 min (Quigley et al., 2002; Alvarado Quiroz et al., 2006). For $^{239, 240}$Pu analysis, $^{242}$Pu yield tracer was added. Gel sections were treated with concentrated HCl and HNO$_3$, and then

passed through anion exchange columns. Pu was micro-precipitated as $LaF_3$ on a Pall Gelman Metricel 0.1 μm filter, mounted on a stainless steel planchet and counted by alpha spectroscopy (Santschi et al., 2002). The activitiy in the blank gels was always very close to the background for both actinides.

The low pH isolate (0-1cm of the IEF gel), where both actinides were the most enriched (Fig. 5.3), was extracted from the gel with 1% SDS and then diafiltered against nanopure water through a 3 kDa regenerated cellulose membrane in an Amicon stirred cell series 8400 (Millipore Corporation, USA) to remove all the electrophoresis reagents. The retentate was freeze-dried and prepared for further characterization. In order to obtain sufficient material for molecular level analysis (e.g., NMR), the IEF focusing was conducted numerous times and the sections of IEF gel which were enriched in Pu activity were pooled. This isolate was called the "IEF extract". IEF blank gels were treated the same way as sample gels through all extraction, diafiltration and freeze drying steps and confirmed that contamination from the reagents (ampholytes, rehydration solutions, extractants, etc.) and the gel material was negligible.
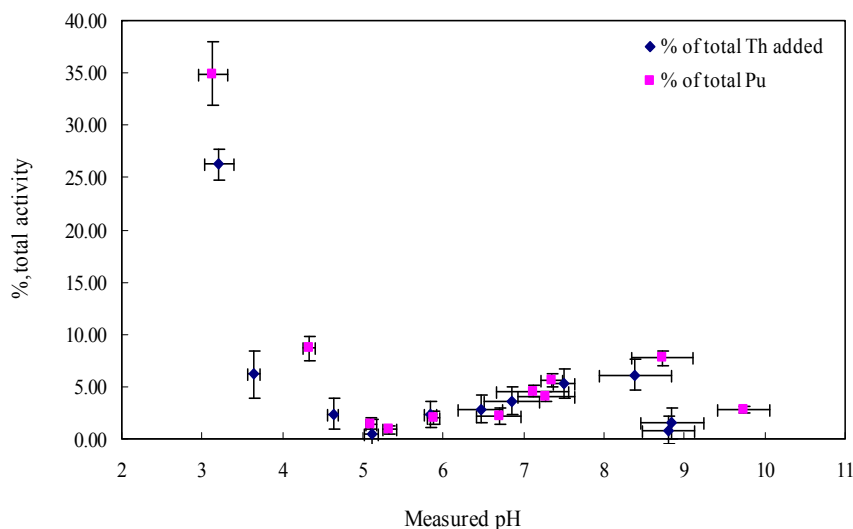
Fig. 5.3 Isoelectric focusing of Pu-containing RFETS soil water extract radiolabeled with $^{234}$Th (IV).

### 5.3.3 HPLC-size exclusion chromatography (SEC)

The molecular weight of this IEF extract was measured by a Waters High Performance Liquid Chromatographic (HPLC) system coupled with Tosoh Biosciences G4000 PWxl guard and analytical size exclusion columns and a 2417 refractive index (RI) detector. Millenium 4.00 software was used to operate the HPLC system and to acquire and integrate the chromatograms. The RI detector was set at a temperature of 30$^{o}$C and a sensitivity of 4. The mobile phase was a solution of 0.078 M NaNO$_3$ with 10 mM phosphate buffer of pH 6.8, maintained at a flow rate of 0.5 ml min$^{-1}$. Solutions of EPS were prepared at concentrations of 1 mg/ml at least 12 hours before analysis to allow uncoiling and solubilization. During this period, the EPS solutions were stored in the dark under refrigeration, and then filtered through 0.2 µm sterile syringe filters

(cellulose acetate, VWR international) before injection into the HPLC to remove non-rehydrated aggregates and bacteria. The injection volume was 150 µL, which is close to 1% of the column bed volume, 14.3 ml. Polysulfonate standards (8, 35, 100, 780 kDa) were used for calibration and prepared exactly the same way as the samples.

**5.3.4 Attenuated total reflection fourier transform infrared (ATR-FTIR)**

In this study, a Varian 3100 FTIR was connected with a single reflection horizontal ATR accessory from PIKE Technologies, Inc. (Madison, WI). A diamond plate was used as the internal reflection element. The freeze-dried sample was mounted at the surface of the diamond. Close contact with the diamond surface to achieve the greatest sampling sensitivity were accomplished by use of pressure clamps. The absorbance spectrum from 4000 to 650 cm$^{-1}$ was collected and integrated using Varian Resolution Pro 4.0 software. A sensitivity of 3 and a resolution of 4 cm$^{-1}$ were used. All ATR spectra used the spectrum of a clean diamond as the background, which was auto-subtracted from the spectra of the sample. Peaks within 2400-2000 cm$^{-1}$ were caused by the interferences of the diamond interface as stated in the manufacturer's instructions. Fortunately, no characteristic peaks of interest in the current study overlapped this region.

**5.3.5 Nuclear magnetic resonance spectroscopy (NMR)**

Solid-state DPMAS $^{13}$C, $^{15}$N NMR, and 1D $^1$H, 2D-HRMAS-NMR (HSQC and COSY) of the IEF extract were acquired on a Bruker Advance II 400 MHz NMR-

spectrometer (Bruker-biospin, Billerica, MA) at ODU. Spectra were obtained using Topspin 2.0 software distributed by Bruker Biospin. Spectral simulations were carried out using Advanced Chemistry Development's (ACD/Labs) Spec Manager (version 9.15) software.

DPMAS $^{13}$C NMR spectra were obtained using the following procedures and optimized parameters: Pu-enriched colloidal IEF extract was placed in a 4 mm rotor and spun at a frequency of 12.4 KHz at the magic angle (54.7º to the magnetic field) and employing the direct polarization pulse sequence; spectral width was 355 ppm; and line broadening set to10 Hz. The chemical shifts were referenced to the carboxyl signal of glycine as an external secondary standard (176.03 ppm).

For HRMAS NMR (1D $^1$H, 2D HSQC and COSY), a 4mm $^1$H-$^{13}$C HRMAS broadband inverse probe was employed. The sample (~30 mg) was swollen with DMSO-$d_6$ in a 4 mm rotor (50 µL). Spectra were obtained while spinning at between 5 and 7 kHz. A $^1$H NMR spectrum was obtained with 1024 scans, 15 ppm spectral width, 5 KHz sample spinning, and 1 s recyle delays. An HSQC spectrum was acquired by spinning at 5 kHz, the spectral width set to 13.3 ppm on the proton channel and 219.9 ppm on the carbon channel with the transmitter frequency set at 6 ppm and 100 ppm, respectively. Exactly 128 points were collected in $t_1$ (carbon channel), with 128 accumulations for each point with a recycle delay of 1s. The time domain for $t_2$ and the $J^1$ ($^1$H-$^{13}$C) were 1024 and 145 Hz, respectively. A magnitude-mode COSY spectrum was acquired with a spectral width of 13 ppm in both $\omega_2$ and $\omega_1$. The sample was spun at 7 kHz. The number of points in $t_1$ (time domain for $\omega_1$) was set to 256 with 128 scans for each point. The

number of points in $t_2$ ($\omega_2$) was 2048. Exactly 1.5 s was used for the recycle delay in the COSY experiment. All $^1$H and $^{13}$C chemical shifts were referenced to DMSO at 2.50 and 39.5 ppm, respectively, for both HSQC and COSY spectra.

**5.3.6 Micro-synchrotron X-ray fluorescence (SXRF) and micro-X ray absorption (μ-XANES) near edge spectroscopy analysis (Brookhaven National Laboratory)**

For both the water and IEF extracts, micro-synchrotron X-ray fluorescence (SXRF) was performed to determine the elemental distribution of Fe, Mn, Ca and Ti in both the water and IEF extracts. Micro-X ray absorption (μ-XANES) near edge spectroscopy analysis was performed at the Fe and Mn K edges to obtain oxidation state information at BNL.

The water extract and IEF extracts of the RFETS colloids were placed in Mylar sample holders having a thickness of 10 mil (250 μm), sealed with Kapton tape and analyzed at the National Synchrotron Light Source (NSLS) on beamline X27A. Micro-synchrotron X-ray fluorescence (SXRF) analysis was performed on the colloids using an incident X-ray energy of 10.04 keV. Data in the absorption edge region (-20 to +50 eV about the edge) was collected at a rate of 0.5 eV/3 sec. This technique permits two-dimensional mapping of calcium and transition metals (e.g. Ti, Mn, Fe) using a focused beam of approximately 10 x 10 μm. The oxidation states for Fe and Mn in the colloids were determined using μ-X ray absorption near edge structure (μ-XANES) analysis at the K edges for Fe (7.112 keV) and Mn (6.539 keV). Calibration standards hematite ($Fe_2O_3$) and birnessite ($MnO_2$) were used to calibrate the absorption edge positions for

Fe(III) and Mn(IV) oxidation states, respectively. Spectra were normalized to the edge-jump using the ATHENA software program. Association of the Pu in the samples was not determined since the concentration was below the detection limit of the technique. Use of the National Synchrotron Light Source, Brookhaven National Laboratory, was supported by the U.S. Department of Energy, Office of Science, Office of Basic Energy Sciences, under Contract No. DE-AC02-98CH10886.

**5.3.7 Csaky test for determination of hydroxamate functional groups**

Soil or the IEF extract was dissolved in 2 mL of nanopure water and mixed with 2 mL of 3 M sulfuric acid in a 15-mL screw capped test tubes. This solution was hydrolyzed by autoclaving at 120°C for 4 hours. After cooling, the hydrolysate was rinsed into a 50-mL graduated test tube. 7 mL of 2M sodium acetate solution was added. This solution was mixed very well and sulfanilamide solution (2 mL, 1% w/v in 30% v/v acetic acid) and 2 mL of iodine solution (0.65% w/v in 1 w/v KI solution, freshly prepared) were added. The mixture was swirled very well on a vortex mixer and allowed to react for at least 5 min. After this, 2 mL sodium arsenite solution (1.5% w/v in nanopure water) was added to remove the excess iodine and 2 mL N-(1-Naphthyl) ethylenediamine solution (0.05% w/v in nanopure water) was added as a coupling reagent in the azo dye formation step. After 30 min, the solution was diluted to 50 mL and its absorbance was measured in at 543 nm. For each sample, three replicates were measured. 2 mL of nanopure water was used as sample blank and went through the whole procedure.

**5.3.8 Other analyses**

Characterization included the spectrophotometric analysis of total carbohydrates, uronic acids (Hung et al., 2001), proteins (Smith et al., 1985), phosphate (Solórzano and Sharp, 1980); elemental analysis of organic C and N by Perkin Elmer CHNS 2400 analyzer (Guo and Santschi, 1997); Fe, Al and Mn by Perkin Elmer 5100 Zeeman GFAAS (Santschi et al., 2002); sulfate by an ion chromatography (Dionex, Houston, TX, USA) with an IonPac AG4A anion guard and analytical columns, after an acid hydrolysis step (Grotjan et al., 1986). Hydrolyzable sugar composition was determined by a Thermo-Finnigan GC-EI-MS after derivatization (Walters and Hedges, 1988). Functional groups were identified by a Varian 3100 FTIR, connected with a single reflection horizontal ATR accessory from PIKE Technologies, Inc. (Madison, WI).

## 5.4 Results and discussion

**5.4.1 Chemical composition**

Fig4.3 presents the result of an IEF run carried out with a $^{234}$Th spiked RFETS soil water extract, having a specific activity of $^{239,240}$Pu of 660±47 pCi/g. It was found that $^{234}$Th (IV) tracked the $^{239,240}$Pu activity fairly well, with a significant peak for both radionuclides at a pH of 3 near the beginning of the gel (0-1 cm), indicating a low isoelectric point and negative charge at neutral pH for the carrier molecules. This suggests that both actinides likely have a similar complexation behavior to specific clustered functional groups of organic matter (Leenheer et al., 1998).

Table 5.2

Comparison of chemical composition of RFETS soil, water extract and IEF extract*.

| | Yield mg/Kg | Pu (pCi/g) | OC (%,wt) | N/C atom ratio | C-AHA/C atom ratio | TCHO-C (%,OC) | Protein-C (%,OC) | URA-C (%,OC) | $PO_4^{3-}$/C mol ratio ($\times 10^{-2}$) | $SO_4^{2-}$/C mol ratio ($\times 10^{-4}$) | Fe/C mol ratio ($\times 10^{-2}$) | Mn/C mol ratio ($\times 10^{-4}$) | Al/C mol ratio ($\times 10^{-2}$) | Size |
|---|---|---|---|---|---|---|---|---|---|---|---|---|---|---|
| Original soil | -1 | 351±7 | 2.0±0.3 | 0.050±0.013 | 0.005 | 17.9±0.8 | 15.9±2.9 | 7.2±0.9 | 0.68±0.07 | 28.0±4.1 | 30.90±0.68 | 43.6±4.3 | 92.07±4.39 | ≤1mm |
| Water extract | 383 | 660±47 | 28.6±0.8 | 0.063±0.026 | ND | 11.5±1.0 | 7.4 | 1.3±0.2 | 0.13±0.01 | 548.7±1.5 | 0.02±0.00 | 3.81±0.95 | 0.18 | 2-450nm |
| IEF extract | 114 | 3222±278 | 48.8±0.3 | 0.203±0.037 | 0.01 | 4.7±1.6 | 1.9±0.7 | 0.4±0.1 | 0.01±0.00 | 139.7±32.1 | 0.05±0.03 | 0.09±0.03 | 0.15±0.01 | (5.9+/-0.7) kDa |

*) Errors are 1 standard deviation from replicate determinations of samples; Activity concentrations of Pu in pCi/g, with 27 pCi = 1 Bq; OC(%,wt), percentage of organic carbon in total mass; C-AHA/C atom ratio: atom ratio of carbon in the hydroxamic acid (AHA) functional group (-CO-N(OH)-) to total organic carbon in sample; TCHO-C (%, OC), percentage of total carbohydrates-C (40%) in total organic carbon; Protein-C (%, OC), percentage of protein-C (analyzed as total protein, and assumed to contain 33% C) in total organic carbon;  URA-C (%,OC), percentage of uronic acid-C (37.11%) in total organic carbon. All other elements, i.e., N, $PO_4^{3-}$, $SO_4^{2-}$, Fe,Mn, Al, were converted into atom ratio to carbon; ND, not determined.

Recoveries of both isotopes ($^{234}$Th (IV) and $^{239,240}$Pu (IV)), calculated as the sum of activity over all gel fractions normalized to the total activity used in IEF, were 83(±4) % and 66(±5) %, respectively, with the remainder adsorbed onto the container walls. The specific activity of Pu is about an order of magnitude greater in the IEF extract than that in the bulk soil. Mass balance calculations also indicate that the colloidal Pu is, for the most part, contained in this IEF extract (pH=3). The amounts of Pu and OC that can be measured in this water extract (i.e., 0.1% of the total Pu and 0.6% of the total OC in the bulk soil) are similar to those that were reported previously (Santschi et al., 2002) for the less vegetated soil case. Furthermore, the mole ratio of Fe to OC of $2x10^{-4}$ in the water extract is lower than that in the IEF extract (by a factor of 2.5), but is similar to that in groundwater samples from this site (Roberts et al., 2004). A comparison of the chemical compositions of the original soil, the water extract, and the IEF extract, is given in Table 5.2.

Hydrolyzable neutral sugars and uronic acids of this IEF extract are quite varied (Fig. 5.4), with a xylose to mannose ratio around 0.3. This suggests a dominant contribution from plant debris and minor levels of carbohydrates from microbial degradation (Murata et al., 1998; Fischer et al., 2007). In addition, the ratio of neutral sugars to uronic acids, a value of 16, confirms this dominance of plant sugars, if it is assumed that uronic acids are mainly microbial oxidation products of neutral sugars (Fischer et al., 2007).
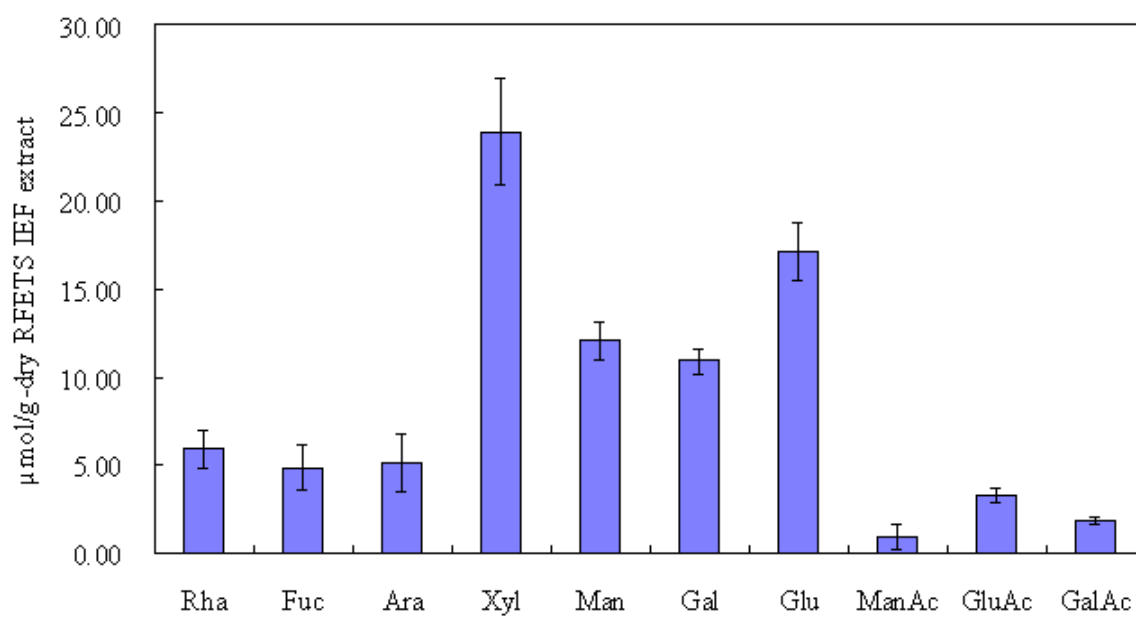
Fig. 5.4 Individual monosaccharides of RFETS soil colloidal IEF extract.
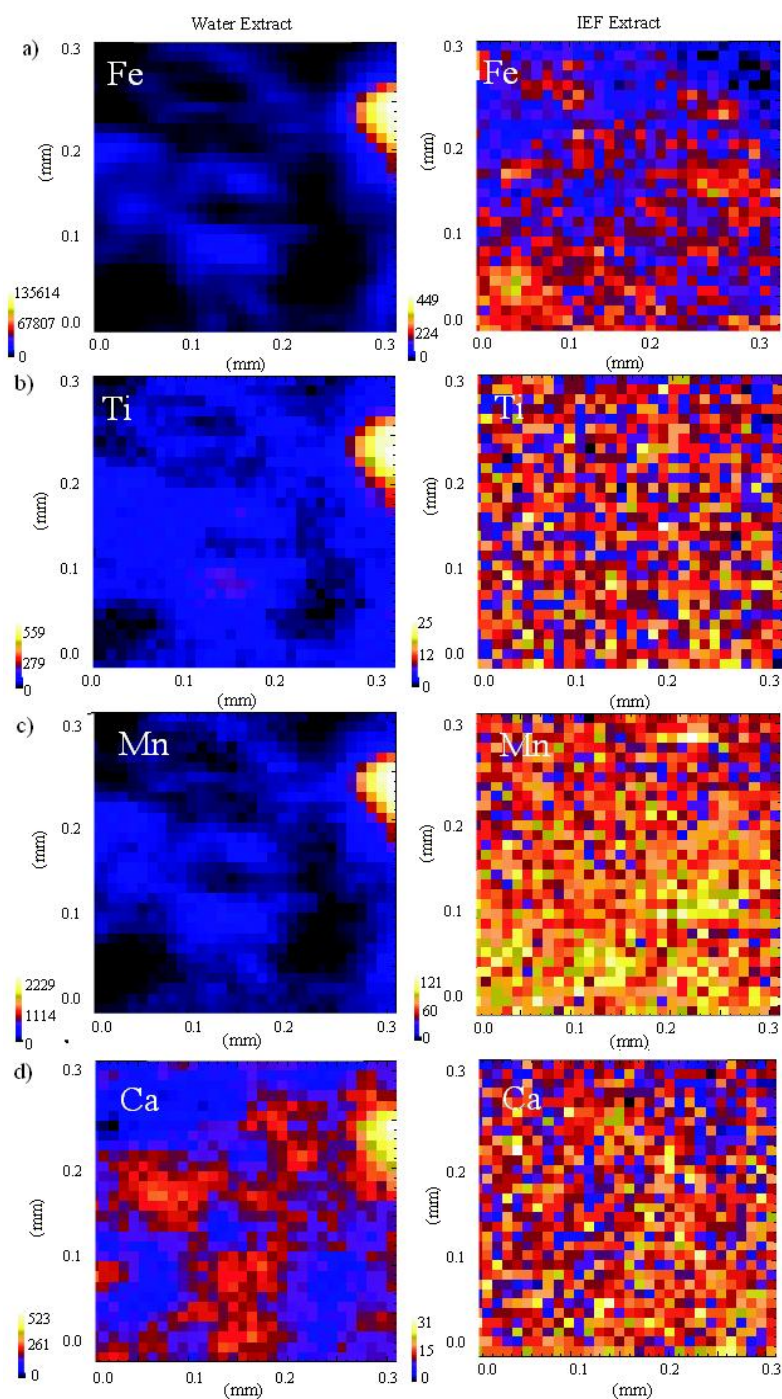
Fig. 5.5 Synchrotron-based -X-ray fluorescence map of Fe (a), Ti (b), Mn (c) and Ca (d) in Rocky Flats colloids. Left, water extract; right, IEF extract. The relative concentration of each metal in the map is given in the ascending color scale at the bottom left of the figure. The intensity maps have not been calibrated so an estimate of metal concentrations in the colloid was not obtained. Each pixel is 10 m x 10 m.

**5.4.2 Elemental mapping**

Elemental mapping obtained by synchrotron-based μ-XRF displays a diffuse and homogenous distribution of Fe in the IEF extract (Figure 4.5a, right), which is very different from the discrete iron oxyhydroxides associated with NOM that exist in the water extract (Figure 4.5a, left). Elemental mapping for Ti (Figure 4.5b) and Mn (Figure 4.5c) shows results similar to that of iron. Calcium is evenly distributed throughout both the water extract and the IEF extract (Figure 4.5d). Cu, Cr, Ni and Zn show results similar to Ca (images not shown).

X-ray absorption near edge spectroscopy (XANES) analysis of the iron and manganese in the water extract performed at the K-adsorption edge (7112 eV and 6539 eV, respectively), indicates that the iron in the colloid is present in the ferric form (Fig. 5.6) and Mn as $Mn^{4+}$(images not shown). Though the Pu concentrations in both samples are below the detection limit of this method, the spatial distribution of other tetravalent elements, e.g., $Ti^{4+}$ and $Mn^{4+}$, closely matches that of iron. Very likely, the IEF extract contains homogenously distributed organic functionalities that complex Fe(III), as well as other tetravalent ions (Ti and Mn), a pattern that is totally different from the previously identified inhomogenously bound Pu-carrying amorphous Fe hydroxide pseudo-colloid reported in groundwater (Novikov et al., 2006). While one could argue that the resolution is not high enough (10μm pixel size) to make this statement, a thermodynamic assessment of the co-occurrence of small iron colloids and hydroxamate and other iron chelating functional groups (see below) strongly argues against such possibility (Holmen and Casey, 1996), as these chelating ligands cause ligand-promoted

dissolution. A similar argument can be made against the presence of plutonium

oxyhydroxides (e.g., Brainard et al., 1992; Ruggiero et al., 2002).
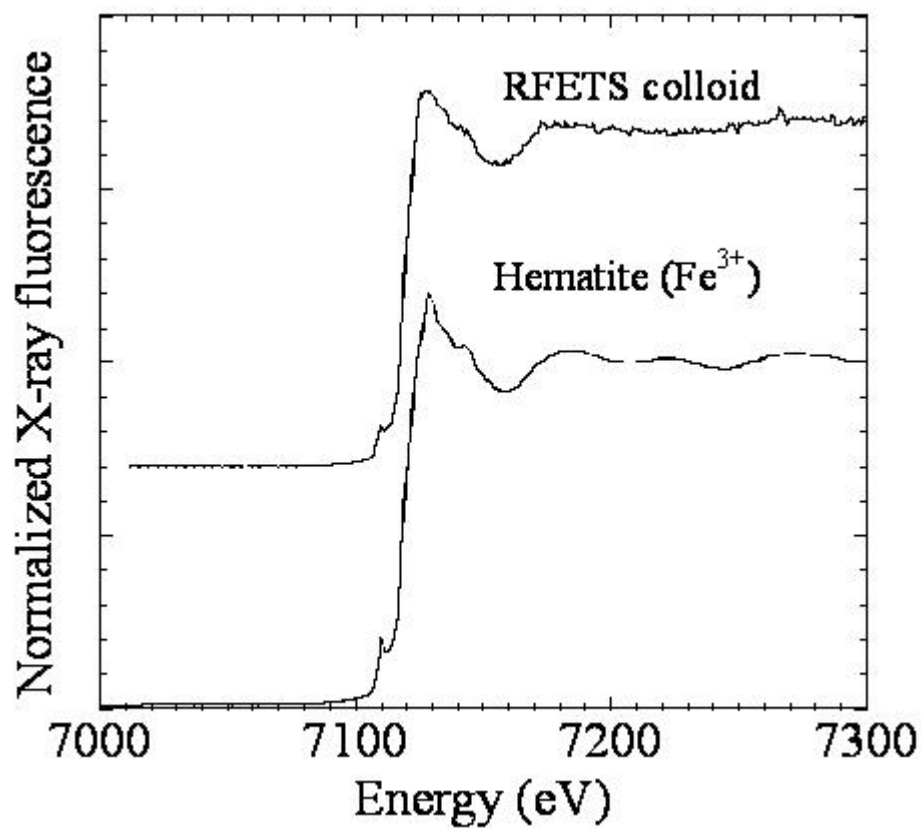


Fig. 5.6 X-ray absorption near edge structure analysis at the Fe K edge of the crude colloid.

### 5.4.3 Functional groups

Functional groups of the IEF extract investigated by ATR-FTIR (Fig. 5.7) show

intense bands at 2920 and 2852 cm$^{-1}$ characteristic of saturated aliphatic C-H stretching.

Very strong aliphatic C-H bending vibrations are also found at 1455 cm$^{-1}$. Both support

the presence of fatty acids or esters. The band at 1724 cm$^{-1}$ can be attributed to the stretching vibrations of carbonyl groups in fatty esters/fatty acids. A rather intense band for the amide I vibration (-C=O stretching, 1660 cm$^{-1}$) is observed and a concomitant shoulder is observed for the amide II (-N-H bending vibration and –CN stretching vibration, 1556 cm$^{-1}$). These suggest the presence of amide or hydroxamate groups. A hump at 3200 cm$^{-1}$ might represent NH$_2$ aminoacidic groups. The presence of sulfate is suggested by two groups of bands: 1247 cm$^{-1}$ (S=O stretching) and 823 cm$^{-1}$ (C-O-S stretching). Carboxylate groups are indicated by the COO$^-$ asymmetric stretching vibration at 1615 cm$^{-1}$ as well as the symmetric stretching vibration around 1400-1377 cm$^{-1}$. The presence of organic phosphate is indicated by two bands at 1247 cm$^{-1}$ and 1218 cm$^{-1}$. However, the band around 1250 cm$^{-1}$ could also be related to the phenolic –OH groups. The band around 1370 cm$^{-1}$ can also be attributed to phenolic C-OH stretching. Except for the band around 1660 cm$^{-1}$, which is usually attributed to the amide I, bands within the region of 1500-1700 cm$^{-1}$ can also be attributed to the C=C stretching of aromatic rings. Distinct bands at 1083 and 1043 cm$^{-1}$ are particularly characteristic of the C-O-C group vibrations of carbohydrates.
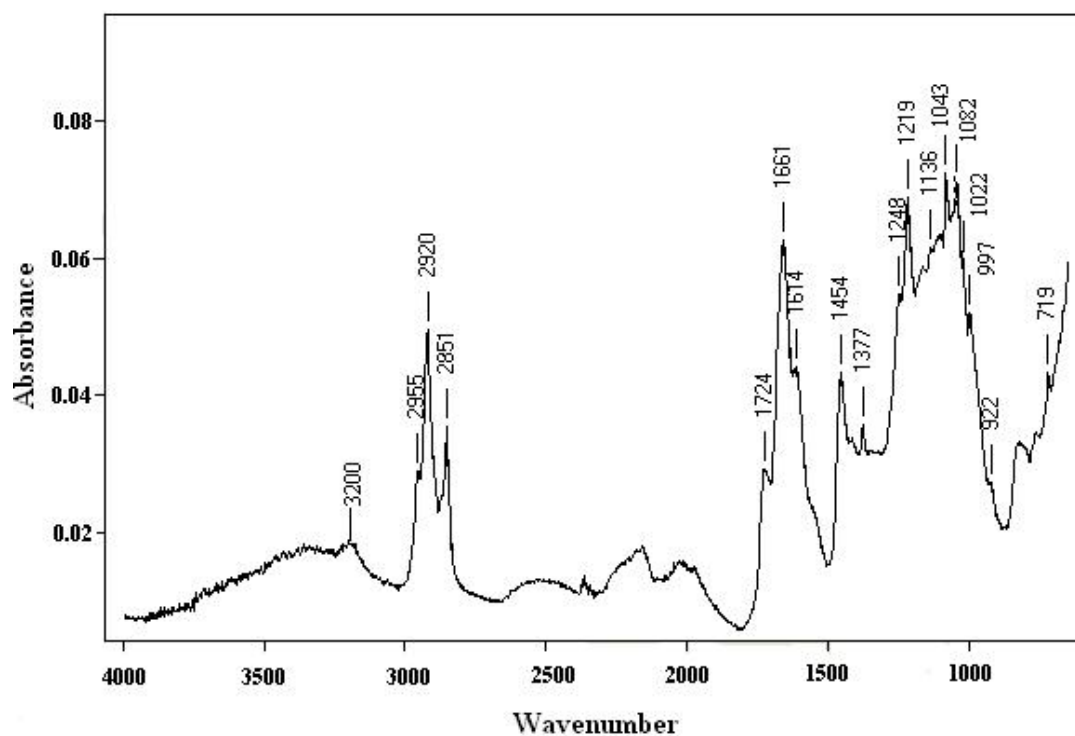
Fig. 5.7 ATR-FTIR spectrum of RFETS soil IEF extract.

The main carbon functionalities are identified in the solid-state DPMAS $^{13}$C NMR (Simpson et al., 2007) as consisting of carboxyl/amide groups, aromatic rings, carbohydrates, and aliphatic chains (Fig. 5.8a), and representing 10.44%, 7.59%, 5.16% and 70.61% of OC, respectively, based on an integration of the individual spectra. Although the lipid and ester content was not independently determined in this study, the carbohydrate content matched well with the spectrophotometric analysis, i.e., 4.7% of OC. The aliphatic signal representing long-chain polymethylenic carbons (~29 ppm) was dominantly composed of $CH_2$ groups having amorphous character (made up of random *cis/trans* orientations). Polymethylenic carbons having a crystalline character, the peak

at ~32 ppm for $CH_2$ units arranged in all *trans* configurations (Hu et al., 2000), is

subordinate. Another important feature of the spectrum is the carboxyl/amide peak at

180 ppm, whose chemical shift indicates the carboxyl or amide groups are clustered

closely together, with the oxygen mainly complexed by metals (Leenheer et al., 1998),

e.g., Fe. Problems like overlapping resonance lines, selective quenching intensity and

loss of signals (Preston et al., 1994) can be ignored due to the relatively low

concentration of Fe (III) (Fe/C atom ratio of 5 x $10^{-4}$, Table 5.2) in the IEF sample. In the

1D $^1$H HRMAS spectrum (Fig. 5.8b), the peaks representing terminal methyl protons

(~1.0 ppm) indicate that this isolate contains an abundance of terminal branching as a

result of extensive diagenesis and, thus, the macromolecule has become more

recalcitrant to biodegradation (Schaeffer et al., 1979). Main-chain $CH_2$ groups are

identified in abundance at around 1.3 ppm. Assignments of other signals, indicated in

Figure 4b, are made on the basis of the 2-D HRMAS data.
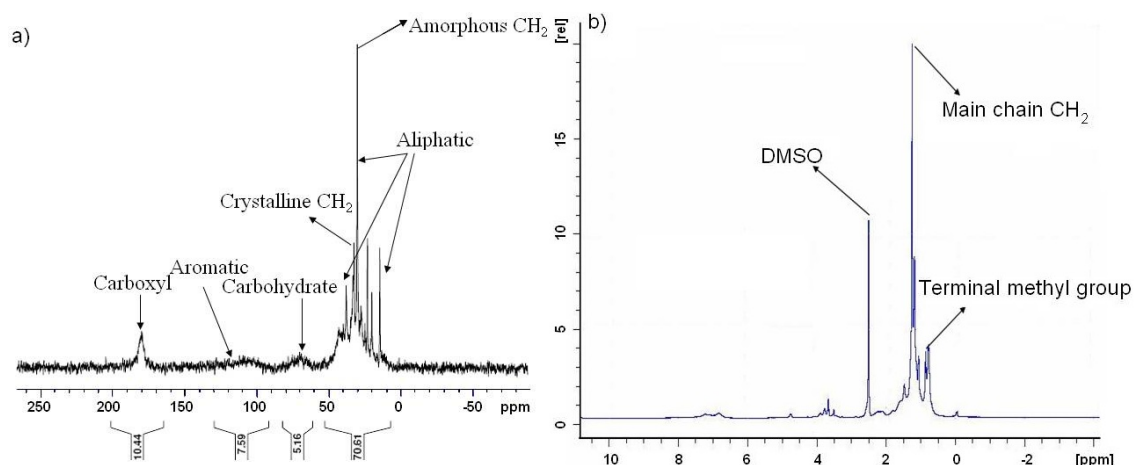
Fig. 5.8 a) Solid-state cross-polarization magic angle spinning (DPMAS) $^{13}$C NMR spectrum of RFETS soil IEF extract (the vertical numbers at the bottom indicate the normalized integrals) b)1D $^1$H HRMAS NMR spectrum of RFETS soil IEF extract in DMSO-d6.

Both HSQC (Fig. 5.9a) and COSY (Fig. 5.9b) NMR spectra indicate the presence of cross peaks that match those shown for cutin (Deshmukh et al., 2005), and, thus, it is very likely that this IEF extract is cuticle-type material. Further support for this conclusion is provided by comparisons to previously identified cutin spectra (Kelleher and Simpson, 2006) and spectral simulations (Fig. 5.9c and 5.9d) of the cutin model structures (Fang et al., 2001; Kolattukudy, 2001), respectively.
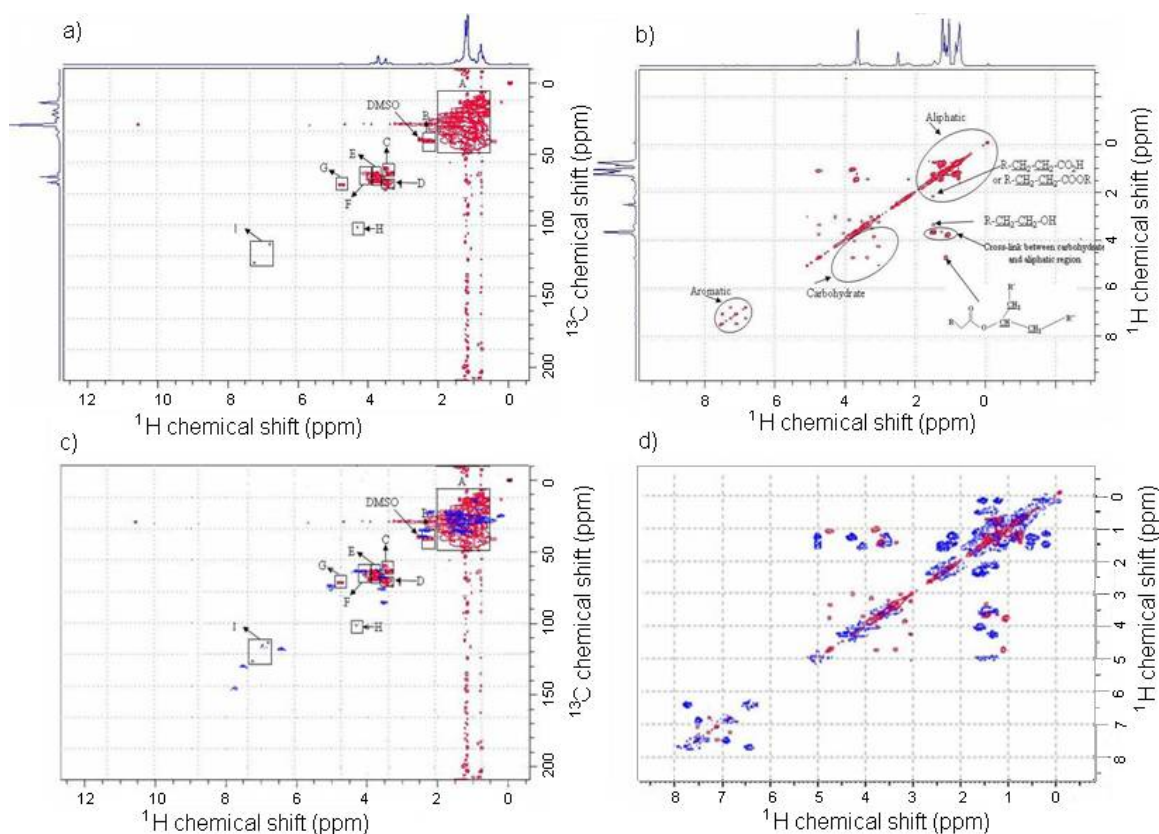
Fig. 5.9 2D NMR spectra of RFETS soil IEF extract swollen in DMSO-d6. a) HSQC
NMR spectrum. b) COSY NMR spectrum. c) Overlapping of the HSQC NMR spectrum
of the IEF extract (red), tomato cuticle (green) (21), and spectral simulations of the
model cutin monomeric unit (22, black; 23, blue); d) Overlapping of the COSY NMR
spectrum of the IEF extract and spectral simulations of the model cutin monomeric unit
(22, black; 23, blue). The spectral assignments for the HSQC spectrum (a) of the IEF
extract are the following: 1) terminal methyls and methylene groups in long-chain
structures (box A); 2) methine structures attached to carbonyl groups in α-methyl
branched fatty acids and esters (box B); 3) methylene structures attached to hydroxyl
groups (box C); 4) methylene structures attached to ether oxygens or methane groups
attached to a secondary alcohol (box D); 5) CH groups in carbohydrates (box E); 6)
methylene structures attached to the singly-bonded oxygen of esters (box F); 7) methines
attached to the singly-bonded oxygen of esters (box G); 8) anomeric carbons in
carbohydrates (box H); and 9) aromatic structures (box I).

The elevated N/C ratio in the IEF extract over that in the water extract is ascribed to the presence of abundant ester/amide groups and some amino acid groups observed by both ATR-FT/IR (Fig. 5.7) and solid state $^{15}$N-NMR (Fig. 5.10), though the signal of the latter is weak due to the limited sample amount. Evidence of cross-linked structures like α-branched fatty acids/esters (box B, Fig. 5.9a) and esters of mid-chain hydroxyls (box G, Fig. 5.9a) have been previously identified in cutin (Deshmukh et al., 2003). The relatively low O-alkyl-C/alkyl-C ratio, the low abundance of aromatic groups and labile components (e.g., polysaccharides), as well as the high nitrogen content would suggest a highly recalcitrant and insoluble property of this substance (Mathers, 2007). The high nitrogen content is of interest because cutin is usually devoid of nitrogen. It is possible that the nitrogen has been incorporated into cutin-like structures by processes yet to be defined.
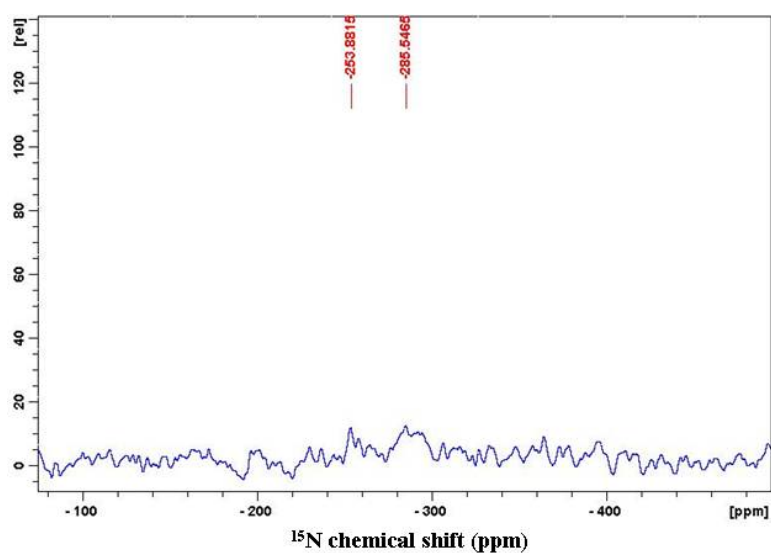


Fig. 5.10 $^{15}$N CP/MAS Solid-state NMR (NO$_3^-$ =0ppm).

Cutin is normally regarded as a water-insoluble macromolecule; this attribute appears to be inconsistent with the fact that this IEF isolate originates from a soil water extract. It could be rationalized that it probably contains sufficient amounts of polar functional groups to induce solubility. The DPMAS spectrum shown in Fig. 5.8a shows the presence of possible carboxyl or amide functionalities that could provide solubility. It is also possible that the isolate exists encapsulated or cross-linked within a hydrophobic domain of an otherwise hydrophilic moiety of colloidal organic matter, e.g., polysaccharides (Table 5.2 and Fig. 5.4), that renders it soluble.

Siderophores produced by bacteria and fungi (Neilands and Leong, 1986; Renshaw et al., 2002) have been proposed as the strongest chelating agents for actinide elements as a result of multinuclear complexation at the carbonyl- or hydroxamate-oxygen, or amide-nitrogen, and their ability to dissolve oxyhydroxides of iron (Brainard et al., 1992; Holmen and Casey, 1996), and, most importantly, also plutonium (Ruggiero et al., 2002). Though NMR analysis applied in this study did not directly show protons associated with the hydroxamate functionality, a high abundance of nitrogen, a strong amide functionality, and a low protein content in this IEF extract indicates the possible presence of hydroxamate, which is regarded as a typical functional group of siderophores. Quantitative determination of hydroxamate functional groups by a modified colorimetric Csaky test (Gillam et al., 1981) showed that about 1.2% of the C is present as hydroxamate, with the IEF extract being enriched by a factor of 10 (%mass) and 2 (%OC) in hydroxamate, compared with the original bulk soil (Table 5.2). Since there are many siderophores that do not contain hydroxamate (e.g., rhizoferrin from soil

fungi, which contains only carboxylates), the presence of even 1% hydroxamate suggests that siderophores decomposition products are important moieties in this mobile Pu-carrying biopolymer. Based on the chemical composition (Table 5.2), a stoichiometry of Fe:Carboxyl-C:N of close to 1:200:400 provides ample opportunities for chelating or clustered Fe (and Pu) binding sites. It is important to point out that the idea of siderophores as carriers of Pu and other actinides has never been tested in the field, where actinide (e.g., Pu or Th) concentrations are many orders of magnitude (e.g., $10^9$ to $10^{12}$) lower than that in laboratory experiments (Boukhalfa et al., 2007b), which makes it very difficult to probe the *in situ* binding environment of Pu. $^{239,240}$Pu/Fe ratios of (7 or 3)x$10^6$ pCi Pu/g-Fe are observed in the water or IEF extracts, equivalent to $^{239}$Pu/Fe atomic ratios of (26 or 11)x$10^{-6}$, respectively, suggesting that Pu would only have to substitute about one in $10^5$ binding sites of Fe(III).

## 5.5 Conclusions

The negatively charged amphiphilic biopolymer that was isolated here has strong metal complexing ability, as well as surfactant and emulsifier qualities (Sanstchi et al., 2002), giving it both high mobility in the surface environment and the ability to at least temporarily adhere to soil particles. Pu is likely complexed by a cutin-like substance containing hydroxamate, carboxylic and amide chelating functional groups that are likely derived from siderophores, which in their pure state normally have a molecular weight of 500-700 Da. This newly characterized 6kDa plutonium carrier likely contains degradation products of cutin, as the backbone, which is the hydrophobic waxy layer

covering plant surfaces and must be abundant in this grassland area, crosslinked to a siderophore degradation product and hydrophilic carbohydrate moieties during microbial degradation. This crosslinking enhances both its complexation ability as well as its mobility, and makes it an ideal collector for actinides and other metals, and a vector for the dispersal of Pu.

# CHAPTER VI

# SUMMARY

$^{129}$I, which is a major by-product of nuclear fission and becomes one of the major radiation risk driver in the Department of Energy (DOE) sites, are present at elevated levels in the surface soils of F-Area of the Savannah River Sites, which used to be an isotope separation facility for the production of nuclear weapons components. The $^{129}$I in soils is thought to be bound predominantly to soil organic matter (SOM). Measurements of stable $^{127}$I and radioactive $^{129}$I in humic acids (HAs) and fulvic acids (FAs) obtained by five successive alkaline, two glycerol and one citric acid-alkaline extraction, demonstrated that these extractable humic substances (HS) together account for 54-56% and 46% of the total $^{127}$I and $^{129}$I in the soil, respectively. The coincident variations in chemical compositions, aromaticity, functional groups (e.g., aliphatic), degree of humification, relative migration in the hydrophobic interaction column, and molecular weight indicated that: 1) iodine in different HAs was bound to a small-size aromatic subunit (~10 kDa); 2) the large-size subunit (~90 kDa), which likely linked the small-size unit through some weak chemical forces (hydrogen bonds, hydrophobic or electrostatic interactions), determined the relative mobility of iodine bound to organic matter; 3) from the strong correlation between iodine content and aromaticity in the HAs, we suggested that iodine incorporation into the SOM via covalent aromatic C-I bond is the key mechanism controlling iodine behavior in this system. However, this relationship is not universal for all fractions of organic matter as evidenced from the

different slopes of this relationship at the two sampling sites, as well as from different relationships among HAs and FAs. These differences in iodination are due to different SOM molecular sizes, compositions, and availability of preferred iodination sites. $^{129}$I in the soil downstream from the contaminated site and near a wetland abruptly dropped below our detection limit (0.5 pCi-$^{129}$I/g-soil), which suggests that the high SOM in the plume soil around the $^{129}$I-contaminated F-Area might be a natural barrier to scavenge radioiodine released from the nuclear waste repository by forming organo-iodine compounds. Water extractable colloid, which was obtained by following the procedure that mimic stormwater, surface runoff and groundwater exfiltration events showed that mobile $^{129}$I was mostly associated with a low molecular weight amphiphilic organic carrier (13.5-15 kDa).

Results from previous field and laboratory experiments indicate that groundwater iodine (I) concentrations near the seepage basin of the F-Area have increased dramatically due to the minor increase in pH in recent 17 years since the remediation actions; while it didn't increase much a few hundred meters downgradient the seepage basin where a moderate pH change was observed. Most importantly, iodine speciation downgradient the seepage basin and along the contaminated plume area cannot be explained by simple transport models that assume iodide being the dominant species. Tracer and soil resuspension experiments that simulate surface runoff or storm and erosion events showed that up to ~72-77% of amended iodide or iodate at both ambient and elevated I concentrations (0.1 μM and 20 μM) could be irreversibly sequestered as organo-iodine in an organic-rich soil during a one-month investigation; while only ~19-

21% were fixed in an organic-poor aquifer sediment. $I^-$ or $IO_3^-$ sorption onto the organic-rich soil exhibited similar kinetics towards a quasi-equilibrium state, indicating that under the presence of sufficient amount of organic matter, formation of organo-iodine is favored in the surface oxic soils. Ultrafiltration of the aqueous phase indicates that a significant amount (9% and13% of the total added $I^-$ or $IO_3^-$ when the addition is 20 μM, 6% and 3% of the total added $I^-$ or $IO_3^-$ when the addition is 0.1 μM) of mobile iodine from the organic-rich soil was present in the >3 kDa colloidial fraction. Even in the permeate (< 3 kDa), organo-iodine accounted for ~100% of total I at the end of the observation period. $^{129}I$ in the permeate and WEC can reach as high as 639 and 1015 pCi/L, accounting for ~9% of the total radioiodine in this soil, which greatly exceeds the drinking water limit issued by EPA (1 pCi/L for $^{129}I$). Transformation of almost all inorganic iodine into colloidal and dissolved organo-iodine species by the organic-rich soil and the resulting remobilization contradicts the conventional view that considers only $I^-$ or $IO_3^-$ as the mobile iodine forms. This novel observation of combined chemical and physical interactions between radioiodine and the organic-rich soil can be depicted as an on-off 'piggy-back' mechanism or a two-way street: the external inorganic iodine is picked up by the SOM through the formation of covalent C-I bond formation and thus buried in this natural trap; while some colloidal and dissolved organic matter carrying parts of the newly-formed organo-iodine as well as some "old" iodine in the aqueous phase, thus becoming an important radioiodine source to the downgradient areas. Laboratory iodination of the HA or WEC obtained from F-Area thus indicate a preferential incorporation of inorganic iodine (in the presence of $H_2O_2$, Fe(II,III) or

Mn(II,IV)) into NOM at acidic pH (3-4), except for the iodination catalyzed by

lactoperoxidase, which favors more alkaline conditions. It is likely that under very acidic

conditions (pH ~3), abiotic iodination of SOM was predominant, while under less acidic

conditions (pH ~5), enzymatically-assisted iodination of SOM by the microbial

community present in the groundwater or soil solution might be predominant. The

organic-rich soil in the vadose zone of F-Area thus acts as a natural attenuation zone to

reduce radioiodine that can be released.

Quantitative structural analyses of carbon and proton functionalities of the eight HAs

and two FAs sequentially extracted from FSI18 surface soil as well as the water

extractable colloid, were obtained through $^{13}$C DPMAS and solution state $^1$H NMR. The

statistical relevances of the carbon or proton functionalities of these soil organic matter

samples to their naturally bound $^{127}$I, $^{129}$I and iodine uptake partitioning coefficients (Kd)

determined at ambient concentration (0.1 μM) were evaluated respectively. It was found

out that incorporations of iodine (I$^-$ or IO$_3^-$) into SOM were iodine concentration-

dependent. Previous studies using elevated iodine concentrations might have overlooked

the fact that iodine binding sites are dependent on the trace-level concentrations of

radioiodine, with different rate constants for the different binding sites. Several

significant correlations were observed: 1) abundance of carbon functionality with a

range of chemical shift of 162-190 ppm was correlated with naturally bound $^{127}$I, $^{129}$I and

laboratory iodine uptake Kd (named "three iodine parameters" below); 2) the product of

integrals of $C_{Ar-H,C}$ (108-162 ppm) and $C_{COO-}$ (162-190 ppm) showed a strong correlation

with the three iodine parameters; 3) the three iodine parameters were closely associated

with the $-O-(C=O)-H$ (8.25-9 ppm) and aromatic protons (6.0-8.25 ppm); 4) strongest statistical correlation with the three iodine parameters (naturally bound $^{127}I$, $^{129}I$ and laboratory determined iodine uptake Kd) were observed for $H_{IV}/H_I$ ratios. Thus it is likely that at ambient concentrations, iodine are preferentially incorporated into the aromatic regions containing esterified products of phenolic and formic acid or other aliphatic carboxylic acids, amide functionalities, and quinone-like structure activated by electron-donating groups (e.g., $NH_2$). These most preferred SOM sites for iodination to occur largely depend on the combined steric and electronic effects on the organic binding molecule. However, the contrasting radioiodine contents among the three types of SOM (HAs, FAs and WEC) cannot only be explained by the difference in the amount of their reactive binding sites. Rather, the results indicate that the overall micro-molecular environment, such as the relative hydrophobic aliphatic periphery that is hindering the active aromatic cores, as well as the hydrophilic polysaccharides favoring the accessibility of the hydrophilic iodine species, also play key roles in the interactions between iodine and SOM. Since environmental processes such as soil erosion, rainfall, surface runoff, etc., as well as anthropogenic site remediation actions, can dramatically change soil physics and chemistry, knowing this nature of the physico-chemical interactions controlling the binding of iodine to SOM can help to better predict the environmental behavior of $^{129}I$.

A colloidal organic vector was obtained from a contaminated soil of the Rocky Flats Environmental Technology Site (formerly Rocky Flats Plants), which used to manufacture components for nuclear weapons for the Nation's defense until 1989.

Surficial soils at RFETS contain elevated $^{239,240}$Pu concentrations due to soil contamination in the 1960's by leaking drums stored on the 903 Pad area whereby Pu-contaminated soil particles were later dispersed by wind and water. Although environmental remediation activities were completed in 2006, residual Pu remains in grassland soils of the site. Soil resuspension experiment was performed to mimic the stormwater and surface runoff events and confirmed that this colloidal vector scavenged $\geq$80% of dissolved Pu (<0.45 μm) in soil leachate aqueous phase. Application of NMR techniques (Solid-state DPMAS $^{13}$C, $^{15}$N NMR, and 1D $^{1}$H, 2D-HRMAS-NMR (HSQC and COSY)) in investigation the molecular composition and structural information of this Pu-enriched colloidal organic carrier revealed that Pu was transported, at sub-pM concentrations, by a cutin-like natural substance containing siderophore-like moieties and virtually all mobile Pu. Most likely, Pu is complexed by chelating groups derived from siderophores that are covalently bound to a backbone of cutin-derived soil degradation products, thus revealing the history of initial exposure to Pu. Features such as amphiphilicity and small size make this macromolecule an ideal collector for actinides and other metals and a vector for their dispersal. Cross-linking to the hydrophobic domains (e.g., by polysaccharides) gives this macromolecule high mobility and a means of enhancing Pu transport. This finding provides a new mechanism for Pu transport through environmental systems that would not have been predicted by Pu transport models.

**REFERENCES**

Allard B. (2006) A comparative study on the chemical composition of humic acids from forest soil, agricultural soil and lignite deposit bound lipid, carbohydrate and amino acid distributions. *Geoderma* **130**, 77-96.

Alvarado Quiroz N.A., Hung C.C. and Santschi P.H. (2006) Binding of Thorium(IV) to carboxylate, phosphate and sulfate functional groups from marine exopolymeric substances (EPS). *Mar. Chem.* **100**, 337-353.

Andersen S. Petersen S.B. and Laurberg P. (2002) Iodine in drinking water in Denmark is bound in humic substances. *Eur. J. Endocrinol.* **147**, 663–670.

Baalousha M. (2009) Aggregation and disaggregation of iron oxide nanoparticles: influence of particle concentration, pH and natural organic matter. *Sci. Total Environ.*, **407**, 2093-2101.

Baglieri A., Ioppolo A., Negre M. and Gennari M. (2007) A method for isolating soil organic matter after the extraction of humic and fulvic acids. *Org. Geochem.* **38**, 140-150.

Beyer L., Blume H.-P., Sorge C., Schulten H.-R., Erlenkeuser H. and Schneider D. (1997) Humus composition and transformations in a pergelic cryohemist of coastal antarctica. *Arctic and Alpine Research*, **29**, 358-365.

Bird G.A. and Schwartz W. (1996) Distribution coefficients, Kds, for iodide in Canadian Shield Lake sediments under oxic and anoxic conditions. *J. Environ. Radioact.* **35**, 261-279.

Bostock A. C., Shaw G. and Bell J. N. B. (2003) The volatilisation and sorption of $^{129}$I in coniferous forest, grassland and frozen soils. *J. Environ. Radioact.* **70**, 29–42.

Boukhalfa H., Icopini G.A. and Reilly S.D. (2007a) Neu M.P. Plutonium(IV) reduction by the metal-reducing bacteria *Geobacter metallireducens* GS15 and *Shewanella oneidensis* MR1. *Appl. Environ. Microbiol.* **73**, 5897-5903.

Boukhalfa H., Reilly S.D. and Neu M.P. (2007b) Complexation of Pu(IV) with the natural siderophore desferrioxamine B and the redox properties of Pu(IV) (siderophore) complexes. *Inorg. Chem.*, **46**, 1018-1026.

Brainard J.R., Strietelmeier B.A., Smith P.H., Langston-Unkefer P.J., Barr M.E. and Ryan R.R. (1992) Actinide binding and solubilization by microbial siderophores. *Radiochim. Acta*, **58/59**, 357–363.

Bruland K. (1983) Trace elements in sea-water. In *Chemical Oceanography* 8, (2nd ed., eds, Rilley J.P. and Skirrow G.), Academic, Orlando, FL, 157–220.

Carlsen L., Lassen P., Christiansen J. V., Warwick P., Hall A. and Randall A. (1992) Radio-labeling of humic and fulvic materials for use in environmental studies. *Radiochim. Acta* **58/59,** 371–376.

Chin Y., Aiken G. and O'Loughlin G. (1994) Molecular weight, polydispersity, and spectroscopic properties of aquatic humic substances. *Environ. Sci. Technol*. **28**(11),1853-1858.

Choppin G.R. and Morgenstern A. (2001) Distribution and movement of environmental plutonium. In *Plutonium in the Environment.* (ed. A. Kudo), Elsevier Science Ltd., New York, 91-105.

Christiansen J.V. and Carlsen L. (1991) Iodinated humic acids. In *Humic Substances in the Aquatic and Terrestrial Environment, Lect. Notes Earth Sci.* **33** (eds. B. Allard, H. Borén and A.Grimvall) Springer Verlag, Sweden, 467-474.

Clark D.L., Janecky D.R. and Lane L.J. (2006) Science-based cleanup of Rocky Flats. *Phys. Today*. **59**, 34-40.

Claret F., Lerouge C., Laurioux T., Bizi M., Conte T., Ghestem J. P., Wille G., Sato T., Gaucher E. C., Giffaut E., and Tournassat C., 2010. Natural iodine in a clay formation: Implications for iodine fate in geological disposals. *Geochim Cosmochim Acta* **74**, 16-29.

Councell T.B., Landa E.R. and Lovley D.R. (1997) Microbial reduction of iodate. *Water, Air, and Soil Pollution*. **100**, 99-106.

Bors J., Martens R. and Kühn W. (1988) Studies on the role of natural and antropogenic organic substances in the mobility of radioiodine in soils. *Radiochimica Acta* **44/45**, 201-206.

Dai J., Zhang M. and Zhu Y. (2004) Adsorption and desorption of iodine by various Chinese soils I. Iodate. *Environmental International*. **30**, 525-530.

Dai M.H., Kelley J.M. and Buesseler K. O. (2002) Sources and migration of plutonium in groundwater at the Savannah River Site. *Environ. Sci. Technol.* **36**, 3690-3699.

Denham M., Kaplan D. and Yeager C. (2009) Groundwater radioiodine: prevalence, biogeochemistry, and potential remedial approaches. SRNL-STI-2009-00463. Savannah River National Laboratory, Aiken, SC.

Deshmukh A.P., Simpson A.J. and Hatcher P.G. (2003) Evidence for cross-linking in tomato cutin using HR-MAS NMR spectroscopy. *Phytochem.* **64**, 1163-1170.

Deshmukh A.P., Simpson A.J., Hadad C.M. and Hatcher P.G. (2005) Insights into the structure of cutin and cutan from *Agave americana* leaf cuticle using HRMAS NMR spectroscopy. *Org. Geochem.* **36**, 1072-1085.

Duan S. and Bianchi T. S. (2007) Particulate and dissolved amino acids in the Lower Mississippi and Pearl Rivers (USA). *Mar. Chem.* **107**, 214-229.

Earnshaw A. and Greenwood N. (2005) The Halogens: fluorine, chlorine, bromine, iodine and astatine. In *Chemistry of the Elements*, 2nd edition, 789-885. Butterworth-Heinemann.

Fang X., Qiu F., Yan B., Wang H., Mort A.J. and Stark R.E. (2001) NMR studies of molecular structure in fruit cuticle polyesters. *Phytochem.* **57**, 1035-1042.

Fischer H., Meyer A., Fischer K. and Kuzyakov Y. (2007) Carbohydrate and amino acid composition of dissolved organic matter leached from soil. *Soil Biol. Biochem.* **39**, 2926-2935.

Fox P.M., Davis J.A. and Luther G.W. III (2009) The kinetics of iodide oxidation by the manganese oxide mineral birnessite ($\delta$-MnO2) in the pH range 4-8. *Water Res.* **43** (14), 3417-3426.

Fox P.M., Douglas B.K. and Davis J.A. (2010) Redox transformations and transport of cesium and iodine (-1, 0, +5) in oxidizing and reducing zones of a sand and gravel aquifer. *Environ. Sci. Technol.* **44**, 1940-1946.

Francis A.J., Dodge C.J. and Ohnuki T. (2007) Microbial transformations of plutonium.

Journal of nuclear and radiochemical sciences. 8, 121. *J. Nucl., Radiochem. Sci.* **8**, 121-126.

Francois R. (1987) The influence of humic substances on the geochemistry of iodine in nearshore and hemipelagic marine sediments. *Geochi. Cosmochim. Acta.* **51**, 2417-2427.

Franke K. Roessler D. and Kupsch H. (2004) Use of radioactive tracers for the characterization of humic and fulvic acids in high performance size exclusion chromatography. In *Humic Substances: Nature's most versatile materials.* (Proceedings of the 11th Biennial Conference of the International Humic Substances Society and the 6th Humic Substances Seminar, Boston, MA, July 21–27, 2002). (eds. E. A. Ghabbour and G. Davies). Taylor and Francis, Inc., New York, 3–8.

Fuge R. and Johnson C.C. (1986) The geochemistry of iodine-a review. *Environmental Geochemistry and health.* **8**, 31-54.

Fujikawa Y., Zheng J., Cayer I., Sugahara M., Takigami H. and Kudo A. (1999) Strong association of fallout plutonium with humic and fulvic acid as compared to uranium and $^{137}$Cs in Nishiyama soils from Nagasaki, Japan. *J. Radioanal. Nucl. Chem.* **240**, 69-74.

Fukui M., Fujikawa, Y. and Satta, N. (1996) Factors affecting interaction of radioiodide and iodate species with soil, *J Environ. Radioact.* **31**, 199-216.

Gallard H., Allard S., Nicolau R., Gunten U. V. and Croué J.P. (2009) Formation of iodinated organic compounds by oxidation of iodide-containing waters with manganese dioxide. *Enviro. Sci. Technol.* **43**, 7003-7009.

Generalova V. A. and Onoshko M. P. (2006) Effects of humus acids on migration of radiostronium and radiocesium in valley deposits of the Sozh River. *Radiochem.* **48**, 99-104.

Gillam A.H., Lewis A.G. and Anderson R.J. (1981) Quantitative determination of hydroxamic acids. *Anal. Chem.* **53**, 841-844.

Gillam A.H. and Wilson M.A. (1985) Pyrolysis-GC-MS and NMR studies of dissolved seawatere humic substances and isolates of a marine diatom. *Org. Geochem.* **8**, 15-25,

Glaus M. A., Muller W., and Van Loon L. R. (2008) Diffusion of iodide and iodate through Opalinus Clay: monitoring of the redox state using an anion chromatographic technique. *Appl. Geochem.* **23**, 3612-3619.

Grotjan Jr. H. E., Padrnos-Hicks P.A. and Keel B.A. (1986) Ion chromatographic method for the analysis of sulphate in complex carbohydrates. *J. Chromatogr.* **367**, 367-375.

Guo L. and Santsch P.H. (1997) Isotopic and elemental characterization of colloidal organic matter from the Chesapeake Bay and Galveston Bay. *Mar. Chem.* **59**, 1-15.

Hatcher P. G. and Spiker E. C. (1988) Selective degradation of plant molecules. In *Humic Substances and Their Role in the Environment.* (eds. F. H. Frimmel and R. F. Christman). Wiley, U.K., 59-74

Hixon A.E., Hu Y.J., Kaplan D.I., Kukkadapu R.K., Nitsche H., Qafoku O., and Powell, B.A. (2010) Influence of iron redox transformations on plutonium sorption to sediments. *Radiochimica Acta* **98,** 685-692.

Holmen B.A. and Casey W.H. (1996) Hydroxamate ligands, surface chemistry, and the mechanism of ligand promoted dissolution of goethite (alpha -FeOOH(s)). *Geochim Cosmochim Acta* **60**, 4403-4416

Hou X., Hansen V, Aldahan A, Possnert G, Lind O. C and Lujaniene G. (2009) A review on speciation of iodine-129 in the environmental and biological samples. *Anal. Chim. Acta* **632,** 181-196.

Hu Q. H., Zhao P. H., Moran J. E. and Seaman J. C. (2005) Sorption and transport of iodine species in sediments from the Savannah River and Hanford Sites. *J. Contaminant Hydro.*, **78**(3), 185-205.

Hu Q. H., Moran J.E. and Blackwood V. (2007) Geochemical cycling of iodine species in soils. In *Comprehensive handbook of iodine*: *Nutritional, Biochemical, Pathological and Therapeutic Aspects*. (eds. V.R. Preedy, N. B., Gerard and R. Watson.) Academic Press, USA, 93-105.

Hu W.G., Mao J.D., Xing, B.S. and Schmidt-rohr, K. (2000) Poly(methylene) crystallites in humic substances detected by nuclear magnetic resonance. *Environ. Sci. Techonol.* **34**, 530-534.

Hung C. -C., Tang D., Warnken K. and Santschi, P. H. (2001) Distributions of carbohydrates, including uronic acids in estuarine waters of Galveston Bay. *Mar. Chem.* **73**, 305–318.

Ivashkina N.V., Yakovleva E.A., Ivanchikova I.D., Moroz A.A. and Shvartsberg M.S. (2005) Iodinated 1,4- naphthoquinones. *Russian Chemical Bulletin, International Edition*, **54**, 1509-1513.

Kaplan D. I., Serne R. J., Parker K. E. and Kutnyakov I. V. (2000) Iodide sorption to subsurface sediments and illitic minerals. *Environ. Sci. Technol.* **24** (3), 399– 405.

Kaplan D. I. (2003) Influence of surface charge of a Fe-oxide and an organic matter dominated soil on iodine and pertechnetate sorption. *Radiochim. Acta* **91**, 173-178.

Kaplan D. I., Roberts K. A., Schwehr K. A., Lilley M. S., Brinkmeyer R., Dehnam M. E., DiPrete D., Li H. -P., PowelB. A., Xu C., Yeager C. M., Zhang S. and Santschi, P. H. (2010) Cause of a multi-species radioiodine plume that is increasing in concentration. *Environ. Sci Technol.* **45**, 489-495.

Kelleher B.P. and Simpson A.J. (2006) Humic substances in soils: are they really chemically distinct? *Enviro. Sci Technol.* **40**, 4605-4611.

Keppler F., Biester H., Puschew A., Silk P. J., Scholer H. F., and Muller G. (2004) Organoiodine formation during humification in peatlands. *Environ. Chem. Let.* **1**, 219-223.

Kersting A. B., Efund D.W., Finnegan D.L., Rokop D.J., Smith D.K. and Thompson J.K. (1999) Migration of plutonium in groundwater at the Nevada Test Site. *Nature*, **397**, 56-59.

Kolattukudy P.E. (2001) Polyesters in higher plants. *Advances in Biochemical Engineering/Biotechnology.* **71**, 1-49.

Krupp G. and Aumann D.C. (1999) The origin of iodine in soil: I. Iodine in rainfall over Germany. Chem. Erde **59**, 57-67.

Leenheer J.A., Brown G.K., MacCarthy P. and Cabaniss S.E. (1998) Models of metal binding structures in fulvic acid from the Suwannee River, Georgia. *Environ. Sci.*

*Technol.* **32**, 2410-2416.

Li L., Huang W., Peng P., Sheng G. and Fu J. (2003) Chemical and molecular heterogeneity of humic acids repetitively extracted from a peat. *Soil Sci. Soc. Am. J.* **67**, 740-746.

Li H.-P., Brinkmeyer R., Jones W.L., Zhang S., Xu C., Schwehr K.A., Santschi P.H., Kaplan D.I., Yeager C.M. (2011) Iodine accumulation by aerobic bacteria isolated from subsurface sediments of a [129]I-contaminated aquifer at the Savannah River Site, SC. *Appl. Environ. Microbiol.* **77**, 2153-2160.

Magnusson R.P., Taurog A. and Dorris M.L. (1984) Mechanism of iodide-dependent catalatic activity of thyroid peroxidase and lactoperoxidase. *The Journal of Biological Chemistry*. **259**, 197-205.

Maillant S., Sheppard M. I., Echevarria G., Denys S., Villemin G., Tekely P., Leclerc-Cessac E. and Morel J. L. (2007) Aged anthropogenic iodine in a boreal peat bog. *Applied Geochem.* **22**, 873-887.

Martin J. M. and Whitfield M. (1983) The significance of the river input of chemical elements to the ocean. In *Trace Metals in Sea Water* (eds. C. S. Wong, E. Boyle, K. Bruland, J. D. Burton and E. D. Goldberg). Plenum Press, New York, 265-269.

Mathers N.J., Jalota R.K., Dalal R.C. and Boyd S.E. (2007) ^{13}C-NMR analysis of decomposing litter and fine roots in the semi-arid Mulga Lands of southern Queensland. *Soil Biol. Biochem.* **39**, 993-1006.

Mauchline J. and Templeton W.L. (1964) Artificial and natural radioisotopes in the marine environment. *Oceanogr. Mar. Biol. Annu. Rev.* **2**, 229–235.

Moran, J.E., Oktay, S.D. and Santschi, P.H. (2002) Sources of iodine and iodine 129 in rivers. *Water Resour. Res.* **38**(8): 1149-1158.

Morrison M. and Bayse G.S. (1970) Catalysis of iodination by lactoperoxidase. *Biochemistry* **9**, 2995-3000.

Moulin V., Reiller P., Amekraz B. and Moulin, C. (2001) Direct characterization of iodine covalently bound to fulvic acids by electrospray mass spectrometry. *Rapid Commun. Mass Spectrom.* **15**, 2488–2496.

Muramatsu Y., Uchida S. and Ohmomo Y. (1990) Determination of I-129 and I-127 in soil and tracer experiments on the adsorption of iodine on soil. *Journal of Radioanalytical and Nuclear Chemistry* **138**, 377-384.

Muramatsu Y., Yoshida S., Fehn U, Amachi S. and Ohmomo Y. (2004) Studies with natural and anthropogenic iodine isotopes: iodine distribution and cycling in the global environment. *J Environ. Radioact.* **74**, 221-232.

Murata T., Nagaishi N., Hamada R., Tanaka H., Sakagami K. and Kato T. (1998) Relationship between soil neutral sugar composition and the amount of labile soil organic matter in Andisol treated with bark compost or leaf litter. *Biology and Fertility of Soils* **27**, 342-348.

Neilands J.B. and Leong S.A. (1986) Siderophores in relation to plant growth and disease. *Ann. Rev. Plant Physiol.*, **37**, 187-208.

Novikov A.P., Kalmykov S. N., Utsunomiya S., Ewing R. C., Horreard F., Merkulov A., Clark S.B., Tkachev V.V. and Myasoedov B.F. (2006) Colloid transport of plutonium in the far-field of the Mayak Production Association, Russia. *Science*,

**314**, 638-641.

Oktay S.D., Santschi P.H., Moran J.E. and Sharma P. (2000) The [129]Iodine bomb pulse recorded in Mississippi River delta sediments: results from isotopes of I, Pu, Cs, Pb and C. *Geochim. Cosmochim. Acta*. **64**, 989-996.

Oktay S.D., Santschi P.H., Moran J.E., and Sharma P. (2001) [129]I and [127]I transport in the Mississippi River. *Environ. Sci. Technol.* **35,** 4470-4476.

Otosaka S., Schwehr K.A., Kaplan D.I., Roberts K.A., Zhang S., Xu C., Li H.-P., Ho Y.-F., Brinkmeyer R., Yeager C.M. and Santschi P.H. (2011) Transformation and transport process of [127]I and [129]I species in groundwater at the F-Area at the Savannah River Site. *Sci. Total Environ.* In press.

Perminova I., Grechishcheva, N.Yu. and Petrosyan, V.S. (1999) Relationships between structure and binding affinity of humic substances for polycyclic aromatic hydrocarbons: relevance of molecular descriptors. *Environ. Sci. Technol.* **33**, 3781-3787.

Piccolo A. (2001) The supramolecular structure of humic substances. *Soil Sci.* **166**, 810-832.

Preston C.M., Newman R.H. and Rother P. (1994) Using ^{13}C CPMAS NMR to assess effects of cultivation on the organic matter of particle size fractions in a grassland soil. *Soil Sci.* **157**, 26-35.

Price N. B. and Calvert S.E. (1977) The contrasting geochemical behaviour of iodine and bromine in recent sediments from the Namibian shelf. *Geochim. Cosmochim. Acta* **41**, 1769–1775.

Quigley M.S., Santschi P.H., Hung C.C. Guo L.D. and Honeyman B.D. (2002) Importance of acid polysaccharides for $^{234}$Th complexation to marine organic matter. *Limnol. Oceanogr.* **47**, 367-377.

Raisbeck G. M. and Yiou F. (1999) $^{129}$I in the oceans: origins and applications. *Sci. Tot. Environ.* ***237/238***, 31-41.

Rechard R.P. (1995) Performance assessment of the direct disposal in unsaturated tuff of spent nuclear fuel and high-level waste owned by the U.S. Department of Energy. Sandia National Laboratories. *SAND*94-2563/1. Sandia National Laboratory, Albuquerque, NM.

Reckhow D.A., Singer, P.C. and Malcolm R.L. (1990) Chlorination of humic materials: byproduct formation and chemical interpretations. *Environ. Sci. Technol.* **24**, 1655-1664.

Reiller P., Mercier-Bion F., Gimenez N., Barre N., and Miserque F. (2006) Iodination of humic acid samples from different origins. *Radiochim. Acta* **94**, 739-745.

Renshaw J.C., Robson G.D., Trinci A.P.J., Wiebe M.G., Livens F.R., Collison D. and Taylor R.J. (2002) Fungal siderophores: structures, functions, and applications. *Mycological Research*, **106**(10), 1123-1142.

Rice J. A. and MacCarthy P. (1992) Disaggregation and characterization of humin. *Sci. Tot. Environ.* **117/118**, 83-88.

Roberts K.A., Santschi P.H., Leppard G.G. and West M. (2004) Characterization of organic-rich colloids from surface and ground waters at the actinide-contaminated Rocky Flats Environmental Technology Site (RFETS), Colorado, USA. *Colloids and*

*Surfaces A: Physicochem. Eng. Aspects*, **244**, 105-111.

Rosa A. H., Simoes M. L., de Oliveira L. C., Rocha J. C., Neto L. M. and Milori D. M. B. P. (2005) Multimethod study of the degree of humification of humic substances extracted from different tropical soil profiles in Brazil's Amazonian region. *Geoderma* **127**, 1−10.

Ruggiero C.E., Matonic J.H., Reilly S.D. and Neu M.P. (2002) Dissolution of plutonium(IV) hydroxide by desferrioxamine siderophores and simple organic chelators. *Inorg. Chem.* **41**, 3593–3595.

Runde W. (2000) The chemical interactions of actinides in the environment. *Los Alamos Science* **26**, 392-411.

Santschi P.H., Schink D.R., Corapcioglu O., Oktay-Marshall S., Sharma P. and Fehn U. (1996) Evidence for elevated levels of iodine-129 in the deep Western Boundary Current in the Middle Atlantic Bight. *Deep-Sea Res.* **43**, 259-265.

Santschi P.H., Guo L., Walsh I.D., Quigley M.S. and Baskaran M. (1999) Boundary exchange and scavenging of radionuclides in continental margin waters of the Middle Atlantic Bight: implications for organic carbon fluxes. *Cont. Shelf Res.* **19**, 609-636.

Santschi P. H., Roberts K. A. and Guo L. (2002) Organic nature of colloidal actinides transported in surface water environments. *Environ. Sci. Technol.* **36**, 3711–3719.

Santschi P.H. and Schwehr K.A. (2004) I-129/I-127 as a new environmental tracer or geochronometer for biogeochemical or hydrodynamic processes in the hydrosphere and geosphere: the central role of organo-iodine. *Sci. Total Environ.*, **321**, 257-271.

Savitzki A., Golay M.J.E., (1964) Smoothing and differentiation of data by a simplified least squares method. *Anal. Chem.* **36**, 1627-1639.

Schaeffer T.L., Cantwell S.G., Brown J.L., Watt D.S. and Fall R.R. (1997) Microbial growth on hydrocarbons: terminal branching inhibits biodegradation. *Appl Environ. Microbiol.* **38**, 742-746.

Schlegel M. L., Reiller P., Mercier-Bion F., Barre N. and Moulin V. (2006) Molecular environment of iodine in naturally iodinated humic substances: insight from X-ray absorption spectroscopy. *Geochim. Cosmochim. Acta* **70** (22), 5536-5551.

Schmitz K. and Aumann D.C. (1995) A study on the association of two iodine isotopes, of natural iodine-127 and of the fission product iodine-129, with soil components using a sequential extraction procedure. *J. Radioanal. Nucl. Chem.* **198** (1), 229-236.

Schwehr K.A. and Santschi P.H., 2003. Sensitive determination of iodine species, including organo-iodine, for freshwater and seawater samples using high performance liquid chromatography and spectrophotometric detection. *Anal. Chim. Acta*, **482**(1): 59-71.

Schwehr K. A., Santschi P. H. and Moran J. E. (2005) [129]Iodine: a new hydrological tracer for aquifer recharge conditions influenced by river flow rate variations and evapotranspiration. *Appl. Geochem.* **20**, 1461–1472.

Schwehr K. A., Santschi P. H., Kaplan D. I., Yeager C. M. and Brinkmeyer R. (2009) Organo-iodine formation in soils and aquifer sediments at ambient concentrations. *Environ. Sci. Technol.* **43**(19), 7258-64.

Sheppard M. I. and Thibault D.H. (1991) A four-year mobility study of selected trace elements and heavy metals. *J. Environ. Qual.* **20**, 101-114.

Sheppard M. I., Hawkins J. L. and Smith P.A. (1996) Linearity of iodine sorption and sorption capacities for seven soils. *Environ. Sci. Technol.* **25**, 1261-1267.

Shimamoto Y.S., Takahashi Y. and Terada Y. (2011) Formation of organic iodine supplied as iodide in a soil-water system in Chiba, Japan. *Enviro. Sci. Technol.* **45**, 2086-2092.

Simpson A.J., Song G., Smith E., Lam B., Novotny E.H. and Hayes M.H.B. (2007) Unraveling the structural components of soil humin by use of solution-state nuclear magnetic resonance spectroscopy. *Environ. Sci. Techonol.* **41**, 876-883.

Smith P.K., Krohn R.I., Hermanson G.T., Mallia A.K., Gartner F.H., Provenzano M.D., Fujimoto E.K., Goeke N.M., Olson B.J. and Klenk D.C. (1985) Measurement of protein using bicinchoninic acid. *Anal. Biochem.* **150**, 76-85.

Solórzano L. and Sharp J.H. (1980) Determination of total dissolved phosphorus and particulate phosphorus in natural waters, *Limnol. Oceanogr.* **25**, 754–758.

Steinberg S.M., Kimble G.M., Schmett G.T., Emerson D.W., Turner M.F. and Rudin M. (2008) Abiotic reaction of iodate with sphagnum peat and other natural organic matter. *J. Radioanal. Nucl. Chem.* **277**, 185-191.

Sutton R., and Sposito G. (2005) Molecular structure in soil humic substances: The new view. *Environ. Sci. Technol.* **39**, 9010-9015.

Swift R. S. (1996) Organic matter characterization. In *Methods of soil analysis. Part 3. SSSA Book Series No.5.* (ed. D. L. Sparks) . Soil Science Society of America Press, Madison, WI. 1011–1069.

Szidat S. Schmidt A., Handl J., Jakob D., Michel R., Synal H.-A. and Suter M. (2000) Analysis of iodine-129 in environmental materials: quality assurance and applications. *J. Radioanal. Nucl. Chem.***244** (1), 45-50.

Takayanagi K. and Wong G.T.F. (1986) The oxidation of iodide to iodate for the polarographic determination of total iodine in natural waters. *Talanta* **33**, 451–454.

Tan W., Lu S., Liu F., Feng X., He J. and Koopal L.K. (2008) Determination of the point-of-zero charge of manganese oxides with different methods including an improved salt titration method. *Soil Science*. **173**, 277-286.

Thurman E. M. and Malcolm R. L. (1981) Preparative isolation of aquatic humic substances. *Environ. Sci. Technol.* **15**, 463-466.

Um W., Serne R.J. and Krupka K.M. (2004) Linearity and reversibility of iodide adsorption on sediments from Hanford, Washington under water saturated conditions. *Water Res.* **38**, 2009-2016.

Walters J.S. and Hedges J.I. (1988) Simultaneous determination of uronic acids and alddoses in plankton, plant tissues, and sediment by capillary gas chromatography of N-hexylaldonamide and alditol acetates. *Anal. Chem.* **60**, 988-994.

Wang, K. and Xing, B., 2005. Chemical extractions affect the structure and phenanthrene sorption of soil humin. *Environ. Sci. Technol.* **39**, 8333-8340.

Warner J. A., Casey W. H. and Dahlgren R. A. (2000) Interaction kinetics of I$_2$(aq) with substituted phenols and humic substances. *Environ. Sci. Technol.* **34**, 3180–3185.

Warwick P., Zhao R., Higgo J. J. W., Smith B. and Williams G. M. (1993) The mobility and stability of iodine-humic and iodine-fulvic complexes through sand. *Sci. Tot. Environ.* **130/131**, 459-465.

Weng L., Fest E. P. M. J., Fillius J., Temminghoff E. J. M. and Van Riemsdijk, W.H. (2002) Transport of humic and fulvic acis in relation to metal mobility in a copper-contaminated acid sandy soil. *Environ. Sci. Technol.* **36**, 1699-1704.

Wershaw R.L. (2004) Evaluation of conceptual models of natural organic matter (humus) from a consideration of the chemical and biochemical processes of humification. Scientific Investigations Report 2004-5121. U.S. Geological Survey: Reston, VA.

WSRC-RP-2006-4011 (2006) Annual Corrective Action Report for the F-Area Hazardous Waste Management Facility, the H-Area Hazardous Waste Management Facility, and the Mixed Waste Management Facility (U). Westinghouse Savannah River Company, Aiken, SC.

Whitehead D.C. (1973) The sorption of iodide by soils as influenced by equilibrium conditions and soil properties. *Journal of the Science of Food and Agriculture* **24**, 547-556.

Whitehead D.C. (1978) Iodine in soil profiles in relation to iron and aluminum oxides and organic matter. *European Journal of Soil Science*. **29**, 88-94.

Whitehead D.C. (1984) The distribution and transformation of iodine in the environment. *Environmental International* 10, 321-339.

Wong G.T.F. (1980) The oxidation state diagram: a potential tool for studying redox chemistry in seawater. *Mar. Chem.* **9**, 1–12.

Wong G.T.F., Takayanagi K. and Todd J.F. (1985) Dissolved Iodine in Waters Overlying and in the Orca Basin Gulf of Mexico. *Mar. Chem.*, **17**(2): 177-183.

Wong G.T.F. and Cheng, X.-H. (2001) The formation of iodide in marine waters from the photochemical decomposition of dissolved organic iodine. *Mar. Chem.* **74**, 53-64.

Xu C., Santschi P. H., Zhong J. Y., Hatcher P. G., Francis A. J., Dodge C. J., Roberts K. A., Hung C. C. and Honeyman. B. D. (2008) Colloidal cutin-like substances cross-linked to siderophore decomposition products mobilizing plutonium from contaminated soils. *Environ. Sci. Technol.*, **42**(22), 8211-8217.

Xu C., Zhang S., Ho Y.-F., Miller E.J., Roberts K.A., Li H.-P., Schwehr K.A., Otosaka S., Kaplan D.I., Brinkmeyer R., Yeager C.M., Santschi P. H. (2011a) Is soil natural organic matter a sink or source for radioiodine ($^{129}$I) in a nuclear waste disposal site? *Geochim. Cosmochim. Acta.* submitted.

Xu C., Miller E.J., Zhang S., Li H.-P., Ho Y.-F., Schwehr K.A., Kaplan D. I., Otosaka S., Roberts K. A., Brinkmeyer R., Yeager C. M. and Santschi P. H. (2011b) Sequestration and re-mobilization of radioiodine ($^{129}$I) by soil organic matter and possible consequences of the remedial action at Savannah River Site. *Environ. Sci. Technol.* Submitted

Yamaguchi N., Nakano M., Takamatsu R. and Tanida H. (2010) Inorganic iodine incorporation into soil organic matter: evidence from iodine K-edge X-ray absorption near-edge structure. *J. Environ. Radioact.* **101**, 451-457.

Yang H., Liu W., Li B., Zhang H., Liu X. and Chen D. (2007) Speciation analysis for iodine in groundwater using high performance liquid chromatography-inductively coupled plasma-mass spectrometry (HPLC-ICP-MS). Geostandards and Geoanalytical Research. **31**, 345-351.

Yoshida S., Muramatsu Y. and Uchida S. (1992) Studies on the sorption of $I^-$ (iodide) and $IO_3^-$ (iodate) onto andosols. *Water Air Soil Pollut*. **63**, 321-329.

Yoshida S. and Muramatsu Y. (1995) Determination of organic, inorganic and particulate iodine in the coastal atmosphere of Japan. *J. Radioanal. Nucl. Chem.* **196**, 295-302.

Yoshida S., Muramatsu Y. and Uchida S. (1998) Soil-solution distribution coefficients, Kds of $I^-$ and $IO_3^-$ for 68 Japanese soils. *Radiochim. Acta* **82**, 293-297.

Yu Z., Warner J.A., Dahlgren R.A. and Casey W.H. (1996) Reactivity of iodine in volcanic soils and noncrystalline soil constituents. *Geochim Cosmochim Acta* **60**, 4945-4956.

Zhang, S., Xu, C. and Santschi, P. H. (2008) Chemical composition and [234]Th binding of extracellular polymeric substances (EPS) produced by the marine diatom Amphora sp. *Mar. Chem.* **112**, 81-92.

Zhang S., Schwehr K. A., Ho Y.-F.,  Xu C., Roberts K. A. and Kaplan D. I, Santschi P. H. (2010) A novel approach for the simultaneous determination of iodide, iodate, and

organo-iodide for $^{127}$I and $^{129}$I in Environmental samples using gas chromatography - mass spectrometry. *Environ. Sci. Technol.* **44**, 9042-9048.

Zhang S., Du J., Xu C., Schwehr K. A., Ho Y. -F., Li H. -P., Roberts K. A., Kaplan D. I., Brinkmeyer R., Yeager C. M. and Santschi P. H. (2011) Concentration dependent mobility, retardation and speciation of iodine in surface sediment from the Savannah River Site. *Environ. Sci. Technol.*, DOI: 10.1021/es1040442.

**VITA**

| | |
|---|---|
| Name: | Chen Xu |
| Address: | Department of Oceanography, Texas A &M University, College Station, TX 77843-3146 |
| Email Address: | xuchen66@hotmail.com |
| Education: | M.S. Chemical Oceanography, Texas A&M University (2007) B.S. Environmental Science and Engineering, Xiamen University (2004) |
| Award: | Erma Lee and Luke Mooney Graduate Student Excellence Research Award (2008) |

Publications:

**Xu, C**., Santschi, P. H., Zhong, J. Y., Hatcher, P. G., Francis, A. J., Dodge, C. J., Roberts, K. A., Hung, C. C. and B. D. Honeyman., 2008. Colloidal Cutin-Like Substances Cross-Linked to Siderophore Decomposition Products Mobilizing Plutonium from Contaminated Soils. Environmental Science & Technology, 42(22): 8211-8217.

**Xu, C.,** Santschi, P.H., Schwher, K., Hung, C.-C., 2009. Optimized isolation procedure for obtaining strongly actinide binding exopolymeric substances (EPS) from two bacteria (*Sagittula stellat*a and *Pseudomonas fluorescens* Biovar II). Bioresource Technology. 100, 6010-6021

Roberts, K.A., **Xu, C.,** Hung, C.-C., Conte, M.H., Santschi, P.H., 2009. Scavenging and fractionation of thorium vs. protactinium in the ocean, as determined from particle-water partitioning experiments with sediment trap material from the Gulf of Mexico and Sargasso Sea. Earth and Planetary Science Letters. 286, 131-138.

**Xu, C.,** Santschi, P. H., Hung, C.-C., Zhang, S. , Schwehr, K,A., Roberts, K.A., Guo, L.D., Gong, G.-C., Quigg, A., Long, R., Pinckney, J., Duan, S.W., Amon, R., Wei, C.-L. 2010. Controls of Th-234 removal from the oligotrophic ocean by polyuronic acids and modified by microbial activity. Marine Chemistry, 123, 111–126.

**Xu, C.,** Zhang, S., Chuang, C.-Y., Miller, E.J., Schwehr, K.A., and Santschi, P.H. 2011. Chemical characterization of strongly actinide binding exopolymeric substances (EPS) from two bacteria (*Sagittula stellata* and *Pseudomonas fluorescens* Biovar II). Marine Chemistry, in press.